EVALUATION OF PREFERENTIAL FLOW PROCESSES IN RECLAMATION SOIL COVERS

A Thesis Submitted to the College of

Graduate Studies and Research

In Partial Fulfillment of the Requirements

For the Degree of Master of Science

In the Department of Soil Science

University of Saskatchewan

Saskatoon

By

DANIELLE CELINE WELTER

Permission to Use

In presenting this thesis in partial fulfilment of the requirements for a Postgraduate degree from the University of Saskatchewan, I agree that the Libraries of this University may make it freely available for inspection. I further agree that permission for copying of this thesis in any manner, in whole or in part, for scholarly purposes may be granted by the professor or professors who supervised my thesis work or, in their absence, by the Head of the Department or the Dean of the College in which my thesis work was done. It is understood that any copying or publication or use of this thesis or parts thereof for financial gain shall not be allowed without my written permission. It is also understood that due recognition shall be given to me and to the University of Saskatchewan in any scholarly use which may be made of any material in my thesis.

Requests for permission to copy or to make other use of material in this thesis in whole or part should be addressed to:

Head of the Department of Soil Science
University of Saskatchewan
Saskatoon, Saskatchewan S7N 5A8
Canada

OR

Dean
College of Graduate Studies and Research
University of Saskatchewan
107 Administration Place
Saskatoon, Saskatchewan S7N 5A2
Canada

ABSTRACT

To predict the effectiveness of land reclamation, it is important to understand how water and solutes are transported within reconstructed landscapes. The objective of this study was to examine the influence of preferential flow on salt leaching in reclamation soil covers. The study site was a reconstructed landscape where saline-sodic minespoil from oil sands mining was capped with layers of glacial and peat mix soil. Preferential flow was investigated using laboratory column experiments and in situ adsorptive dye and conservative tracer experiments.

Results from column experiments and dye tracer experiments indicate that preferential flow is an important and prevalent mechanism of solute transport. Column experiments, which used time-domain reflectometry to monitor the transport of a chloride tracer through an undisturbed core of peat mix soil, determined immobile water fractions (θ_{im}/θ) ranging from 80-99% and diffusive mass transfer rates (α) between 0.15 - 2.0 h^{-1}. Breakthrough curves showed the early arrival of chloride and extended tailing. Dye tracer experiments, in which Brilliant Blue dye was applied in solution to the soil surface, were carried out at 6 hillslopes plots. Approximately 24 hours after dye application, a vertical soil face was excavated to reveal stained flow patterns. Preferential flow as macropore flow, fingering, and / or funneling was observed at each plot.

Results from the conservative tracer field study indicated soil solutes were flushed by a combination of vertical and lateral flow processes. A large pulse of bromide and chloride was applied across the lower slope of the 0.35-m cover. Soil sampling at approximately 1 and 2 years later determined vertical leaching, lateral translocation downslope, and upwards movement of soil solutes. Matrix flow during the spring melt, combined with matrix flow and / or preferential flow during summer and fall periods, was responsible for the vertical leaching of solutes. Subsurface flow generated in response to the spring melt or due to differences in soil hydraulic conductivity was responsible for the lateral transport of solutes. As a result of advective or diffusive processes, solutes were transported upwards into the overlying soil. These results suggested that despite the existence of preferential flow, there

were other mechanisms of solute transport which served to leach and flush salts from the soil.

ACKNOWLEDGMENTS

It is with utmost gratitude that I thank my husband, Kevin Welter, dear friend, Alanna Dickson, and parents, Denis and Lynda Renaud, for their unwavering support and encouragement.

I thank my supervisor, Dr. Bing Cheng Si, and his colleagues, Dr. Diane Knight, Dr. Mike Grevers, Dr. M. Jim Hendry, and Dr. Derek Peak, for the guidance received while acting as my Advisory Committee. I also thank Dr. Terry Fonstad for acting as my external examiner and Dr. Lee Barbour for his continuous support.

I would like to acknowledge the help of several individuals whose assistance in the project was invaluable. Heidi Lazorko, Sophie Kessler, and Heather Rodger, thank you for all the help in conducting field research and data compilation. Sincere thanks to Dr. Xulin Guo for her invaluable assistance in image processing and to Dr. Gang Liu for his help with the CXTFIT model.

Funding for this project was provided by Syncrude Canada Ltd. and the National Science and Engineering Research Council (NSERC). I thank Mike MacKinnon at Syncrude's Environmental Research Laboratory for his technical support and Clara Qualizza at Environmental Affairs for her faith in the importance of industry-based research.

Last, but definitely not least, I thank Elaine Farkas for everything she does to help graduate students, near and far.

“Energy and persistence conquer all things.”
Benjamin Franklin

To my son, Noah, and in memory of my sister, Nicole

TABLE OF CONTENTS

page

ABSTRACT ii

ACKNOWLEDGMENTS iv

LIST OF TABLES viii

LIST OF FIGURES ix

LIST OF ABBREVIATIONS xii

1. INTRODUCTION 1

1.1 Background 1
1.2 Research Hypotheses 6
1.3 Research Objectives 7
1.4 Outline of Thesis 7
2. LITERATURE REVIEW 8

2. 1 Description of Preferential Flow Processes 8
2.1.1 Macropore flow 8
2.1.2 Fingered flow 9
2.1.3 Funneled flow 10
2.2 Characterization of Preferential Flow 11
2.2.1 Field experiments 12
2.2.1.1 Adsorptive dye tracer studies 12
2.2.1.2 Dye tracer selection 14
2.2.2 Laboratory column experiments 15
2.2.2.1 Mobile-immobile model of solute transport 15
2.2.2.2 Time domain reflectometry 18
2.2.2.3 Conservative tracer selection 19
3. SUSCEPTABILITY OF SOIL COVERS TO PREFERENTIAL FLOW 21

3.1 Introduction 21
3.2 Materials and Methods 22
3.2.1 Study site 22
3.2.2 Laboratory column experiments 23
3.2.3 Dye tracer experiments 28
3.3 Results and Discussion 30
3.3.1 Laboratory column experiments 30
3.3.2 Dye tracer experiments 37
3.4 Conclusions 48
4. FIELD STUDY OF VERTICAL AND LATERAL SOLUTE TRANSPORT 49

4.1 Introduction 49
4.2 Materials and Methods 50

4.2.1 Study site 50
4.2.2 Experimental design 51
4.2.3 Sampling scheme 53
4.3 Results and Discussion 54
4.3.1 Soil chemistry 54
4.3.1.1 2004 sampling program 55
4.3.1.2 2005 sampling program 61
4.3.2 Subsurface water chemistry 72
4.4 Conclusions 74
5. CONCLUSIONS AND RECOMMENDATIONS 75

5.1 Summary 75
5.2 Implications for Design 77
5.3 Recommendations for Future Research 78
5.4 Lessons Learned 79
6. REFERENCES 80

Appendix A - Non-Linear Least Squares Analysis For Estimation Of Transport Parameters 90

Appendix B - Soil Water Chemistry from Soil Sampling Program 93

LIST OF TABLES

Table page

Table 3.1 Physical and chemical properties for the three soil materials comprising the reclamation soil covers at the SW30 research site, Mildred Lake mine site, as determined in 2002. Mean values are reported. (Kessler, 2007) 24

Table 3.2 Measured water contents (θ) and estimated solute transport parameters, including the fraction of mobile water (β), dispersivity of the mobile region (D_m), mass transfer rate co-efficient (α), mean travel velocity (v), and peak travel velocity (v_{pk}) for column experiments where q = 0.002 m hr^{-1}..... 35

Table 3.3 Measured water contents (θ) and estimated solute transport parameters, including the fraction of mobile water (β), dispersivity of the mobile region (D_m), mass transfer rate co-efficient (α), mean travel velocity (v), and peak travel velocity (v_{pk}) for column experiments where q = 0.010 m hr^{-1}..... 35

Table 3.4 Percent of soil area stained by preferential flow for toe, middle, and upper slope positions on the 0.35-m and 1-m soil covers, one day after soil plots were irrigated with a total application of 0.04 m dye solution..... 46

Table 4.1 Mass of bromide ions determined in soil samples downslope of initial tracer application, as measured in September 2004. 71

Table 4.2 Mass of bromide ions determined in soil samples downslope of initial tracer application, as measured in June 2005. 71

Table 4.3 Bromide concentrations in subsurface water as collected in downslope shallow monitoring wells. 73

LIST OF FIGURES

Figure page

Figure 1.1 Aerial view of the South West 30 Dump (SW30) research site showing the three prototype reclamation soil covers situated along the north-facing slope (photo courtesy of Syncrude Canada Limited). 2

Figure 1.2 The South West 30 Overburden Dump is located approximately 35km north of Fort McMurray, Alberta, on Syncrude Canada's Mildred Lake mine site (OSERN, 2004). 3

Figure 3.1 Schematic diagram of solute transport experiment, in which the transport of chloride through an undisturbed soil core from the South West 30 Overburden Dump was monitored. A humidifier supplied flushing water (a solution of calcium sulfate) to a secondary reservoir. Water flowed from the reservoir to the core below through transmission tubes. Horizontally installed time domain reflectometry (TDR) probes were used to measure soil water content and electrical conductivity. Unsaturated conditions were obtained by placing the core atop a porous glass plate and using sand to increase hydraulic contact. When steady state conditions were achieved, the reservoir was drained and a pulse of potassium chloride (KCl) was applied. Once the pulse was completed, the supply to the reservoir was returned. 26

Figure 3.2 Concentrations of total dissolved solids (TDS) versus time elapsed since tracer application in peat mix soil cores under a flux (q) of 0.002 m hr^{-1}. Cores labeled 6, 16, and 25 are identified as a, b, and c, respectively. Concentrations are plotted as determined experimentally (normalized to a mass per area of applied chloride of 48 g m^{-2}) and as fit by inverse modeling using CXTFIT. The dashed line represents the expected time, t_v, for the solute peak to arrive based on piston flow velocity, v. 32

Figure 3.3 Concentrations of total dissolved solids (TDS) versus time elapsed since tracer application in peat mix soil cores under a flux (q) of 0.010 m hr^{-1}. Cores labeled 6, 3, and 25 are identified as a, b, and c, respectively. Concentrations are plotted as determined experimentally (normalized to a mass per area of applied chloride of 48 g m^{-2}) and as fit by inverse modeling using CXTFIT. The dashed line represents the expected time, t_v, for the solute peak to arrive based on piston flow velocity, v. 33

Figure 3.4 Vertical flow patterns of Brilliant Blue dye one day after soil plots were irrigated with a total application of 0.04 m dye solution. Profiles are presented for the: a)top, b)middle, and c)toe slope positions of the 0.35-m soil cover. 38

Figure 3.5 Vertical flow patterns of Brilliant Blue dye one day after soil plots were irrigated with a total application of 0.04 m dye solution. Profiles are

presented for the: a)top, b)middle, and c)toe slope positions of the 1-m soil cover. 39

Figure 3.6 Vertical flow patterns of Brilliant Blue dye, and the corresponding digital classification of dyed pixels and non-dyed pixels, one day after soil plots were irrigated with a total application of 0.04 m dye solution. Profile shown is representative of the middle slope position of the 1-m soil cover. 42

Figure 3.7 Vertical flow patterns of Brilliant Blue dye, and the matching one-dimensional profile of dye coverage, one day after soil plots were irrigated with a total application of 0.04 m dye solution. Profile shown is representative of the middle slope position of the 1-m soil cover. 43

Figure 3.8 Percentage of stained soil versus soil depth for the 0.35-m cover. Error bars represent the standard error associated with the method of digital classification. 44

Figure 3.9 Percentage of stained soil versus soil depth for the 1-m cover. Error bars represent the standard error associated with the method of digital classification. 45

Figure 4.1 Schematic diagram of tracer application and monitoring well locations on the 0.35-m soil cover. Sodium bromide was applied to the soil surface (black boxes) while sodium chloride was applied in the soil trenches (white boxes). The black dots represent the locations of the monitoring wells. 52

Figure 4.2 Mean concentrations of bromide and chloride (g m^{-3}soil) as a function of soil depth, as measured at the locations of the initial tracer application in September 2004. Error bars were not presented due to the particularly large variability in concentrations. 56

Figure 4.3 Mean concentrations of soil bromide (g m^{-3} soil) as a function of distance downslope from the source (the site of initial tracer application). Measurements occurred during the September 2004 soil sampling program for depths of 0-0.15 m, 0.15-0.35 m, and 0.35-0.50 m. Error bars represent standard deviation. Source data was previously presented in Figure 4.2. 58

Figure 4.4 Mean concentrations of soil chloride (g m^{-3} soil) as a function of distance downslope from the source (the site of the initial tracer application). Measurements occurred during the September 2004 soil sampling program for depths of 0-0.15 m, 0.15-0.35 m, and 0.35-0.50 m. Error bars represent standard deviation. Source data was previously presented in Figure 4.2. 62

Figure 4.5 Mean concentrations of bromide and chloride (g m^{-3}soil) as a function of soil depth, as measured at the locations of the initial tracer application in June 2005. Error bars were not presented due to the particularly large variability in concentrations. 63

Figure 4.6 Mean concentrations of soil bromide (g m^{-3} soil) as a function of distance downslope from the source, as determined during the June 2005 sampling program for depths of 0-0.15 m, 0.15-0.35 m, and 0.35-0.50 m. Error bars represent standard deviation. Source data was presented previously is Figure 4.5. 65

Figure 4.7 Mean concentrations of soil chloride (g m^{-3} soil) as a function of distance downslope from the source, as determined during the June 2005 sampling program for depths of 0-0.15 m, 0.15-0.35 m, and 0.35-0.50 m. Error bars represent standard deviation. Source data was presented previously is Figure 4.5. 66

Figure 4.8 Change in soil bromide concentrations at the 0-0.15 m sampling depth from fall 2004 to spring 2005. Box plot illustrates the median, 10th, 25th, 75th, and 90th percentiles. Outliers are shown as black circular dots. Concentration distributions were significantly different at α=0.05 according to the Wilcoxon Rank Sum Test (n= 15). 67

Figure 4.9 Change in soil bromide concentrations at the 0.15-0.35 m sampling depth from fall 2004 to spring 2005. Box plot illustrates the median, 10th, 25th, 75th, and 90th percentiles. Outliers are shown as black circular dots. Results were not statistically different at α=0.05 according to the Wilcoxon Rank Sum Test (n= 15). 68

Figure 4.10 Change in soil bromide concentrations at the 0.35-0.50 m sampling depth from fall 2004 to spring 2005. Box plot illustrates the median, 10th, 25th, 75th, and 90th percentiles. Outliers are shown as black circular dots. Concentration distributions were significantly different at α=0.05 according to the Wilcoxon Rank Sum Test (n= 15). 69

LIST OF ABBREVIATIONS

ADE	Advection dispersion equation
BDL	Below detection limit
BTC(s)	Breakthrough curve(s)
CDE	Convection dispersion equation
IC	Ion chromatography
MIM	Mobile-immobile model of soil water
MPA	Mass of solute applied per area
NDVI	Normalized difference vegetation index
SW30	South West 30 Overburden Dump
TDR	Time domain reflectometry
TDS	Total dissolved solids

1. INTRODUCTION

1.1 Background

In post-mining landscapes, reclaimed minespoil piles form an integral part of the environment. Capped with salvaged soil suitable as a vegetative medium, minespoil piles form the foundation for future self-sustaining ecosystems. Contaminants within minespoil piles can, however, be highly mobile. Once mobile in the environment, these contaminants may adsorb onto soil particles, leach into groundwater or adjacent rivers and streams, or be taken up by vegetation. All of these possibilities pose a risk to the ecosystem and threaten the success of reclamation practices. It is therefore important to understand how water and solutes are transported within these reconstructed landscapes. This will serve not only to help predict the long-term sustainability of land reclamation techniques, but also to help ensure long-term environmental protection and continued public health and safety.

Mining of the Athabasca Oil Sands, located north of Fort McMurray, Alberta, is occurring at an unparalleled rate. Consequently, the amount of reclamation required is unprecedented. To access the oil sands, large quantities of Cretaceous marine shales must first be removed. These shales, which are highly saline and sodium saturated, form large volumes of waste material, referred to as saline-sodic minespoil. Due to the detrimental effects of salinity on vegetation and the negative impacts of sodicity on soil structure, saline-sodic minespoil is not suitable as a vegetative medium when left in its original state. Reclamation of this material occurs by capping the shale with a layer of clean soil to reduce the upwards migration of salts into the rooting zone and to provide enough moisture for a vegetative cover.

To investigate the sustainability of reclamation practices and the best design for reclamation soil covers capping saline-sodic minespoil, Syncrude Canada Ltd. constructed a research site known as the South West 30 Overburden Dump (SW30) (Figure 1.1). The SW30 is located 35 km north of Fort McMurray at the Mildred Lake mine site (Figure 1.2). From 1980 – 1996, saline-sodic minespoil resulting

Figure 1.1 Aerial view of the South West 30 Dump (SW30) research site showing the three prototype reclamation soil covers situated along the north-facing slope (photo courtesy of Syncrude Canada Limited).

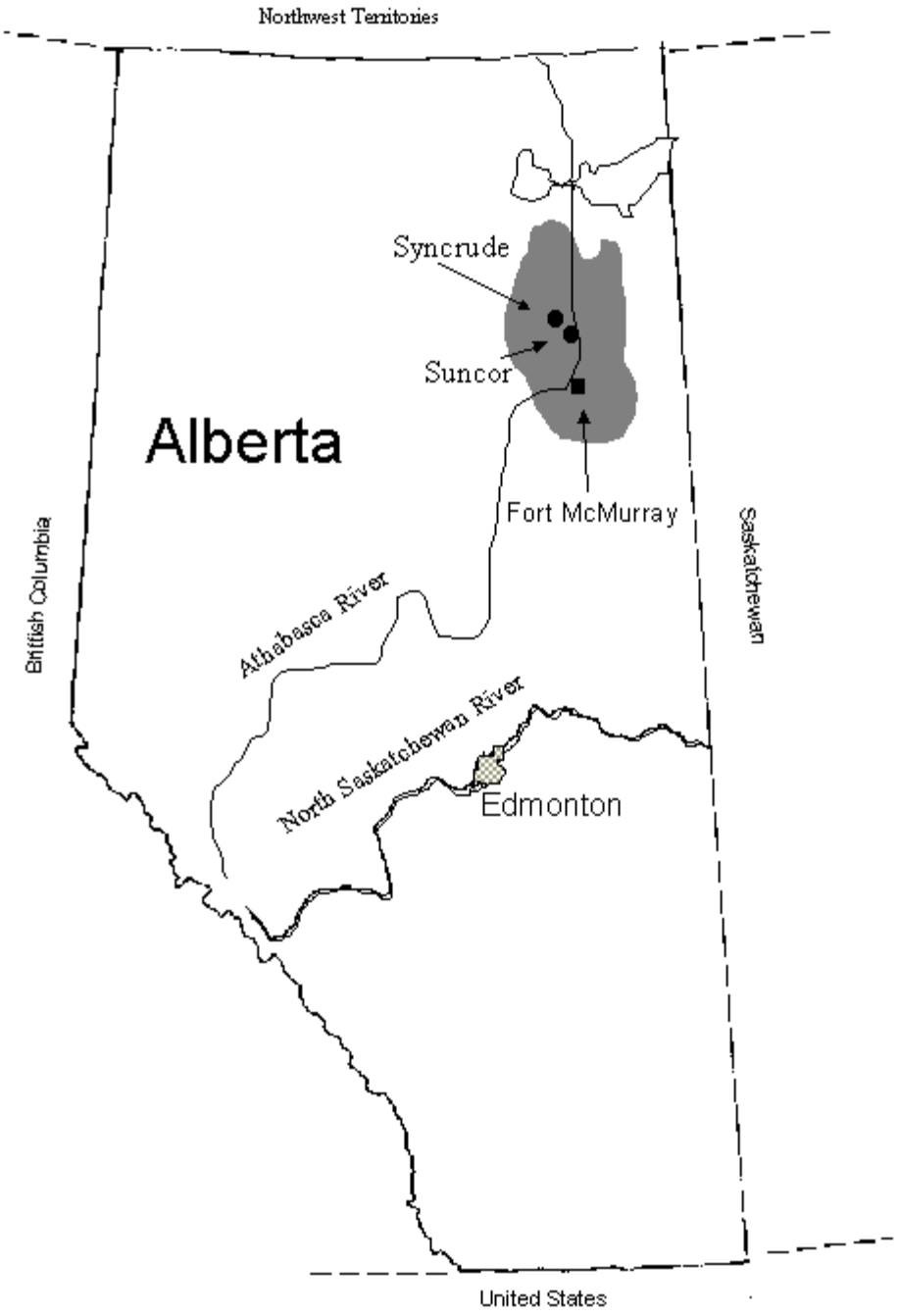

Figure 1.2 The South West 30 Overburden Dump is located approximately 35km north of Fort McMurray, Alberta, on Syncrude Canada's Mildred Lake mine site (OSERN, 2004).

from oil sands mining was dumped to form a large surface deposit, which was then contoured to resemble a natural watershed. The SW30 is 2 km^2 in area with a plateau elevation that rises 60 m above the nearby landscape. In 1999, three 1 ha prototype soil covers of varying thicknesses (0.35, 0.50 or 1 m) were placed over the saline-sodic minespoil. Each cover consisted of a selected depth of peat mix soil overlying a clay-rich glacial soil. Since establishment, the three soil covers have provided the basis for research into reclamation-specific geochemistry and hydrology.

The geochemical characterization of salt distribution within the reconstructed landscape was investigated by Wall (2005) and Kessler (2007). Within the shale, Wall (2005) observed that sulphide mineral oxidation was consuming oxygen (O_2) to produce soluble sulfate (SO_4), which in turn leads to sulphuric acid (H_2SO_4) production. In response to acid production, carbonate mineral dissolution reactions were occurring, resulting in the production of carbon dioxide (CO_2) and the release of calcium (Ca^{2+}). Cation exchange on clay mineral surfaces was found to increase available sodium (Na^+). Therefore, within the shale, the elevated concentrations of SO_4^{2-} (from sulphuric acid production), Ca^{2+} (from carbonate dissolution), and Na^+ (from cation exchange) serve as sources of salts which could migrate into the overlying soil covers.

Kessler (2007) confirmed that within four years following cover placement, salts had indeed migrated from the shale to the overlying reclamation soil covers. The majority of these salts were SO_4^{2-} and Na^+, both of which were attributed to the sulphide oxidation observed by Wall (2005). Soil salinity profiles showed that salt migration was so prevalent that salinity indices for plant growth were at critical levels at the base of each soil cover. Diffusion was identified as the dominant mechanism of salt transport.

The hydrology of the reconstructed landscape was investigated by Boese (2003), Shurniak (2003), Meiers et al. (2006), and Kelln et al. (2007). Boese (2003) and Shurniak (2003) implemented a field instrumentation program to monitor water movement within the reclamation soil covers. Two weather stations, three soil monitoring stations, a runoff monitoring system, and an interflow collection system were installed on the SW30. One weather station was constructed in the centre of the

3 ha test plot while the other was placed outside of the test plot on the flat top of the waste dump. Measurements from these stations included wind speed and direction, air temperature, relative humidity, and precipitation. Three soil stations were installed in the middle of each 1 ha soil cover. Each station consisted of calibrated thermistor, thermal conductivity, and time domain reflectometry (TDR) sensors to measure soil temperature, matric suction and volumetric water content, respectively, at selected depths throughout both the shale and overlying cover. Neutron and capacitance probe access tubes were also installed near the soil stations to further aid in the measurement of soil moisture. Snowmelt and rainfall runoff was measured by sonic sensors attached to weirs constructed upstream and at the toe of each soil cover. Interflow was collected at the base of each cover in a large collection well that was pumped out regularly to measure flow volumes. Two rows of shallow monitoring wells were also installed at 5 and 20 m upslope of the interflow collection well to monitor solute transport. From the data collected with the field instrumentation and additional in situ measurements, Shurniak (2003) was able to model moisture movement within the covers and found that saturated hydraulic conductivity, K_s, was the most critical parameter in model accuracy.

Meiers et al. (2003) studied the evolution of K_s since cover placement and observed its change from 2.5×10^{-6} cm s^{-1} to 2.1×10^{-4} cm s^{-1} to 4.3×10^{-4} cm s^{-1} from 2000 to 2001 to 2002 in the secondary glacial layer. These results showed that within four years of cover placement, the hydraulic conductivity of the covers had increased by two orders of magnitude. Meiers et al. attributed the large increase in K_s to an increase in soil macroporosity caused by annual freeze-thaw cycles.

Soil macroporosity, and its impact on water movement, was investigated by Kelln et al. (2007). The study found that preferential flow (i.e. flow through macropores) was responsible for infiltration during spring melt or in times when antecedent soil moisture conditions were high. Interflow was found to initiate during spring melt when water from the preferential flow paths migrated into the soil matrix during saturated conditions to form a perched water table at the soil cover-shale interface.

Taken together, the results from the previous geochemical and hydrological research on the SW30 suggest that the reclamation soil covers may be at risk for

salinization. Salts remaining in the pore fluid of the unoxidized shale and salts produced from sulphide mineral oxidation are diffusing upwards into the overlying soil covers (Wall, 2005; Kessler, 2007). Flow through the soil matrix has the ability to dissolve the upwards diffusing salts and flush them vertically and horizontally out of the soil profile. Meiers et al. (2003) and Kelln et al. (2007) have, however, observed that macroporosity is impacting water movement within the soil covers. Kelln (2007) found that flow through soil macropores was a primary means of water and solute transport when the ground was frozen or moisture conditions were high. When this occurs, infiltrating water bypasses the soil matrix and is no longer capable of flushing the upwards diffusing salts, thus causing concern over the salinization of the soil covers. Therefore, the great potential that macropore flow will impact salt flushing necessitates further research into the mechanisms of water and solute transport within the soil.

1.2 Research Hypotheses

Preferential flow, commonly referred to as macropore flow but also including fingering and funneling, is an important mechanism of water and solute transport within natural environments. Cited as the rule rather than the exception (Flury et al., 1994), preferential flow is the result of flow through macropores or due to wetting front instability and the creation of fingered or funneled flow. Preferential flow bypasses the soil matrix and flow at speeds greater than can be predicted with traditional laws of water movement (Kung, 1990a). Preferential flow paths often account for a very small portion of the soil volume; however, these paths have the ability to conduct a large majority of water and solutes (Kung, 1990a).

Salt redistribution within natural landscapes is generally accepted as being related to water movement within the soil. In situations where water moves through the soil matrix, soluble salts within the soil are often leached and transported in the direction of water flow. In situations such as the SW30, the leaching and subsequent flushing of salts by flow through the soil matrix may counteract the upwards diffusion observed by Kessler (2007). However, if water becomes funneled through preferential flow paths and avoids the soil matrix, as was observed by Kelln (2007)

at the SW30, there may not be enough contact area or time with the salts to effectively flush them from the soil profile. Furthermore, preferential flow paths may also cause water to be confined to select macropores while diffusion of salts will occur in all pores, thus resulting in the selective leaching of salts.

Within the reconstructed landscape of the SW30, it is assumed that water and solute transport processes will mimic those in the natural environment. It is therefore hypothesized that preferential flow, due to flow through macropores or the development of wetting front instability, will be an important mechanism of water and solute transport within the reclamation soil covers. Moreover, because of its nature, preferential flow will bypass the soil matrix and restrict the vertical and horizontal flushing of salts within the reconstructed landscape.

1.3 Research Objectives

Based on the potential for preferential flow to play a large role in salt redistribution within the reconstructed landscape, the objectives of this study were to:

1) Examine localized water flow through the soil matrix in comparison to flow through macropores. An examination of water transport will aid in better understanding the role of preferential flow on solute leaching within the soil column;

2) Assess the effect of vertical and lateral flow processes on solute transport within reconstructed landscapes. Determining the extent to which salts may be flushed from the soil profile will aid in evaluation of current reclamation practices.

1.4 Outline of Thesis

This thesis is organized into 5 chapters. Chapters 1 and 2 provide an introduction and review of relevant scientific literature, respectively. Chapter 3 presents the results from laboratory column experiments and in situ dye tracer experiments that were used to meet Objective 1. Chapter 4 subsequently presents the data to meet Objective 2, which was obtained from a field study using conservative tracers to track solute movement. Chapter 5 provides a summary of the results, implications for soil cover design, and recommendations for future research.

2. LITERATURE REVIEW

2. 1 Description of Preferential Flow Processes

Preferential flow results when a more or less spatially uniform precipitation flux becomes very non-uniform as flow converges towards conducting macropores or other areas of rapid water flow (Beven and Germann, 1982). The occurrence of preferential flow has long been accepted as the rule rather than the exception (Flury et al., 1994). Preferential flow paths often account for a very small portion of the soil volume; however these paths can conduct a large majority of water and solutes (Kung, 1990a). Consequently, preferential flow and their pathways have important implications for water and solute movement. Therefore, it is essential to understand preferential flow processes to accurately develop conceptual and numerical models to predict water and solute transport within the soil.

2.1.1 Macropore flow

Within the vadose zone, numerous large pores and cracks exist as a result of soil structure, root decay, biological activity, or physical processes such as freeze-thaw and shrink-swell cycles or management techniques. Termed macropores, these large soil pores tend to conduct water and solutes at rates greater than the soil matrix, thus resulting in the creation of preferential flow (Beven and Germann, 1982). Macropores are described as large continuous, non-capillary pores, cracks or channels within a soil profile (Beven and Germann, 1982). According to Luxmoore (1981), macropores are characterized by an effective diameter of >1mm, often reflecting soil structure, root decay, or the presence of biological activity. Macropores can arise from cracks or fissures (resulting from freeze/thaw, shrink/swell, and management strategies) and/or from natural pipes (resulting from the erosive action of subsurface flows). They can be generally divided into distinct categories: those formed biologically and those resulting from non-biological factors (Li and Ghodrati, 1994). Biologically formed macropores are those that result from

biological activities within the soil, such as animal or insect boring or vegetation growth. Types of macropores in this category include reptile and fauna burrows, worm holes, ant tunnels, and root channels. Non-biologically induced macropores are those resulting from physical stress which results in an alteration to the soil structure. Examples include interaggregate pores, interpedal voids, cracks or fissures resulting from shrink and swell cycles, and natural soil pipes formed by erosive action (Beven and Germann, 1982; Li and Ghodrati, 1994). While it is useful to distinguish macropores as being biologically or non-biologically created for description purposes, soils will often contain many different types of macropores and their abundance, continuity, and distribution depends on the combination of multiple soil altering factors.

The presence of macropores within the soil may, under certain conditions, dictate water and solute transport processes. Flow through soil macropores will often result in a non-laminar flow regime (Chen and Wagenet, 1992) that is characterized by the rapid transport of water and solutes through a relatively small portion of the soil medium. In undisturbed soil column experiments, Wildenschild et al. (1994) found that water and solute transport was dominated by the presence of macropores, as evidenced by non-uniform outflow distribution, early breakthrough of solutes, and extended tailing. Under saturated or near-saturated field conditions, macropores have been observed to induce the transport of considerable water and solute fluxes at the local scale (Watson and Luxmoore, 1986). These occurrences suggest that macropores are important controlling mechanisms causing preferential flow of water and contaminants within the vadose zone.

2.1.2 Fingered flow

Another cause of preferential flow is related to wetting front instability. Wetting front instability can result in the formation of fingers (Glass et al., 1989; Yao and Hendrickx, 1996) that have the potential to move water and solutes through the vadose zone at velocities approaching the saturated hydraulic conductivity (Glass et al., 1988). Fingered flow occurs when an initially distributed flow field breaks into distinct and spatially separate flow streams called fingers (Hillel and Baker, 1988).

Fingers themselves are important mechanisms of preferential flow pathways as they extend from the wetting zone and provide high regions of hydraulic conductivity and water content for which water and solutes can be rapidly transported (Glass et al., 1989). While the complete mechanism behind wetting front instability is not entirely understood, wetting front instability and the consequent creation of fingered flow are thought to result from pore scale permeability dissimilarities (Hillel and Baker, 1988).

Several authors have offered more detailed explanations for why an initially distributed wetting front would become unstable and result in fingered flow. Certain hypotheses suggest that wetting front instability occurs when there is an increase in soil hydraulic conductivity with depth (Hill and Parlange, 1972); redistribution of infiltration following a precipitation event (Philip, 1975; Tamai et al., 1987); or non-ponding rainfall (Raats, 1973; Selker et al., 1992). Raats (1973) and Philip (1975) also suggest air trapped within the soil can result in wetting front instability while other studies found water repellency to be the leading cause of instability (van Dam et al., 1990; Ritsema and Dekker, 1994). Depending on local circumstances, any or all of these conditions may apply and potentially lead to wetting front instability and the creation of fingered flow (de Rooij, 2000).

2.1.3 Funneled flow

Funneled flow in sloping layered soils has also been recognized an important mechanism of preferential flow in soil. Funneling is the increase in the rate of water transport associated with sloping interfaces separating texturally different materials such as fine sand overlying coarse sand (Kung, 1990b). This type of preferential flow is so named because the sloping layer collects and directs water to the end of the layer, where it can then be transported vertically into the soil profile in a concentrated form. In these situations, where a soil profile has abrupt textural discontinuity and inclined bedding planes, four factors will influence the existence of funneled flow (Kung, 1990b): the conductivity of the upper fine layer, the slope of the inclined layer, the retention potential of the upper fine layer, and the ponding

potential. Both the conductivity and retention potentials are determined by the soil texture while the slope and ponding potential are impacted soil structure.

2.2 Characterization of Preferential Flow

Characterization of water and solute transport within the vadose zone is difficult, due in part to the large natural heterogeneity of soil. The difficulty is, however, compounded in situations where preferential flow exists. To assess how preferential flow impacts water and solute transport, preferential flowpaths must first be identified (Kung, 1990b; Ju et al., 1997). This task is complicated, largely due to the three-dimensional aspect of preferential flow, its small volumetric fraction of the soil, and the fact that preferential flow cannot be quantified by the conventional techniques used to measure the hydraulic properties of the soil matrix (Kung et al., 2000a; Kung et al., 2000b).

Conventional sampling protocols, such as soil cores and lysimeters, have long been used to examine the mechanisms of water and solute transport within the soil. However, these methods fall short of accurately evaluating preferential flow since they assume that water and solutes move through the entire soil profile (Kung et al., 2000b). These methods rely on the random collection of samples and averaging of results, consequently resulting in substantial scattering in the data set (Ghodrati and Jury, 1992; Ju et al., 1997). As a result, the random samples collected by the coring method and lysimeter method may significantly underestimate solute breakthrough in soil with preferential flow paths (Kung et al., 2000b).

The use of adsorptive and conservative tracers, on the other hand, can provide a means for tracking all types of water movement, even preferential flow which moves rapidly through only a small portion of the soil. The tracers are soluble in water and upon infiltrating the soil, are transported similarly. Detection of the tracer often occurs through visualization (with dyes) or chemical analyses (with conservative tracers).

2.2.1 Field experiments

2.2.1.1 Adsorptive dye tracer studies

Tracers have long been used in hydrology to investigate flow pathways, velocities and travel times, hydrodynamic dispersion, and transport mechanisms. In the study of preferential flow, using dyes as tracers has proven to be extremely useful. Most dyes are organic molecules with various attached functional groups. They have the ability to sorb to solid surfaces, and thus enable the direct observation of the spatial structure of water and solute flow in an excavated section of the soil profile. Dyes are advantageous because they are detectable at low concentration, easily quantified in water, highly visible, and often non-toxic. Many of the dyes also differ in physical and chemical properties thus enabling their usage in a wide variety of water and solute transport studies (Ghodrati and Jury, 1990).

Several studies have established the use of adsorptive dyes as tracers to stain flowpaths as a method for assessing preferential flow in field soils (Ghodrati and Jury, 1990; Flury et al., 1994; Forrer et al., 2000, Weiler and Fluhler, 2004). Ghodrati and Jury (1990) and Flury et al. (1994) were among the first researchers to use dyes to not only visualize preferential flow pathways in soil but also quantify the area of dye coverage per vertical soil profile. Ghodrati and Jury (1990) used dye tracers to characterize the spatial structure of preferential flow pathways and investigate the role of soil structure and irrigation methods on preferential flow. Several field plot experiments were conducted where a narrow pulse of Acid-Red 1 dye solution was applied to the surface of the test plots. Each test plot was then subjected to 100 mm of irrigation water, either under ponding or daily sprinkler irrigation. Following irrigation, vertical and horizontal soil profiles were excavated to reveal stained flowpaths. The distribution of the dye patterns illustrated that preferential flow occurred at each test plot, under both ponding and irrigation conditions. Soil structure was found to influence the type of preferential flow that occurred, namely vertical fingering or funneling associated with wetting front instability.

Flury et al. (1994) used adsorptive dyes to assess flowpaths in different field sites comprising a wide range of soil variation. At each of the sites, test plots were irrigated with a solution of water and 4 g L^{-1} Brilliant Blue FCF dye. Following a 24 hour waiting period, a vertical soil profile was excavated to reveal stained flow pathways. A grid was placed onto the soil profile and the dye pattern was photographed. Digital analysis of the photograph yielded a one-dimensional profile of dye coverage versus soil depth. Results from the study highlighted a large variation in flow patterns among soil types, although in most soils preferential flow was prevalent. The study also found that preferential flow was responsible for transporting water deeper within the soil profile in structured soils versus non-structured soils.

Forrer et al. (2000) was among the first studies to quantify dye tracer concentrations in the field although the study is better recognized for establishing methodology for the excavation and photography of dye patterns. Field plot experiments were conducted where Brilliant Blue FCF dye was applied in solution form at various infiltration rates and amounts to soil plots. One day after tracer application, vertical soil profiles were dug perpendicular to the direction of tracer application. To avoid shadows caused by uneven or rough soil aggregates, the face of each profile was leveled. The soil profiles were photographed in daylight, under a white opaque tent placed over each soil pit to diffuse the light and avoid direct radiation. White reflection panels were used to counteract light differences throughout the depth of the pit. A 1 m^2 grid type frame was placed in front of the soil profile to correct images for geometrical distortion and provide a frame of reference. Kodak color scales were attached to the grid to enable color correction. The profiles were then photographed without the use of optical filters. The images were digitized and treated for any geometric distortion, variation in illumination, or alteration to color. Based on soil color from the images, concentration maps of Brilliant Blue dye were computed. Validation of the technique showed that the method predicted dye concentrations well, provided that the corrected images contained only the colors used in calibration.

Weiler and Fluhler (2004) further developed the processing and classification of dye patterns to identify flow types in soil. Test plots at three field sites were irrigated with one of two irrigation rates and a solution of water and 4g L^{-1} Brilliant Blue FCF dye. One day after irrigation, several parallel vertical and horizontal soil profiles were excavated to reveal the colored patterns of the dye tracer. Photographs were taken and processed by image analysis to identify stained areas from non-stained areas. Stained areas were classified as macropore flow with either low, mixed, or high interaction with the soil matrix. Non-stained areas were divided into heterogeneous and homogenous matrix flow. From the flow type delineation and a statistical relationship between macropores and stained areas, the amount of water flowing preferentially in macropores was compared to water flowing within the soil matrix. The study found that at all sites investigated, both macropore and matrix flow existed, although macropore flow was the primary mechanism of water and solute transport during extreme precipitation events.

The previous studies are only a few, among the multitude (Booltink and Bouma, 1991; Schwartz et al., 1999; Kung et al., 2000b; Weiler and Naef, 2003; Morris and Mooney, 2004) of studies using adsorptive dyes to characterize in situ preferential flow. This illustrates that it is feasible and appropriate to characterize preferential flow by the application of adsorptive dyes to field plots.

2.2.1.2 Dye tracer selection

For adsorptive dyes to be useful in transport studies, it is imperative that they meet several criteria. Flury and Wai (2003) say that good visibility is required in either the sorbed or solution phase. The dyes should have a stable spectrum such that they are resistant to color changes when sorbed to solid surfaces. Adsorptive dyes should also be easily discernable from the soil background, be relatively robust and insensitive to changes in solution chemistry, and not pose a toxicological risk to the environment (Flury and Wai, 2003).

Many adsorptive dyes have complicated chemical and physical interactions that make it important to choose a dye that is best suited to the individual experiment. Several studies have investigated the most suitable vadose zone dye tracer.

Methylene Blue has one of the highest visibilities in soil and has been used widely to characterize macropore flow in soils. Methylene Blue is, however, a cation that sorbs strongly to soil particles and its mobility is thus limited compared to that of anionic dyes (Flury and Wai, 2003). Kung (1990a) recommends the use of Rhodamine WT while other authors suggest Brilliant Blue FCF (Flury and Fluhler, 1995). Compared to Rhodamine WT, the use of Brilliant Blue is often advantageous in certain soils due to its blue color compared to the red color of Rhodamine WT.

Brilliant Blue is further advantageous because, depending on pH, the dye is neutral or dissociates to a mono- or bivalent anion (Flury and Fluhler, 1995). As such, Brilliant Blue is not strongly sorbed by negatively charged soil particles. The toxicity of Brilliant Blue is also advantageous over other dyes. It is used in food because its general toxicity is low. In the environment, Brilliant Blue does not accumulate in plants or animals and is not recognized as a carcinogenic or mutagenic (Flury and Fluhler, 1994).

2.2.2 Laboratory column experiments

2.2.2.1 Mobile-immobile model of solute transport

Understanding and predicting the transport of water and solutes within the soil is often quite difficult due to physical non-equilibrium transport conditions caused by preferential flow. Early studies of soil solute movement initially predicted transport using the convective-dispersive equation (CDE). The CDE assumes that all water moving through the soil does so with the same velocity. The solute becomes dispersed around the downward moving solute front and can be described by a dispersion co-efficient that varies linearly with the average solute velocity (Jury et al., 1991). While successfully used to model transport in repacked columns, the CDE could not adequately explain groundwater contamination under field conditions (Steenhuis et al., 1994; Ritsema, 1998). This suggested that water moving through the vadose zone did not move at the same velocity, thus implying the existence of non-equilibrium (in other words, preferential) flow.

In non-equilibrium models of mass transport, the sorptive process is slow when compared to the flow velocity. Consequently, solutes cannot reach equilibrium with respect to chemical reactions that are occurring. One of the most common models used to describe non-equilibrium transport in soil is the mobile-immobile model (MIM) of soil water (Coats and Smith, 1964). This model was first developed to characterize preferential flow of a solute governed by convection-dispersion processes and was later applied to transport in soil columns (van Genuchten and Wierenga, 1977). This model assumes that soil water can be divided into two distinct regions: the mobile soil water content, θ_m and the immobile soil water content, θ_{im}, where the total water content, θ [L^3 L^{-3}], is given by:

$$\theta = \theta_m + \theta_{im} \qquad [2.1]$$

The mobile soil water region occupies the center of saturated pores and represents the flowing water within the system. The immobile soil water is representative of stagnant water existing as the thin coatings of water on soil particles, water within dead-end pores, and water trapped in small unsaturated pores.

Using this approach, the solute concentration is divided into an average concentration, C_m, for the concentration in the mobile fraction and C_{im}, for the concentration in the immobile fraction. The model assumes that one dimensional solute transport occurs in the mobile fraction by convection-dispersion processes. It also assumes that there is solute exchange with the immobile fraction by a rate-limited diffusion process. As such, the transport of a conservative solute through unsaturated soil containing mobile and immobile water can be expressed as (Jaynes et al., 1995):

$$\theta_m \frac{\partial C_m}{\partial t} + \theta_{im} \frac{\partial C_{im}}{\partial t} = \theta_m D_m \frac{\partial^2 C_m}{\partial x^2} - q \frac{\partial C_m}{\partial x} \qquad [2.2]$$

where θ_m and θ_{im} [L^3 L^{-3}] are the mobile and immobile water contents, respectively, C_m and C_{im} [M L^{-3}] are the solute concentrations in the mobile and immobile domains, t [T] is time, D_m [L^2 T^{-1}] is the dispersion co-efficient for the mobile domain, q [L T^{-1}] is the Darcy flux density, and x [L] is the depth. Furthermore, the rate-limited mass transfer between the mobile and immobile fractions can be expressed as (Jaynes et al., 1995):

$$\theta_{im} \frac{\partial C_{im}}{\partial t} = \alpha(C_m - C_{im}) \qquad [2.3]$$

where α [T^{-1}] is the diffusive mass transfer rate co-efficient. The temporal and spatial distribution of solutes thus depends on the mobile and immobile water contents, the dispersion co-efficient, the flux, and the rate of mass exchange.

Preferential flow is accounted for in the MIM as water flowing in the mobile region. Since the total water-filled pore space is comprised of both mobile and immobile regions and yet water flows only throughout the mobile region, this water is said to flow preferentially through the soil. Within the literature, the ratios of immobile water to total soil water content were found to vary from 0, as in no preferential flow reported by Cassel (1971), to 98% (Jaynes et al., 1995). The latter shows that water and solutes could be transported through soil twice as fast as predicted with models not including immobile water (Jaynes et al., 1995). Within surface layers, individual studies have reported θ_{im}/θ values ranging from 4–7% (Ilsemann et al., 2002) for fine loamy – medium sand, 35-55% (Smeettem, 1984) for a well structured clay loam, and from 21-88% (Alletto et al., 2006) for organic mineral surface layers. Within the surface layer of the same loam soil but through the use of different techniques, several studies have reported different θ_{im}/θ values: 11-27% (Ilsemann et al., 2002), 36 – 88% (Al-Jabri et al., 2002), 28-95% (Casey et al. 1998). Within subsurface horizons, Alletto et al. (2006) found θ_{im}/θ values in the range of 35-52% for clay enriched illuvial horizons, 26-36% for heavy clay horizons, and 51-93% for limestone materials.

The application of the MIM depends on the determination of θ_m, θ_{im}, D_m, q, and α. These parameters are normally found by applying inverse methods to breakthrough data (i.e. adjusting the parameters until the calculated concentrations match the observed) (Parker and van Genuchten, 1984; van Genuchten and Wagenet, 1989; Gamerdinger et al., 1990). Consequently, solute breakthrough curves are required before the MIM can be used to examine preferential flow.

2.2.2.2 Time domain reflectometry

Time domain reflectometry (TDR) is a proven method of accurately, inexpensively, and nondestructively monitoring solute transport within soil (Kachanoski et al., 1992). For the past two decades, TDR has been established as a method of measuring soil water content, θ (Topp et al., 1980; Topp et al., 1982; Topp and Davis, 1985). Subsequent studies have shown that the attenuation of the TDR signal can be used as a measure of bulk soil electrical conductivity, σ (Dalton et al., 1984). As soil solute concentration is related to θ and σ, TDR has become a recognized tool for measuring ionic solute breakthrough curves (Vanclooster et al., 1993; Wraith et al., 1993; Mallants et al. 1994; Ward et al., 1994; Risler et al., 1996).

Kachanoski et al. (1992) was one of the first studies to use TDR to monitor soil solute transport. TDR probes were installed vertically into repacked soil columns and field plots to monitor the transport of a conservative solute tracer (Cl^-) under saturated steady state conditions. Solute mass flux of the applied solute out of the laboratory column was in agreement with TDR measurements. Solute mass flux measurements in the field using ceramic solution samplers were also comparable to those obtained using the TDR method. As such, the authors concluded that TDR was a dependable means of determining solute breakthrough curves (BTCs) under saturated steady state conditions. The method was, however, limited to soils in which the addition of a solute tracer would result in a measurable change in the reflected signal of the TDR.

Wraith et al. (1993) further investigated the reliability of using TDR to monitor solute breakthrough, although under unsaturated steady flow conditions. Laboratory transport experiments were conducted using an undisturbed soil column into which TDR probes were installed horizontally. A pulse of a conservative solute tracer (Br^-) was added to the top of the soil column and transport was monitored through effluent collection and the TDR method. Results were very similar between the column effluent and the TDR method, proving that TDR could be used in unsaturated conditions and further supporting the use of TDR in chemical transport studies.

The research carried out by Kachanoski et al. (1992) and Wraith et al. (1993) pioneered the use of TDR in solute transport studies. Their work indicated that TDR

could be used under a wide range of experimental conditions, such as under saturated or unsaturated steady state conditions, with both vertically and horizontally installed probes. Other studies have supported these findings, proving the effectiveness of using TDR in laboratory column experiments (Ward et al., 1994; Mallants et al., 1996; Comegna et al., 1999) and in the field (Kachanoski et al., 1994; Ward et al., 1995). Studies by Risler et al. (1996) and Nissen et al. (1998) have shown that TDR can also be used under transient flow conditions. Lee et al. (2001) even successfully used to TDR to directly estimate preferential flow parameters.

TDR has been proven to be a highly reliable means of monitoring solute transport within soil. From the TDR method, ionic solute breakthrough curve data can be used to estimate the parameters of the MIM and aid in the characterization of preferential flow. The success of TDR in monitoring solute transport is, however, dependent on the choice of solute tracer to be monitored.

2.2.2.3 Conservative tracer selection

Much like the adsorptive dyes used to stain flowpaths; conservative tracers are also capable of providing evidence on the movement of soil water and solutes. In transport experiments, the breakthrough pattern of a non-adsorbing chemical tracer through an undisturbed soil column can provide information on soil hydraulic and transport properties. These properties can then be used to characterize water and solute transport at field-scale.

Flury and Wai (2003) suggest that an ideal tracer of water must be conservative in nature, meaning that it moves similar to water, without sorption to soil and without degradation during the time of interest. The tracer should have a low background concentration or at least be clearly discernable from background values. The tracer must be fairly robust and insensitive to changes in solution chemistry. Adequate detection of the tracer must also be possible, either through chemical analyses or through visualization. Finally, the tracer must not generate a toxicological risk to the study environment. That said, an ideal water tracer is non-existent (Davis et al., 1980; Flury and Wai, 2003). The best tracer would be the water molecule itself, either deuterium (2H) or oxygen-18 (18O). However, these isotopes are often

limited in their use because of the expense involved. The next most common so-called ideal tracers are the ions of chloride (Cl^-) and bromide (Br^-). These tracers have relatively low toxicological impact, are easily detected by chemical analyses, relatively insensitive to minor changes in solution chemistry, and background concentrations can easily be discerned. Both tracers rarely sorb to soil particles and often mimic water molecule movement. When compared to deuterium or tritium, chloride and bromide have been observed as having faster breakthroughs, largely due to a phenomenon called anion exclusion. Anion exclusion results from the repulsion of anions from the negatively charged soil particles, thus resulting in non-adsorbing tracer molecules. However, in positively charged soils it is important to note that these tracers may not behave conservatively since electrostatic adsorption of anions will occur, possibly leading to considerable retardation (Flury and Wai, 2003).

3. SUSCEPTABILITY OF SOIL COVERS TO PREFERENTIAL FLOW

3.1 Introduction

Over the last several decades, studies have observed the rapid transport of strongly adsorbing chemicals deep within the soil profile (Jury et al., 1986; Everts et al., 1989; Kladivko et al., 1991; Kung et al., 2000b). This expeditious transport of water and solutes is termed preferential flow and has important implications for the fate and transport of contaminants within the environment. One of the most important characteristics of preferential flow is its ability to transport water and solutes to depths far exceeding those predicted by the uniform flow of Richard's equation. Resulting in the non-uniform wetting of the soil profile, preferential flow occurs because water tends to be transported faster within soil macropores or other regions of the soil due to fingering or funneling (Simunek et al., 2003). In further contrast to uniform flow, preferential flow is also a non-equilibrium flow regime. With preferential flow, infiltrating water does not equilibrate with the slowly moving resident water of the soil matrix. This results in different hydrological patterns that combine flow processes occurring in the soil matrix with those occurring in adjacent macropores or other areas of higher conductivity.

The effects of the combined flow on solute transport can be seen through solute breakthrough curves (BTCs). Studies using structured soil columns have shown that preferential flow results in asymmetrical BTCs, characterized by early breakthrough and evident tailing (van Genuchten and Wierenga, 1977; Smeetem, 1984; Khan and Jury, 1990). The early arrival of solutes has been related to the accelerated transport of water and solutes through preferential flowpaths. The long tailing of solutes is attributed to the diffusion of solutes from the less active flow region.

A common approach to describing the asymmetrical BTCs typical of preferential flow is to use the mobile-immobile model (MIM) of soil water (van Genuchten and Wierenga, 1977). The MIM separates pore water into 2 regions: the mobile soil water region, θ_m, which occupies the center of saturated pores, and the immobile soil water region, θ_{im}, which consists of dead-end pores. Dispersion of solutes occurs

within the mobile region and can be described using convective and dispersive processes. Solute transfer between the two regions occurs by diffusive transport only and is described by a first-order mass transfer rate co-efficient, α. The MIM transport parameters θ_m, θ_{im}, and α, are often determined by inverse methods, using solute transport data from observed BTCs of a conservative tracer.

Another common approach in the investigation of preferential flow is the use of adsorptive dye tracers to track water and solute movement (Ghodrati and Jury, 1990; Flury et al., 1994). Adsorbing dyes stain flowpaths, enabling the visualization of flow patterns to determine if water is flowing preferentially or within the soil matrix. From the stained flow patterns, qualitative inferences can be made regarding the type of flow dominating transport processes and quantitative evaluations can determine the amount of dye coverage or concentrations of dye within the soil profile.

The objective of this study was to combine both the MIM and adsorptive dye methods of analysis to evaluate preferential flow processes and their impact on water and solute transport.

3.2 Materials and Methods

3.2.1 Study site

The study site is the South West 30 Overburden Dump (SW30), located at Syncrude Canada's Mildred Lake mine, north of Fort McMurray, Alberta, Canada (57°2' N, 111° 33' W). The SW30 is an experimental watershed comprising of three 1 ha reclamation soil covers capping saline-sodic shale resulting from oil sands mining. Situated along a 5H:1V north facing slope, the covers are approximately 50 m wide by 200 m long.

The reclamation soil covers were constructed by placing selected depths of a peat-glacial soil mix (here after called peat mix) over that of reworked glacial mineral soil (here after termed glacial soil) to form nominal soil thicknesses of 0.35, 0.50, and 1 m. The 0.35-m cover consists of 0.15 m of peat mix overlying 0.20 m of glacial soil. The 0.50-m cover was constructed by placing 0.20 m of peat mix over 0.30 m of glacial soil. The 1-m cover, consisting of 0.20 m of peat mix and 0.80 m of glacial

soil, acts as the control cover as it meets the 1 m criteria for soil depth required by the provincial government for reclamation standards.

Although reconstructed, the soil at the SW30 is classified as an Orthic Gray Luvisol. The A horizon comprises the peat mix. The B horizon is the glacial soil while the C horizon is the saline-sodic shale. Selected physical and chemical properties of the soil are presented in Table 3.1 and available in more detail in Kessler (2007).

Kelln et al. (2007) reported porosity of the glacial layer to be 0.40 – 0.43 (n=4). Field saturated hydraulic conductivity, K_s, for the shale, glacial soil, and peat mix has increased since cover placement (Meiers et al., 2006; Kelln et al., 2007). From 2000 to 2002, the K_s for the shale increased one order of magnitude to $1x10^{-8}$ m s^{-1}. The glacial soil was found to have the greatest change in K_s, from $1x10^{-8}$ m s^{-1} in 2000 to $6x10^{-6}$ m s^{-1} in 2003. In the same time span, the peat-glacial soil mix K_s increased by only one-half an order of magnitude to approximately $4x10^{-5}$ m s^{-1}. In 2004 and 2005, the values of K_s showed little change.

The climate is classified as subhumid continental (Koppen Classification, McKnight and Hess, 2005 as cited in Kelln et al., 2007). The mean annual air temperature is 1.5° C, with monthly mean temperatures ranging from -20.7° C in January to 18° C in June. The mean annual precipitation is 442 mm (1945-1995), of which approximately 20% occurs as snow during winter months. Surface runoff is largely attributed to the spring snow melt and does not typically occur in the summer due to the large moisture deficit (70 to 80 mm, Elshorbagy et al., 2005).

3.2.2 Laboratory column experiments

Laboratory column experiments were conducted under unsaturated steady-state conditions for undisturbed soil cores. Sixteen polyvinyl chloride columns (0.15 m inside diameter and 0.30 m length) were pushed vertically into the 0.35-m soil cover on the SW30. The columns were vibrated while being pushed into the soil surface to minimize the incidence of soil compaction. Of the 16 columns, 3 (labeled 6, 16, and 25) were randomly chosen to represent field conditions.

Table 3.1 Physical and chemical properties for the three soil materials comprising the reclamation soil covers at the SW30 research site, Mildred Lake mine site, as determined in 2002. Mean values are reported. (Kessler, 2007)

	Peat mix	Glacial soil	Saline-sodic shale
Physical Properties			
Sand, %	24.9	28.1	25.5
Silt, %	33.6	29.1	37.7
Clay, %	41.5	42.8	36.8
BD, Mg m^{-3}[†]	0.89	1.56	1.41
Chemical Properties			
pH (H_20)	6.2	7.2	7.2
EC, dS m^{-1}[‡]	1.1	2.1	10.0
SAR, $mmol_c\ L^{-1}$[¶]	1.5	3.7	16.9
CEC, $cmol_c\ kg^{-1}$[§]	55.6	18.0	20.4

[†]BD, bulk density.

[‡]EC, electrical conductivity in saturation extracts.

[¶]SAR, sodium adsorption ratio

[§]CEC, cation exchange capacity.

Previous studies have indicated the potential for artificial flowpaths to exist along the soil-wall interface in experiments involving soil columns (Till and McCade, 1976; Saffigna et al., 1977). These artificial flowpaths are often caused by the shrinkage of soil away from the column walls during wetting-drying cycles. The resulting open channels can transport water preferentially down the sides of the column wall. Resulting in what is termed sidewall flow, this anomalous flow is not representative of field conditions and may impact solute transport studies.

While sidewall flow cannot be completely eliminated, efforts were made to limit its existence in the cores from the SW30 by ensuring that the soils were brought up to field capacity prior to the start of the solute transport experiments. Moreover, the columns were placed atop a porous glass plate (air entry value of 0.30 m, providing -0.03 m suction) which maintained unsaturated flow conditions and minimized the channeling of water to selected surface pores.

A thin layer of fine sand was used between the soil core and glass plate to improve hydraulic contact. The cores were instrumented at soil depths of 0.05, 0.10, and 0.15 m with horizontally installed, parallel TDR probes, which were used to measure water content, θ, and EC in the peat mix soil. TDR measurements, collected every 2 minutes over the experiment duration, were stored in a datalogger (CR10X model, made by Campbell Scientific, AB). Figure 3.1 shows a schematic of the experimental design.

Rainfall was simulated at the top of the soil cores at rates of approximately 0.002 and 0.01 mhr^{-1} using a modified room humidifier, secondary reservoir, and transmission tubes. The rainfall rates were chosen to best match the SW30 climate and K_s of the peat mix layer. The humidifier served to supply water to a smaller (0.5 L) secondary reservoir that was fitted with spaghetti-like transmission tubes (0.38 mm inside diameter and 400 mm long). The transmission tubes hung down from the reservoir, ending approximately 0.10 m above the surface of the core. Once primed, the tubes trickled water onto the soil surface, simulating rainfall.

To ensure uniform wetting and leaching of the soil, the cores were flushed with 3x pore volume water content (determined from known soil volume and θ) prior to the tracer experiments. The flushing solution consisted of 0.68 g L^{-1} calcium sulfate,

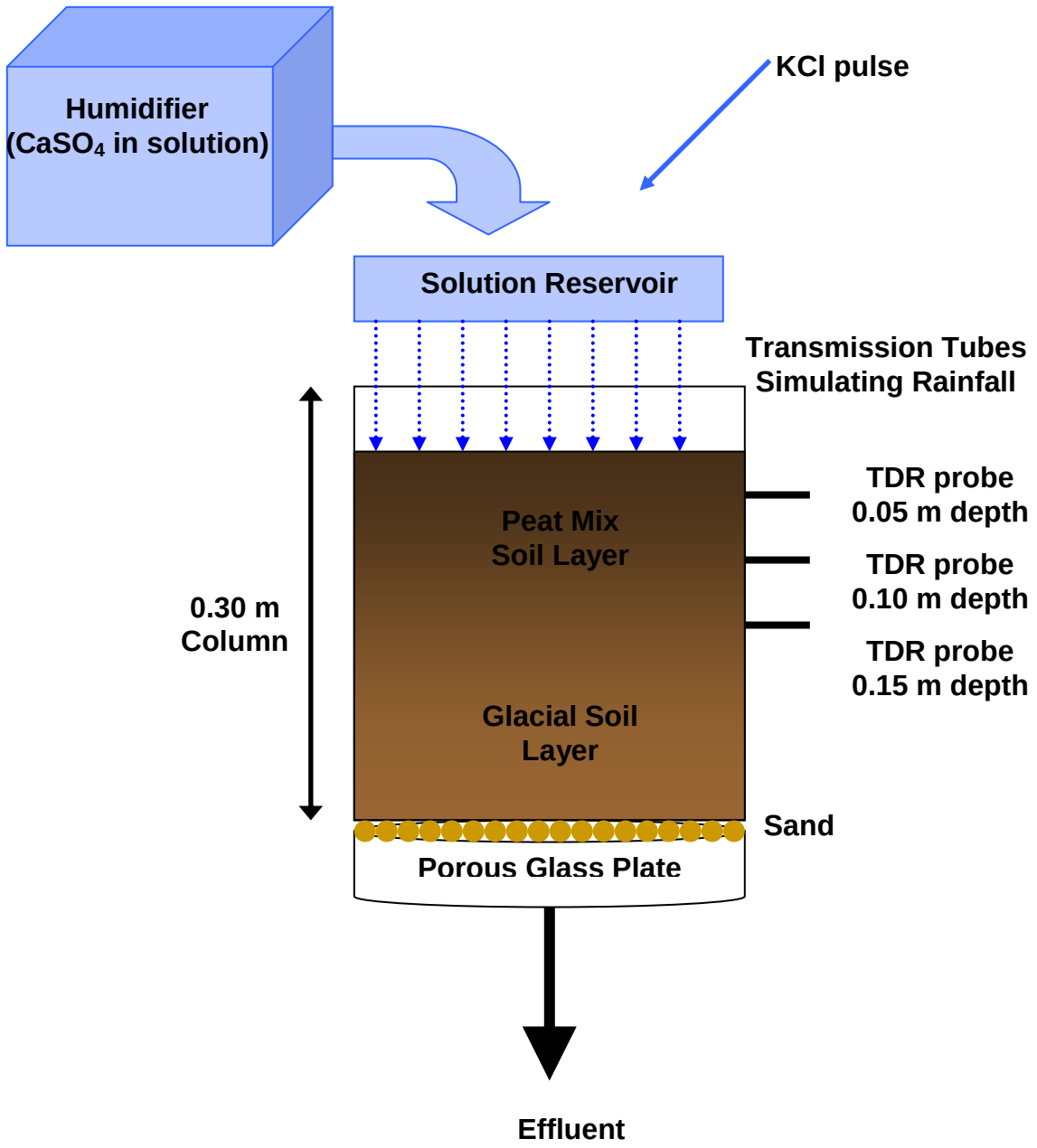

Figure 3.1 Schematic diagram of solute transport experiment, in which the transport of chloride through an undisturbed soil core from the South West 30 Overburden Dump was monitored. A humidifier supplied flushing water (a solution of calcium sulfate) to a secondary reservoir. Water flowed from the reservoir to the core below through transmission tubes. Horizontally installed time domain reflectometry (TDR) probes were used to measure soil water content and electrical conductivity. Unsaturated conditions were obtained by placing the core atop a porous glass plate and using sand to increase hydraulic contact. When steady state conditions were achieved, the reservoir was drained and a pulse of potassium chloride (KCl) was applied. Once the pulse was completed, the supply to the reservoir was returned.

which was used to maintain soil aggregate stability, in solution with distilled water. Measurements of θ were conducted during the initial infiltration to ensure steady state ($\delta\theta/\delta t=0$) conditions were reached.

After steady state was achieved, the water supply to the secondary reservoir was briefly interrupted and the reservoir was drained to near empty (so as to not interrupt steady state). When only a few milliliters of solution remained in the reservoir, a pulse of solute corresponding to a specific mass, M = 48 g m^{-2} of chloride (Cl^-, in the form of KCl solution), was applied. Cl^- was chosen as the tracer as it rarely sorbs to soil particles, moves with water molecules, is easily detected, and inexpensive (Flury and Wai, 2003). Once the pulse was completed, the water supply to the secondary reservoir was returned and the flushing solution once again simulated rainfall. Rainfall was ceased and the experiments were concluded when the concentrations of total dissolved solids (TDS) in the soil returned to background or near background (due to tailing) levels.

To determine solute transport parameters under field conditions for the peat mix layer of the soil covers, experiments were performed using the entirety of the soil core for each of the three columns. One of the concerns with this method was the potential for differences in soil hydraulic conductivity to impact solute transport. In situations where a soil layer is underlain by soil of lower hydraulic conductivity, the vertical percolation of water is restricted and ponding at the layer interface may occur. To ensure that this did not occur in the SW30 columns, the TDR was used to ensure that there was no change in θ with time.

However, to determine solute transport parameters for the glacial layer of the soil covers, the columns were hand-excavated to separate the peat mix from the glacial soil. This was done to not only determine separate transport parameters for each layer but also to clarify the depth at which the glacial layer began.

Movement of the Cl^- pulse through the core was assessed using TDR measurements of EC (dS m^{-1}). The measurements of EC were transformed into concentrations of total dissolved solids (TDS), C_t, based on the mass of solute applied per area of soil, *MPA*, as follows:

$$MPA = \int_0^{\infty} (C_t - C_o) \cdot q \cdot dt \qquad [3.1]$$

given

$$C_o = a + b \cdot EC_o \quad [3.2]$$

$$C_t = a + b \cdot EC_t \quad [3.3]$$

where C_o is the original concentration of TDS, q is flux, t is time, a is an empirical value, b is the calibration constant for the TDR, and EC_o and EC_t are the measured original and final conductivities, respectively. Substituting Equations 3.2 and 3.3 in Equation 3.1 yields:

$$MPA = b \cdot q \int_0^\infty (EC_t - EC_o) dt \,. \quad [3.4]$$

Solving for b:

$$b = \frac{MPA}{q \int_0^\infty (EC_t - EC_o) dt} \,. \quad [3.5]$$

It was now possible to solve for a in Equation 3.2, and then knowing both a and b, solve for C_t using Equation 3.3. Plotting the results from Equation 3.3 against time yielded concentration BTCs.

Solute transport properties, β (which is θ_m/θ), D_m, and α, were estimated from the concentration BTCs using an inverse curve-fitting method (CXTFIT Version 2.1, Toride et al., 1999). The value of q from the experiments was used for the curve fitting of the BTC, so that CXTFIT had to solve for only three parameters. Values of θ_{im} were obtained from β and TDR measured θ.

3.2.3 Dye tracer experiments

Dye tracer experiments were conducted in July of 2004 on the 0.35-m and 1-m reclamation soil covers. The dye used to stain flowpaths was the food-grade Brilliant Blue FCF, chosen for its low toxicity and good visibility (Flury et al., 1994). On each cover, three 1 x1 m soil plots were identified, with one each at the top, middle, and toe of the SW30 hillslope. Surface vegetation was removed manually from each plot.

Each plot was manually irrigated with a solution containing 4 kg m^{-3} Brilliant Blue dye (Flury et al., 1994). Care and attention was used during the irrigation to

ensure that a uniform flux was applied to the entire plot. A total of 0.04 m of irrigation solution was used each time. One day after the dye solution was added to the soil, a soil pit was dug to a depth of approximately 1 m. To reveal the stained flowpaths, a vertical soil profile was prepared 0.25 m from the plot's border and perpendicular to the direction of the tracer application. To avoid shadows caused by an even soil face, a trowel was used to clean and flatten the face of each profile. A 1 m^2 frame with number gradations was then mounted on the soil profile to correct for any possible geometric distortion and uneven illumination. The frame was also used to provide location reference within the soil profile.

Photography of the stained flowpaths was performed according to the procedure of Forrer et al. (2002). Soil profiles were photographed in mid-afternoon with the use of a tarping system that ensured lighting conditions were similar among profiles. A digital camera was used to take the photographs and no optical filters were necessary.

Soil photographs were analyzed using a remote sensing software program that was trained to distinguish dyed pixels from non-dyed pixels. The software program used was PCI Geomatica Version 9.1.0 Copyright © 2003 PCI Geomatics (Ontario, Canada). Due to the heterogeneity of the layered soils, soil photographs were divided horizontally into ten 0.10 m subsections prior to analysis. This was performed to reduce the spectral complexity of the images, which served to increase the accuracy of the analysis.

The first step in image analysis was to provide a clear distinction between the dyed and non-dyed pixels. To do this, a model known as the Normalized Difference Vegetation Index (NDVI) was used to highlight spectral differences between the dyed pixels and the highly variable background soil colors. The NDVI is based on the differential reflectance response of solar radiation in the visible and near infrared wavelengths. Green vegetation commonly has larger reflectances in the near infrared than in the visible range while the differential is almost zero for soil. Thus, the spectral differences identified using the NDVI were useful in differentiating vegetation and soil from the dyed pixels.

By combining the results of the NDVI with the red and blue spectral channels, a manual (supervised) classification was then used to differentiate the spectral identity of the dyed pixels from the non-dyed pixels. Once the supervised classification was complete, an unsupervised (software-based) classification continued to categorize pixels as either dyed or non-dyed. This classification was based on the Maximum Likelihood with Null Probability division. Following classification, the software program summed up the area consisting of dyed pixels and calculated a percentage accuracy of the results.

3.3 Results and Discussion

3.3.1 Laboratory column experiments

Laboratory column experiments were performed for three cores of each of the peat mix and glacial soil layers and repeated for each applied flux. The experiment for Core 16 under the 0.010 m hr^{-1} flux was not completed successfully as the transmission tubes simulating rainfall lost tension, resulting in the drying of the core. To preserve the 1-2 weeks preparation time to rewet and flush the core, a pre-wet core (labeled Core 3) was substituted to represented field conditions under the 0.010 m hr^{-1} flux. Difficulties were also experienced while using the glacial soil for the experiments and again when modeling the subsequent transport parameters. The manual separation of the peat mix and glacial soil layers was destructive as scraping at the layer interface resulted in blocking soil pores at the surface of the glacial soil. This blockage of pore space resulted in an impeded solute entrance into the soil, such that ponding conditions occurred and hindered the natural transport of Cl^- in the soil. Moreover, the CXTFIT method failed to accurately fit the experimental data from these BTCs (likely due to the large number of iterations required). Other inverse models were used to fit the data from the glacial soil; however, the same errors were encountered. In hindsight, the soil cores should have remained undisturbed, with solute transport parameters being determined as a function of depth and then related to soil material following experiment completion. As a result of the difficulties

encountered with the glacial soil, the solute transport parameters presented below are limited to the peat mix layer.

Figures 3.2 and 3.3 show tracer concentrations plotted as a function of time for three peat mix soil cores under q = 0.002 m hr^{-1} and 0.010 m hr^{-1}, respectively. Concentrations are plotted as determined experimentally (normalized to a mass per area of applied chloride of 48 g m^{-2}) and as fit by inverse modeling using CXTFIT. All curves shown are representative of concentrations found at the 0.10m soil depth.

In Figure 3.2a, the abnormality of the solute breakthrough pattern in core 6 resulted in very few data points being used in the inverse curve-fitting method. From the resulting BTC, two things were clear: the peak of solute concentrations was small and there was prolonged tailing in comparison to other BTCs in the peat mix. This shows that the majority of the tracer was transported very slowly through the soil, suggesting that solutes had been retained in immobile soil regions.

Figures 3.2b and 3.2c are representative of solute breakthrough patterns in which there was a rapid and early rise in TDS concentrations. The early arrival of the solutes in cores 16 and 25 was confirmed quantitatively by comparing the peak solute velocity, v_{pk}, based on the arrival time, t_{pk}:

$$v_{pk} = \frac{L}{t_{pk}} \qquad [3.6]$$

to piston flow velocities, v:

$$v = \frac{q}{\theta}. \qquad [3.7]$$

According to Butters et al. (1989), the v_{pk} is important in environmental studies as threshold groundwater contamination may already be surpassed at the time of peak contaminant arrival. Therefore, when $v_{pk}>v$ this is representative of preferential flow conditions. Consequently, when v_{pk} and v were determined for the BTCs (Tables 3.2 and 3.3), it quantitatively verified that preferential flow occurred in cores 16 and 25 as $v_{pk}>v$.

In Figures 3.3a and b, there was no early arrival of Cl^-, as verified by $v_{pk}<v$. This indicated that no preferential flow occurred. There was, however, evident tailing meaning that Cl^- was adsorbed by the soil and released later. This suggested that

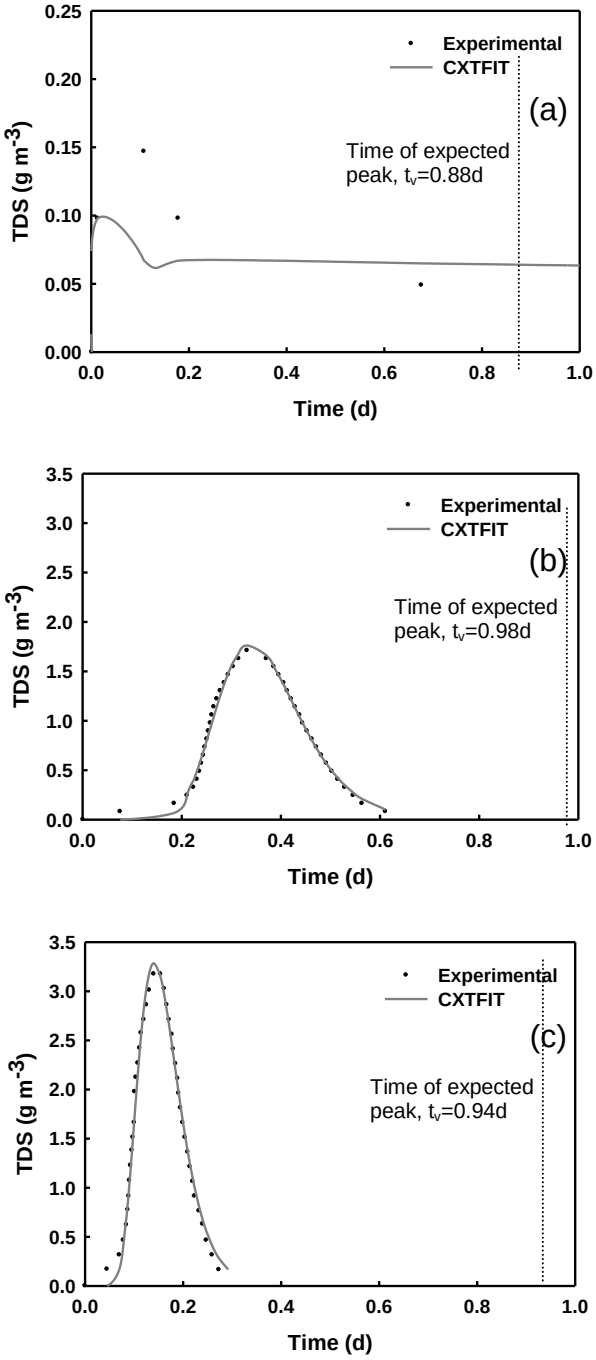

Figure 3.2 Concentrations of total dissolved solids (TDS) versus time elapsed since tracer application in peat mix soil cores under a flux (q) of 0.002 m hr^{-1}. Cores labeled 6, 16, and 25 are identified as a, b, and c, respectively. Concentrations are plotted as determined experimentally (normalized to a mass per area of applied chloride of 48 g m^{-2}) and as fit by inverse modeling using CXTFIT. The dashed line represents the expected time, t_v, for the solute peak to arrive based on piston flow velocity, v.

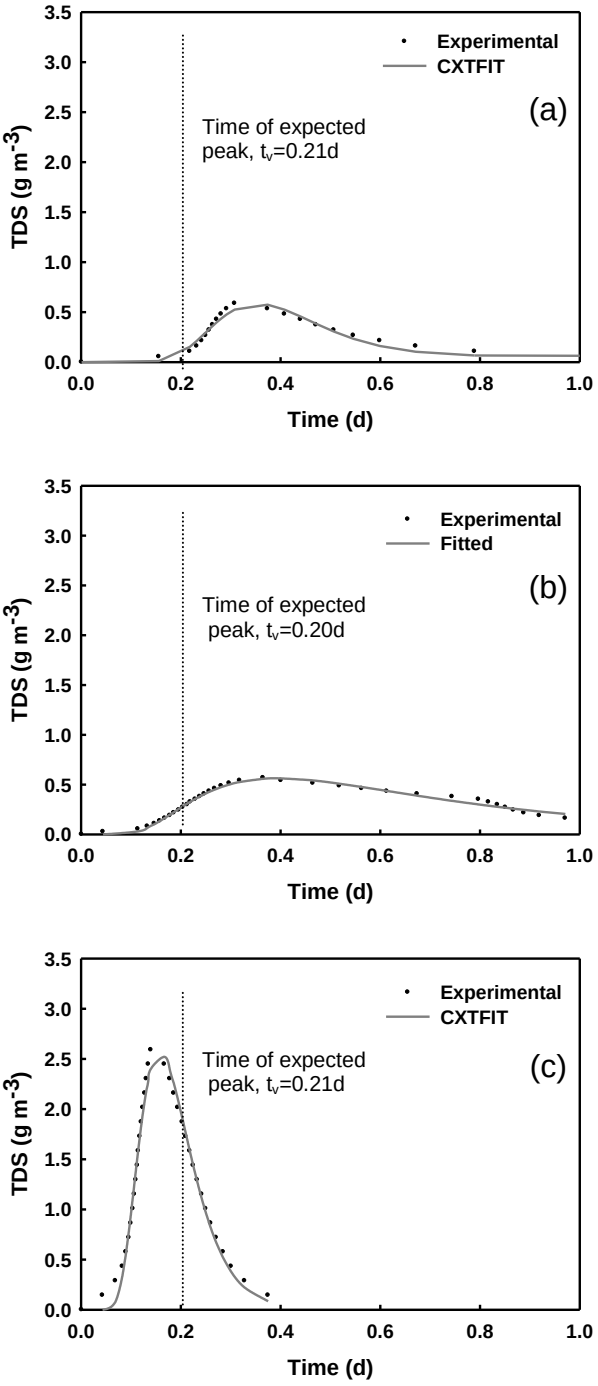

Figure 3.3 Concentrations of total dissolved solids (TDS) versus time elapsed since tracer application in peat mix soil cores under a flux (q) of 0.010 m hr^{-1}. Cores labeled 6, 3, and 25 are identified as a, b, and c, respectively. Concentrations are plotted as determined experimentally (normalized to a mass per area of applied chloride of 48 g m^{-2}) and as fit by inverse modeling using CXTFIT. The dashed line represents the expected time, t_v, for the solute peak to arrive based on piston flow velocity, v.

residual solutes had become trapped in immobile regions. Upon comparing solute breakthrough patterns in core 6 under the 0.002 m hr^{-1} and 0.010 m hr^{-1} fluxes (Figures 3.2a and 3.3a, respectively), it was clear that tailing was common in this core. With the faster flux, there was a greater rise in measured solute concentrations and a larger percentage of the applied mass was recovered earlier. This, combined with the evident tailing, suggests that this core had an extensive immobile region and a high rate of mass transfer. Hence, when the applied flux was slow, there was a greater potential for the diffusive transfer of solutes into immobile regions. This would account for the smaller peak concentrations and much of the tailing.

Conversely, in Figure 3.3c, there was a rapid decrease in solute concentrations following the early arrival of the solute. The early arrival of solutes in core 25 was confirmed based on $v_{pk}>v$. Upon comparing solute breakthrough patterns in core 25 under the 0.002 m hr^{-1} and 0.010 m hr^{-1} fluxes (Figures 3.2c and 3.3c, respectively), it appeared that both solute breakthrough patterns were typical of the fast arrival of preferential flow.

All the BTCs presented in Figures 3.2 and 3.3 were representative of asymmetrical solute breakthrough patterns. For some, the asymmetry was related to a rapid and earlier than predicted rise in solute concentrations while in others, the asymmetry was caused by the slow elucidation of the solute. Qualitatively, these observations of asymmetry related to early solute breakthrough were suggestive of preferential flow conditions (van Genuchten and Wierenga, 1977; Smeetem, 1984; Khan and Jury, 1990; Camobreco et al., 1996; Kim et al., 2005). The early arrival of solutes showed the accelerated transport of water and solutes through preferential flowpaths. This was confirmed quantitatively for cores 16 and 25 under the 0.002 m hr^{-1} flux and core 25 under the 0.010 m hr^{-1} flux as $v_{pk}>v$. The long tailing of solutes, meanwhile, indicated the diffusion of solutes from the less active flow region suggesting nonequilibrium adsorption. Moreover, the large variability between column BTCs indicated that there was a significant spatial variability in the peat mix soil.

Table 3.2 Measured water contents (θ) and estimated solute transport parameters, including the fraction of mobile water (β), dispersivity of the mobile region (D_m), mass transfer rate co-efficient (α), mean travel velocity (v), and peak travel velocity (v_{pk}) for column experiments where q = 0.002 m hr^{-1}.

Core	θ	β	D_m	α	v	v_{pk}
	%	%	m^2 hr^{-1}	h^{-1}	m hr^{-1}	m hr^{-1}
A (Core 6)	42	0.22	0.0014	2.0	0.0048	nd†
B (Core 16)	47	9.7	0.0055	0.24	0.0043	0.013
C (Core 25)	45	0.04	0.010	0.30	0.0044	0.030
Average	45	3.3	0.0056	0.85	0.0045	0.022‡

† nd means not determinable as peak was insignificant

‡ Average based on B and C only

Table 3.3 Measured water contents (θ) and estimated solute transport parameters, including the fraction of mobile water (β), dispersivity of the mobile region (D_m), mass transfer rate co-efficient (α), mean travel velocity (v), and peak travel velocity (v_{pk}) for column experiments where q = 0.010 m hr^{-1}.

Core	θ	β	D_m	α	v	v_{pk}
	%	%	m^2 hr^{-1}	h^{-1}	m hr^{-1}	m hr^{-1}
A (Core 6)	51	11	0.0090	1.2	0.020	0.011
B (Core 3)	47	20	0.041	0.15	0.021	0.014
C (Core 25)	50	4.9	0.066	1.7	0.020	0.030
Average	49	12	0.039	1.0	0.020	0.018

Measured water contents and estimated values for β, D_m, and α are listed in Tables 3.2 and 3.3 for the 2 and 10mm hr^{-1}fluxes, respectively. Across the experiments, the computed solute transport parameters were quite variable. Values for β were found to vary from 0.04 – 20% with an average of 7.6. Resultant immobile water fractions (θ_{im}/θ), calculated from β and θ, were thus found to range from 80 – 99%, with a mean of 92%. Dispersion co-efficients were estimated to vary from 0.0090 – 0.066 m^2 hr^{-1} while values of α ranged from 0.15 - 2.0 h^{-1}.

The estimated values of θ_{im}/θ, D_m, and α are comparable to those reported in previous studies. For a repacked sandy loam, Nkedi-Kizza et al. (1983, 1984) reported θ_{im}/θ values ranging from 0.04 – 0.56 and α values between 0.01 and 2.15 h^{-1}. For a silt loam, Jaynes et al. (1995) found θ_{im}/θ values to range from 25 – 98% and values of α were in between 0.0030 and 0.021 h^{-1}. Using similar methods and soil as Jaynes et al. (1995), Casey et al. (1997) reported values of θ_{im}/θ to be between 39 and 95% with α values ranging from 0.014 – 0.289 h^{-1}. For the surface layer of a loam soil, Casey et al. (1998) measured θ_{im}/θ values ranging from 28 - 95% and α values in between 0.015 and 0.3 h^{-1}. Using the same soil but different methods, Al-Jabri et al. (2002) reported θ_{im}/θ values that ranged from 36 – 88% and α values that ranged from 0.002 - 0.12 h^{-1}. Within organic mineral surface layers, Alletto et al., 2006 measured θ_{im}/θ values between 21 and 88% corresponding with α values ranging from 0.0006 to 0.0115 h^{-1}.

The large measured values for θ_{im}/θ demonstrated that the effective transport volume of the soil (θ_m) was much less than the total water-filled pore space (θ). Because only a small portion of the soil was therefore hydraulically active, this meant that solutes were moving at a faster rate than if all the water-filled pore space had been active. As such, these results show that there was considerable preferential flow within the peat mix soil.

The large values determined for α were not unexpected. Both Casey et al. (1997) and Al-Jabri et al. (2002) have noted that estimates for α are proportional to θ_{im}/θ. Al-Jabri et al. (2002) explains that large θ_{im}/θ values yield large contact regions between the mobile and immobile domains such that more solute transport is

expected to occur. As such, a large immobile region results in a large rate of mass transfer.

The column experiments, therefore, provided evidence that preferential flow was an important hydrological process governing solute transport in the peat mix soil. Patterns of conservative solute breakthrough showed early arrival and extended tailing, which suggest preferential flow and non-equilibrium adsorption. The early arrival of the solute peak was confirmed quantitatively such that $v_{pk}>v$ for three of the six experiments. Moreover, the large measured values for θ_{im}/θ and α also supported the existence of preferential flow. Large θ_{im}/θ values showed that only a small portion of the soil was hydraulically active, meaning that water and solutes were transported rapidly and preferentially through the soil. The high α values suggested that solutes, despite being transferred preferentially through the soil, have a high likelihood of being trapped within the soil matrix in dead-end pores or as interaggregate water. This effect was further supported by observations of extended tailing in some of the BTCs. As such, the combination of early arrival, extended tailing, and large θ_{im}/θ and α values proves that the peat mix soil is susceptible to preferential flow. The large variability in breakthrough patterns and estimated solute transport parameters does, however, suggest that there may be unique soil structure within the peat mix that serves to impact solute transport differently within the same soil.

3.3.2 Dye tracer experiments

The adsorptive dye Brilliant Blue FCF was applied to 6 test plots on the SW30 to determine the occurrence of preferential flow and its role in solute transport. Excavated vertical soil profiles revealed stained flow patterns that were generally similar from plot to plot (Figures 3.4 and 3.5). The largest staining occurred in the peat mix soil layer of each plot and was attributed to flow through the soil matrix and/or diffusive mass transfer from mobile regions to immobile regions. Preferential flowpaths were identified at each soil plot. The minor differences observed in

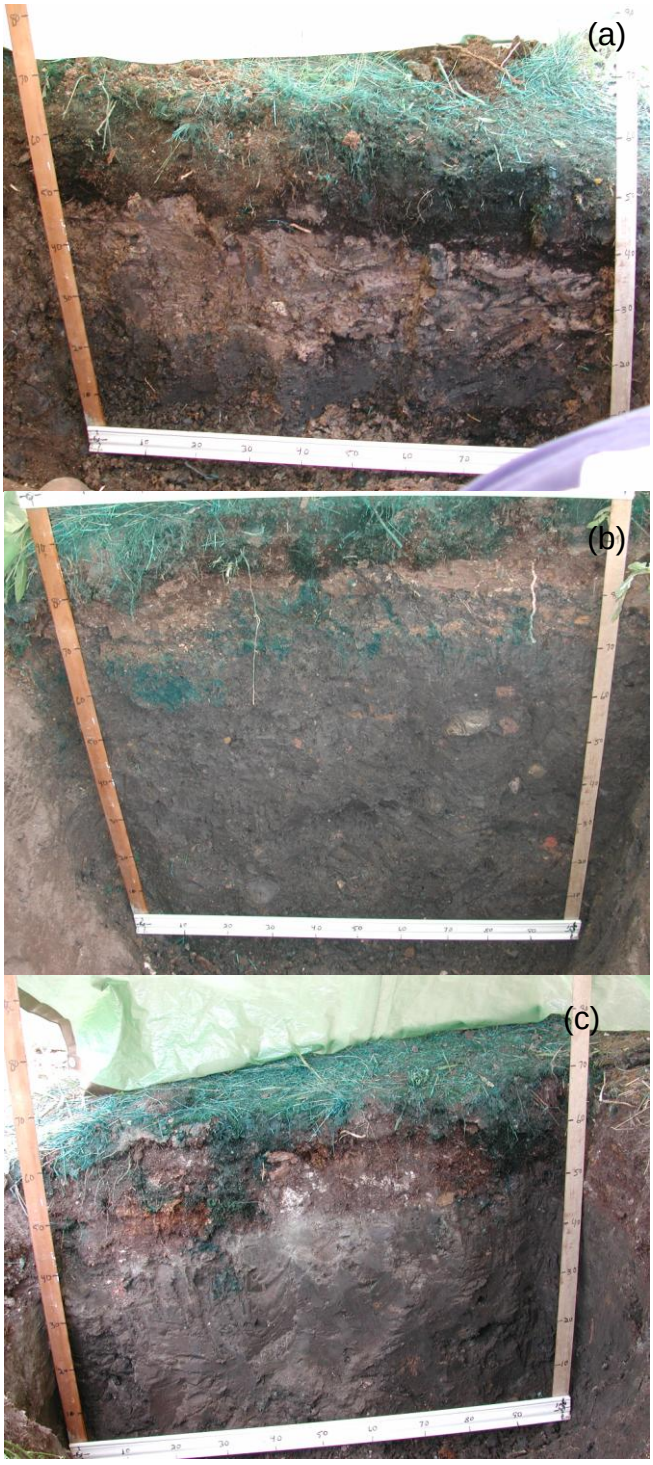

Figure 3.4 Vertical flow patterns of Brilliant Blue dye one day after soil plots were irrigated with a total application of 0.04 m dye solution. Profiles are presented for the: a)top, b)middle, and c)toe slope positions of the 0.35-m soil cover.

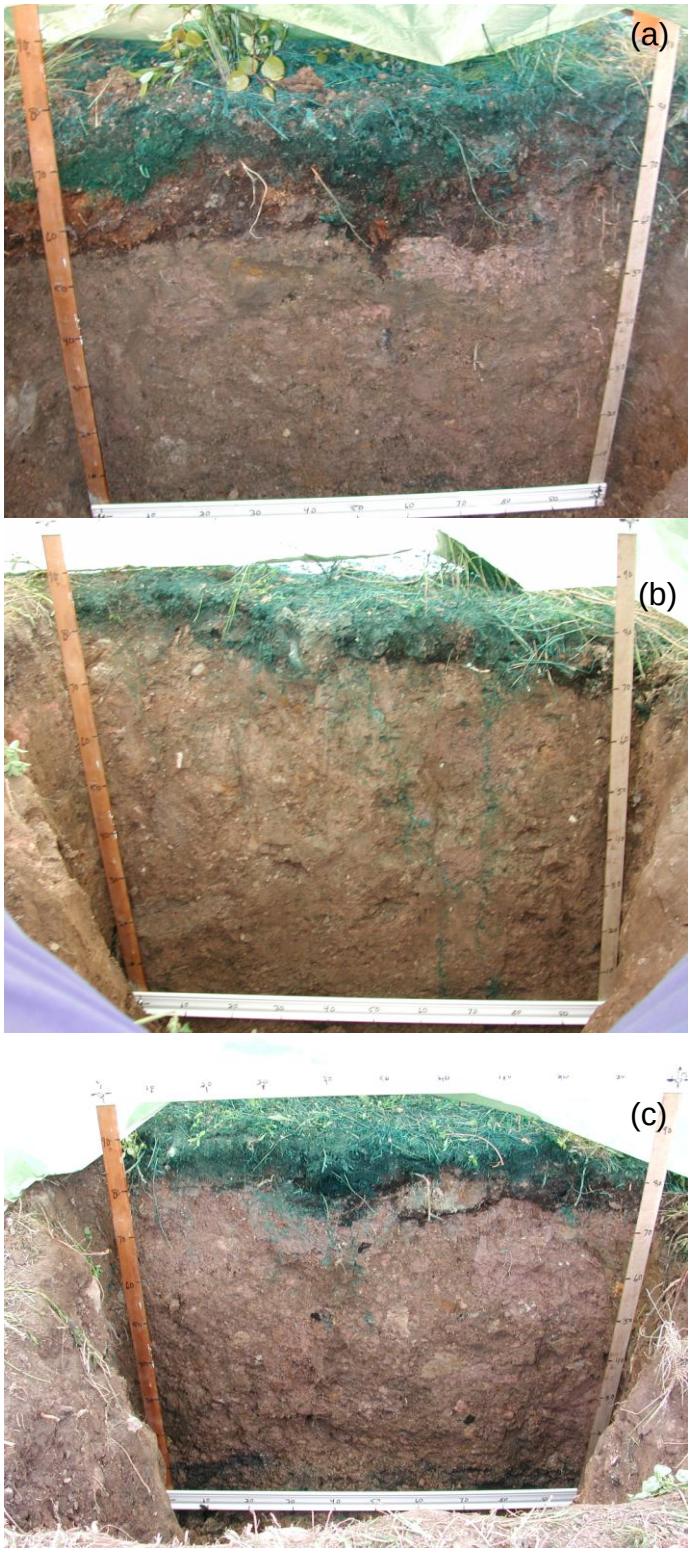

Figure 3.5 Vertical flow patterns of Brilliant Blue dye one day after soil plots were irrigated with a total application of 0.04 m dye solution. Profiles are presented for the: a)top, b)middle, and c)toe slope positions of the 1-m soil cover.

stained flow patterns among plots were attributed to the type of preferential flowpaths in existence and related differences in the depth of dye penetration.

Between the 6 soil plots, there is evidence of each major source of preferential flow: macropores, fingering, and funneling. Stained flow patterns indicated that some form of macropore flow occurred in each soil plot. The most obvious example is seen in the middle slope position (Figure 3.5b) of the 1-m cover where two large macropores channeled the infiltrating dye solution deep (>0.9 m) within the soil profile. Close inspection revealed that these macropores were most likely the decayed root channels from surface vegetation, such as the yellow sweet clover herb (*Melilotus officinalis (L.) Pallas*), which was abundant on the covers and known for its quick growing and lengthy taproot.

Preferential flow through fingering was evident in the toe slope position of the 0.35-m cover. In the upper left hand corner of Figure 3.4c, the development of a finger can be seen in the dyed flow pattern. This finger appears to have formed from water initially flowing in the peat mix that separated into a distinct flow stream when a zone of higher conductivity (i.e. finer textured material) was encountered. At the bottom of the finger, at approximately 0.3 m below the soil surface, it appears as if the finger met up with a macropore (origin unknown), which served to transport the dye even deeper within the soil. Between the finger and macropore, preferential flow paths transported the dye solution to about 0.4 m below the soil surface.

The effect of funneling on solute transport is shown in soil plot located in the middle slope position of the 0.35-m cover (Figure 3.4b). In this soil profile, the interface between the peat mix and the glacial soil formed a slight local depression (or concave shape). The depression between the texturally different materials served to funnel the dye solution through the bottom of the peat depression where it was transported vertically into the glacial layer. Once in the glacial layer, the dye solution appeared to encounter a lens of finer textured material which served to preferentially transport the dye. As such, there is zone of lateral spreading evident 0.25 – 0.45 m below the soil surface in this location.

One-dimensional profiles of dye coverage were determined for each soil plot using classification data that differentiated dyed pixels from non-dyed pixels. An

example of the stained flow pattern and the corresponding digital analysis is presented in Figure 3.6. In Figure 3.7, the same dye pattern is once again presented, this time alongside the resulting one-dimensional profile of dye coverage. To calculate the amount of staining as a function of soil depth, the sum of dyed pixels in each 0.1 m subsection was divided by the total sum of pixels in said subsection and then expressed as a percentage. This calculation was performed successfully (i.e. measured accuracy of >90%) for subsections from 0-0.9 m below the soil surface. Below the 0.9 m depth, several difficulties were encountered which limited the identification of stained patterns. At each soil plot on the 0.35-m cover, the presence of the compacted shale made manual digging to the 1m depth extremely arduous and thus most profiles could not be excavated in their entirety. The sloping nature and large heterogeneity of the soils also limited the classification of stained flow patterns, especially in the 1-m cover plots. The slope of the covers posed problems when it came to cropping the images into horizontal subsections. Because of the slope, some areas of the images had background interference from surface vegetation or the reference grid. As a result of these difficulties, data was presented for the 0-0.9 m soil depths only to ensure a consistency among results.

The profiles of dye coverage as a function of soil depth further illustrate the similarity in transport processes between plots and confirm the existence of preferential flow (Figures 3.8 and 3.9). As expected, the greatest amount of dyed pixels corresponds to the depth of the peat mix (about 0.15-0.20 m) in each soil plot. The amount of soil stained with dye at this depth varies from plot to plot, averaging 18% across the site. All soil plots showed a marked decrease in dye coverage with depth of soil past the 0.15-0.20 m depth, with the exception of the middle slope position of the 0.35-m cover that was subjected to lateral subsurface flow as described previously.

Assuming that stained flow patterns up to 0.20 m depth represented matrix flow and/or diffusive mass transfer into immobile regions in the peat mix, any dye that penetrated past this layer could be seen as evidence of preferential flow. As such, the stained soil below the 0.20 m depth is representative of the soil area used by preferential flowpaths (Table 3.4). Preferential flowpaths in the 0.35-m soil plots

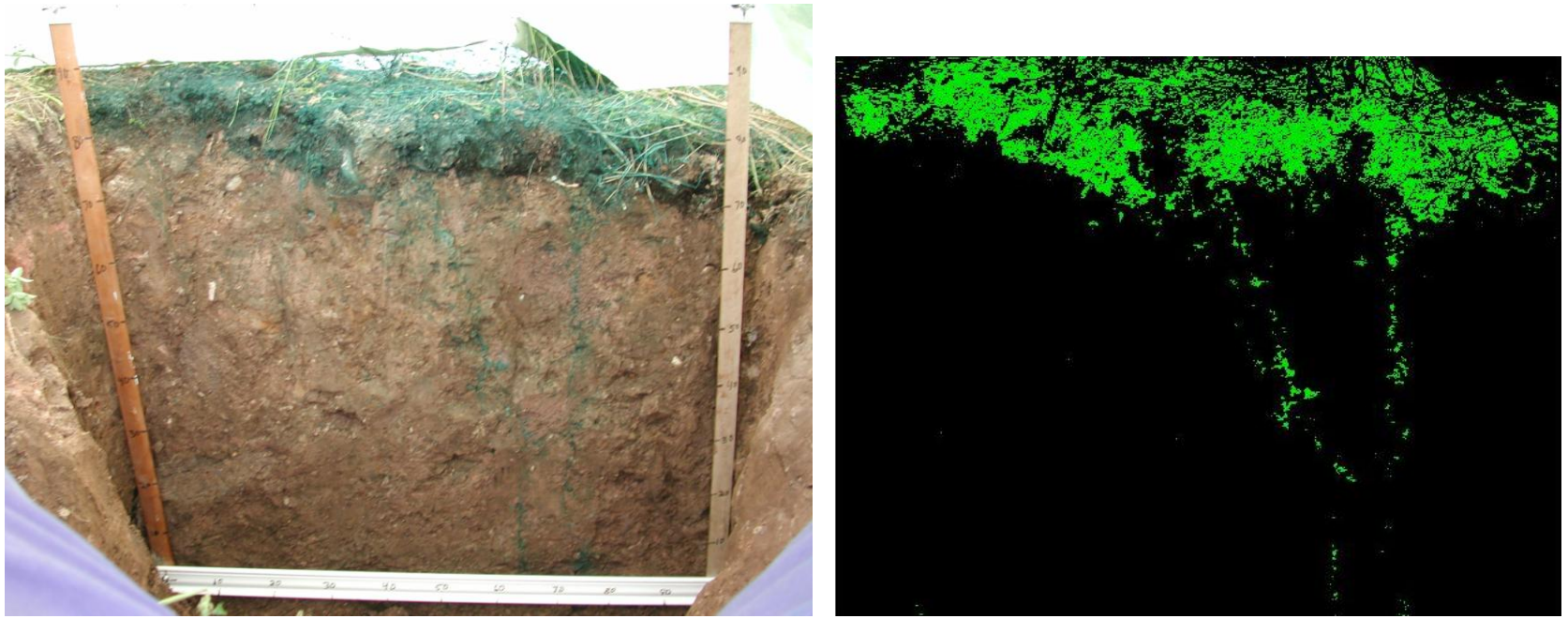

Figure 3.6 Vertical flow patterns of Brilliant Blue dye, and the corresponding digital classification of dyed pixels and non-dyed pixels, one day after soil plots were irrigated with a total application of 0.04 m dye solution. Profile shown is representative of the middle slope position of the 1-m soil cover.

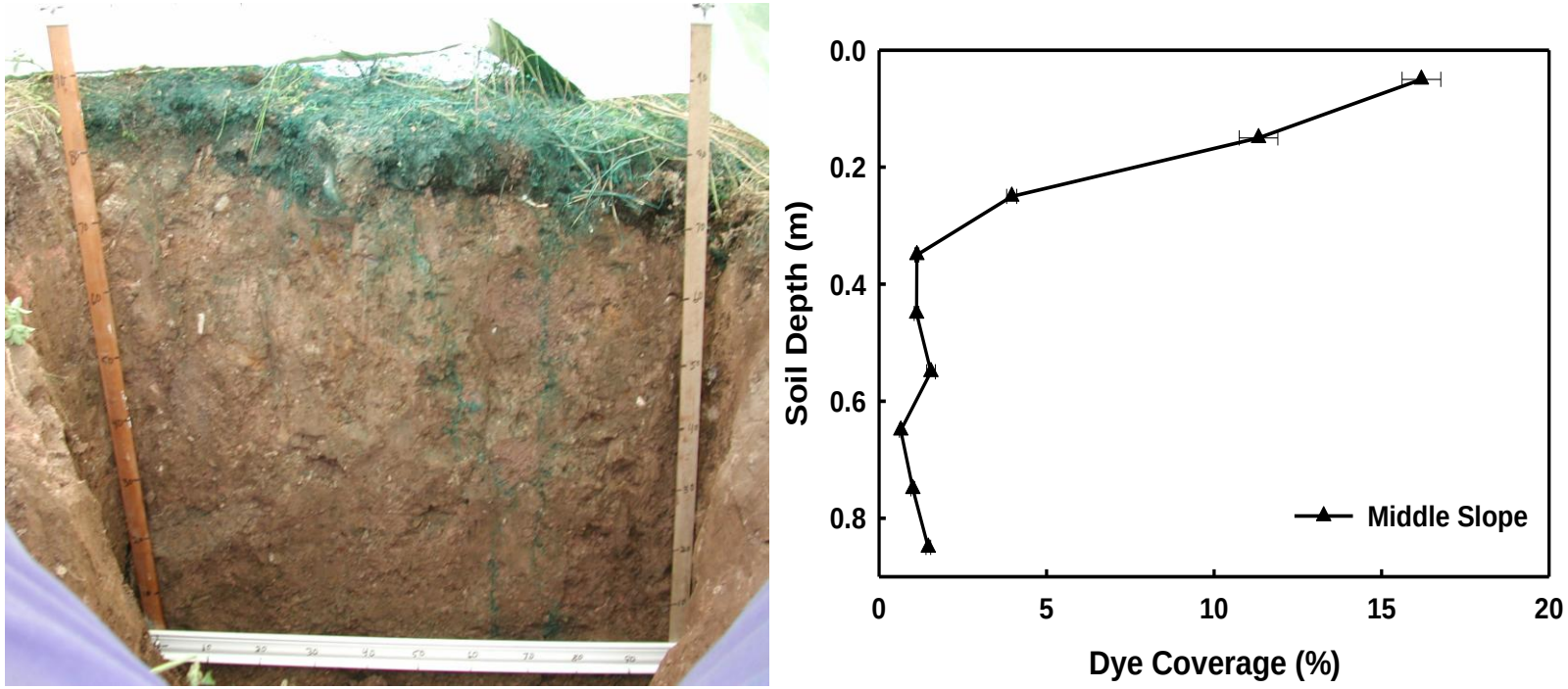

Figure 3.7 Vertical flow patterns of Brilliant Blue dye, and the matching one-dimensional profile of dye coverage, one day after soil plots were irrigated with a total application of 0.04 m dye solution. Profile shown is representative of the middle slope position of the 1-m soil cover.

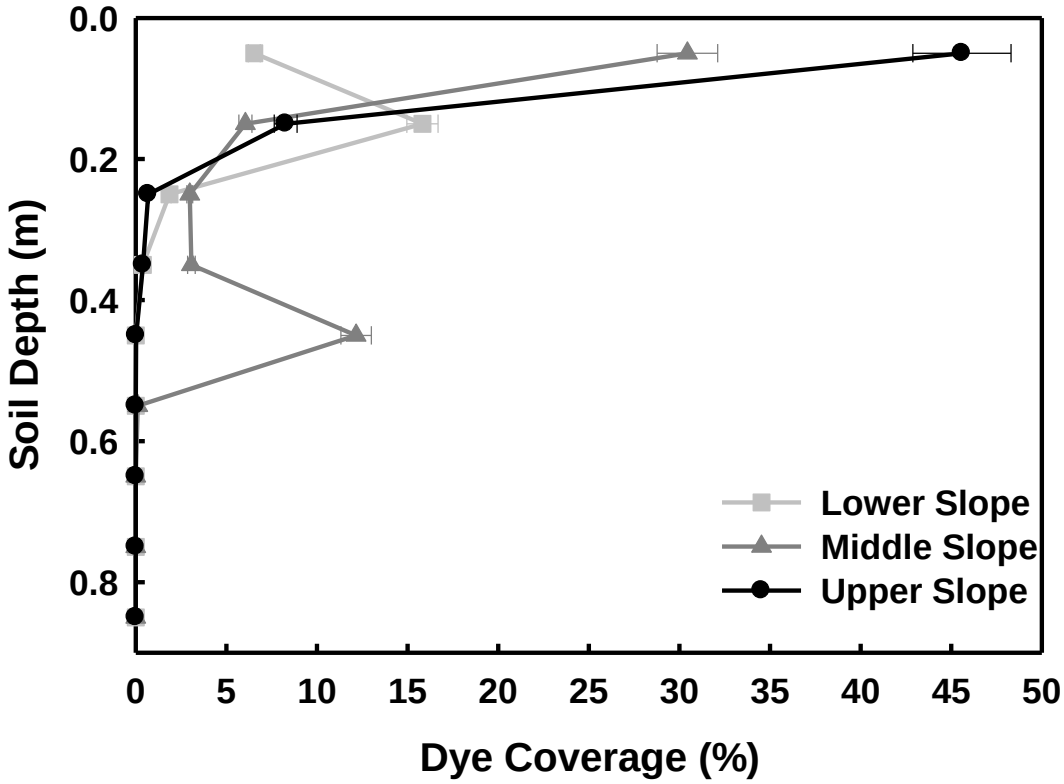

Figure 3.8 Percentage of stained soil versus soil depth for the 0.35-m cover. Error bars represent the standard error associated with the method of digital classification.

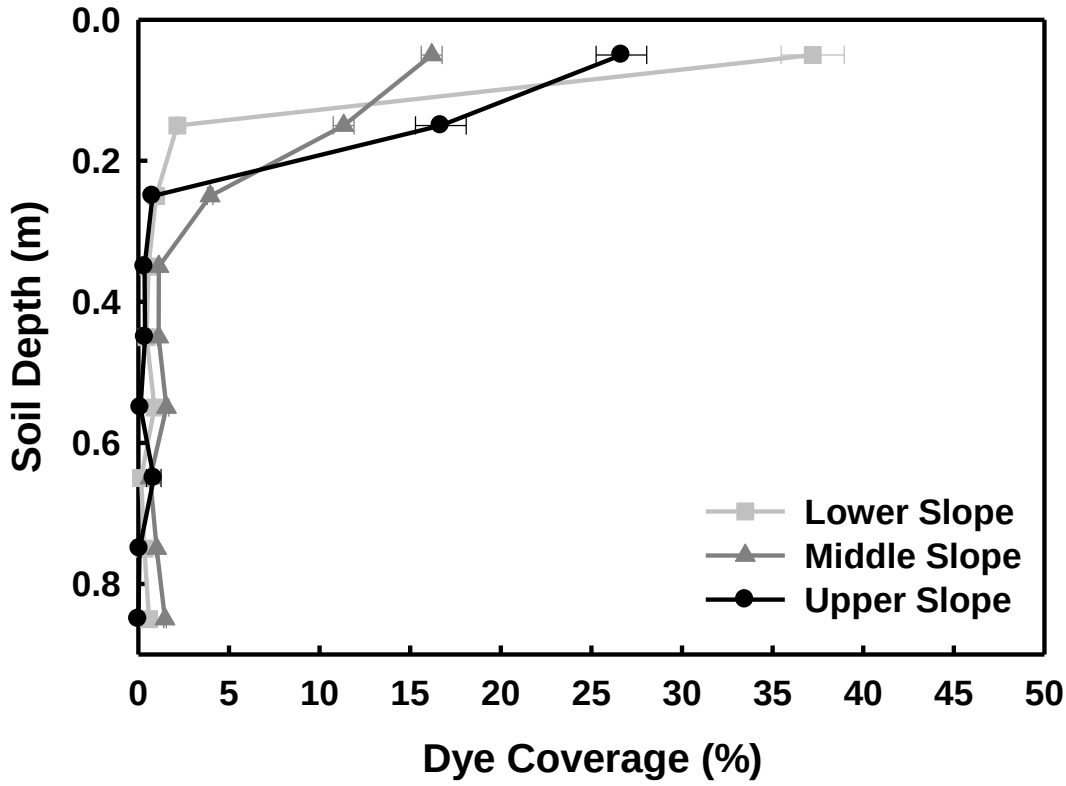

Figure 3.9 Percentage of stained soil versus soil depth for the 1-m cover. Error bars represent the standard error associated with the method of digital classification.

Table 3.4 Percent of soil area stained by preferential flow for toe, middle, and upper slope positions on the 0.35-m and 1-m soil covers, one day after soil plots were irrigated with a total application of 0.04 m dye solution.

	0.35-m Cover			1-m Cover		
Soil Depth	Toe Slope	Middle Slope	Upper Slope	Toe Slope	Middle Slope	Upper Slope
m	%					
0.25	1.9	3.0	0.69	0.98	4.0	0.78
0.35	0.40	3.0	0.40	0.56	1.1	0.34
0.45	NDP[†]	12	0.02	0.45	1.1	0.37
0.55	NDP	0.10	NDP	0.89	1.6	0.12
0.65	NDP	NDP	NDP	0.15	0.65	0.85
0.75	NDP	NDP	NDP	0.33	1.0	0.07
0.85	NDP	NDP	NDP	0.59	1.5	NDP

[†]NDP, no dyed pixels were present.

generally used <5% in soil area at each depth. The exception was of course the middle slope location, in which funneling to a zone of higher conductivity resulted in lateral subsurface flow around the 0.45 m depth, as was discussed previously. Soil plots in the 1-m cover also had <5% of the soil stained by preferential flowpaths. On average, the area consumed by preferential flow paths below the 0.20 m depth and across the soil plots was 2%.

The maximum depth of dye penetration was variable between soil plots (Table 3.4), depending on the type of preferential flowpaths available. When flow occurred within macropores, such as those created by decayed roots, the dye was transported deep within the soil profile, nearing the 1 m depth as was observed with the middle and toe slope positions of the 1-m cover. When fingering dominated transport mechanisms, in the instance of the toe slope position of the 0.35-m cover, the depth of dye penetration was confined to nearer to the soil surface (0.35 m). In the case of funneling, as seen in the middle slope of the 0.35-m cover, the vertical extent of the finer textured material determined the depth of dye penetration.

The results from the dye tracer experiments illustrate similarity in flow processes within each plot of the reclamation soil covers and support the laboratory findings. The three main sources of preferential flow (i.e. macropores, fingering, and funneling) were identified in at least one of the 6 soil plots. Macropore flow was identified in each plot. The dye solution was largely retained in the upper 0.15-0.20 m of each soil profile, suggesting infiltrating water flowed through the soil matrix and/or was a result of mass transfer into the immobile region of the peat mix soil. Based on the laboratory findings that identified a large immobile region and a high rate of diffusive mass transfer into this region, it is therefore hypothesized that water flowed preferentially through the peat mix; however, the dye pattern was masked as there was a large transfer of dye to immobile soil regions. This explains why a large proportion of dye was retained in the peat mix and why there was evidence of preferential flow further within the soil profile. Although preferential flowpaths were shown to consume only a small portion of the soil volume, they still served to transport solutes rapidly deep within the soil profile. This proved that

preferential flow within the reclamation soil covers would have important implications on water and solute transport.

3.4 Conclusions

Combining the mobile-immobile model of solute transport with adsorptive dye tracer experiments has provided a relatively inexpensive and yet exact method of assessing preferential flow processes within the soil matrix and macropores. Breakthrough patterns from conservative solute transport experiments provided evidence of the early arrival of solutes and extended tailing. Combined with large computed values for the immobile water fraction and high rates of diffusive mass transfer, these results suggest that preferential flow and non-equilibrium adsorption were important mechanisms affecting solute transport in the peat mix soil. Stained flow patterns from adsorptive dye experiments further support this conclusion. Evidence of preferential flow through macropore flow, fingering, and / or funneling was found at each test plot. From these results, it is assumed that preferential flow would be ubiquitous across the reconstructed landscape under similar experimental conditions.

The large variability in breakthrough patterns, estimated solute transport parameters, and conducting areas of the soil shows that there is a strong spatial variability in flow processes within the peat mix. Given that preferential flow is three-dimensional, this means that solutes will be transported differently within the same soil. The highly variable nature of preferential flow may therefore reduce the leaching of salts within reclamation soil covers. Salt migration into the covers will be matrix-driven, meaning that salts will accumulate in all pore spaces. Preferential flow, as observed in this study, will result in the selective leaching of salts which may have implications on salt accumulation in the soil. As such, this study has highlighted the importance of using research methods which examine flow processes occurring in both the soil matrix and macropores.

4. FIELD STUDY OF VERTICAL AND LATERAL SOLUTE TRANSPORT

4.1 Introduction

Preferential flow paths can act as important conduits of subsurface flow in forested hillslopes (Mosley, 1979; Tsuboyama et al., 1994; Sidle et al., 2001; Buttle and McDonald, 2002). Even the most shallow and permeable soil on a steep hillslope will generally respond to an intense rainfall with the slow subsurface transport of water, where percolation and downslope flow occur via Darcy's Law (Freeze, 1972). However, in situations where these soils contain numerous preferential flowpaths (e.g. macropores), subsurface flow can result in rapid response to precipitation events.

Macropores allow infiltrating water to bypass the soil matrix and be rapidly transported to the basal saturated zone and/or move downslope as pipe flow at speeds greater than predicted by Darcy's Law (Kirkby, 1988). Macropore flow is initiated when rainfall intensity exceeds the hydraulic conductivity of the soil matrix (Beven and Germann, 1982). This results in infiltration-excess overland flow that stimulates water entry into macropores. High antecedent moisture conditions in the soil matrix reduce the lateral movement of macropore flow into the surrounding soil, and thus also play an important role in allowing bypass flow to reach greater depths in the profile (Beven and Germann, 1982).

Vertical transport through macropores has been the basis of much research (Beven and Germann, 1982; Watson and Luxmoore, 1986; Ghodrati and Jury, 1990; Booltink and Bouma, 1991; Booltink et al., 1993; Flury et al., 1994; Li and Ghodrati, 1994; Wildenschild et al., 1994, Turton et al., 1995), while studies on lateral transport via preferential flowpaths have been limited. Research has shown that lateral preferential flow can take a variety of forms, such as: a saturated layer at the soil-bedrock interface (Smettem et al., 1991; Collins et al., 2000), pipe flow at the base of the soil profile (McDonnell, 1990), and flow through a network of macropores and mesopores imbedded in the soil matrix (Sidle et al., 2001). Only recently has the importance of lateral subsurface flow systems been recognized as

providing a direct link between macropore flow and the rapid runoff response often observed in forested ecosystems (Mosley, 1979; Noguchi et al., 1999; Noguchi et al., 2001; Sidle et al., 2001; Buttle and McDonald, 2002, Kelln et al., 2007).

Within reclamation soil covers capping saline-sodic shale, lateral subsurface flow via preferential flowpaths can be a significant mechanism of water and solute transport. Previous work in this landscape (Kelln et al., 2007) has shown that subsurface flow is initiated during spring snow melt in response to water migrating from macropores to the soil matrix, encouraging the development of a perched water table at the cover-shale interface if saturated conditions develop. In summer and fall, the occurrence of saturated conditions above the interface is rare and thus, the interaction between vertical transport through macropores and lateral preferential flow remains largely undetermined.

Therefore, to better understand vertical and lateral flow processes occurring within reclamation soil covers, the objectives of this study were to: 1) determine how vertical flow through soil macropores contributed to solute transport and, 2) evaluate the role of lateral subsurface flow in solute movement.

4.2 Materials and Methods

4.2.1 Study site

The study site was the South West 30 Overburden Dump (SW30), located north of Fort McMurray, Alberta at Syncrude Canada's Mildred Lake mine site. In 1999, three reclamation soil covers were constructed to cap saline-sodic shale resulting from oil sands mining. Each 1 ha cover is situated along a 5H:1V north facing slope and consists of selected depths of peat mix and glacial soil to form nominal cover thicknesses of 0.35, 0.50, and 1 m. This study deals with the 0.35-m cover only, which was constructed from 0.15 m peat mix overlying 0.20 m of glacial soil. For a more detailed description of the study site, including soil and climatic data, refer to section 3.2.1.

4.2.2 Experimental design

To evaluate the effects of macropore flow on solute transport, a large field-scale tracer study was conducted. Two conservative tracers, bromide (Br^-) and chloride (Cl^-), were applied to the surface of the 0.35-m soil cover at the SW30. Tracer movement was tracked over time using downslope soil sampling at each of approximately 14 months and 24 months later. Water chemistry from previously installed shallow monitoring wells was also used to monitor tracer transport. The application of the tracers to the soil surface occurred in July of 2003. A 50 m long by 1 m wide transect was staked across the lower portion of the 0.35-m soil cover. The soil transect, which was located approximately 20 m upslope from the bottom of the cover, was divided into ten segments (Figure 4.1). Each segment, labeled alphabetically from A to J, was 5 m in length and manually cleared of surface vegetation. At every second segment (i.e. B, D, F, H, J), a soil trench measuring 0.20 m deep and 0.35 m wide was dug while the remaining segments were left undisturbed. The soil trenches were manually irrigated with a solution of sodium chloride (NaCl) at a rate of 250 g L^{-1}, with an application volume of approximately 4 L. A solution of sodium bromide (NaBr), at the same rate and volume, was manually applied to the undisturbed soil segments (i.e. A, C, E, G, I). The objective of applying the tracers to both the soil surfaces and trenches was to evaluate if there was a difference in transport mechanisms between the top and bottom of the soil covers. Following application of the NaCl, the soil surface was replaced as best possible to mimic the natural soil profile.

Two rows of shallow monitoring wells were previously installed on the 0.35-m cover to monitor water flowing along the cover-shale interface (Boese, 2003). Since the tracers were applied approximately 1m upslope of the well locations (Figure 4.1), water from the monitoring wells was used to trace solute transport.

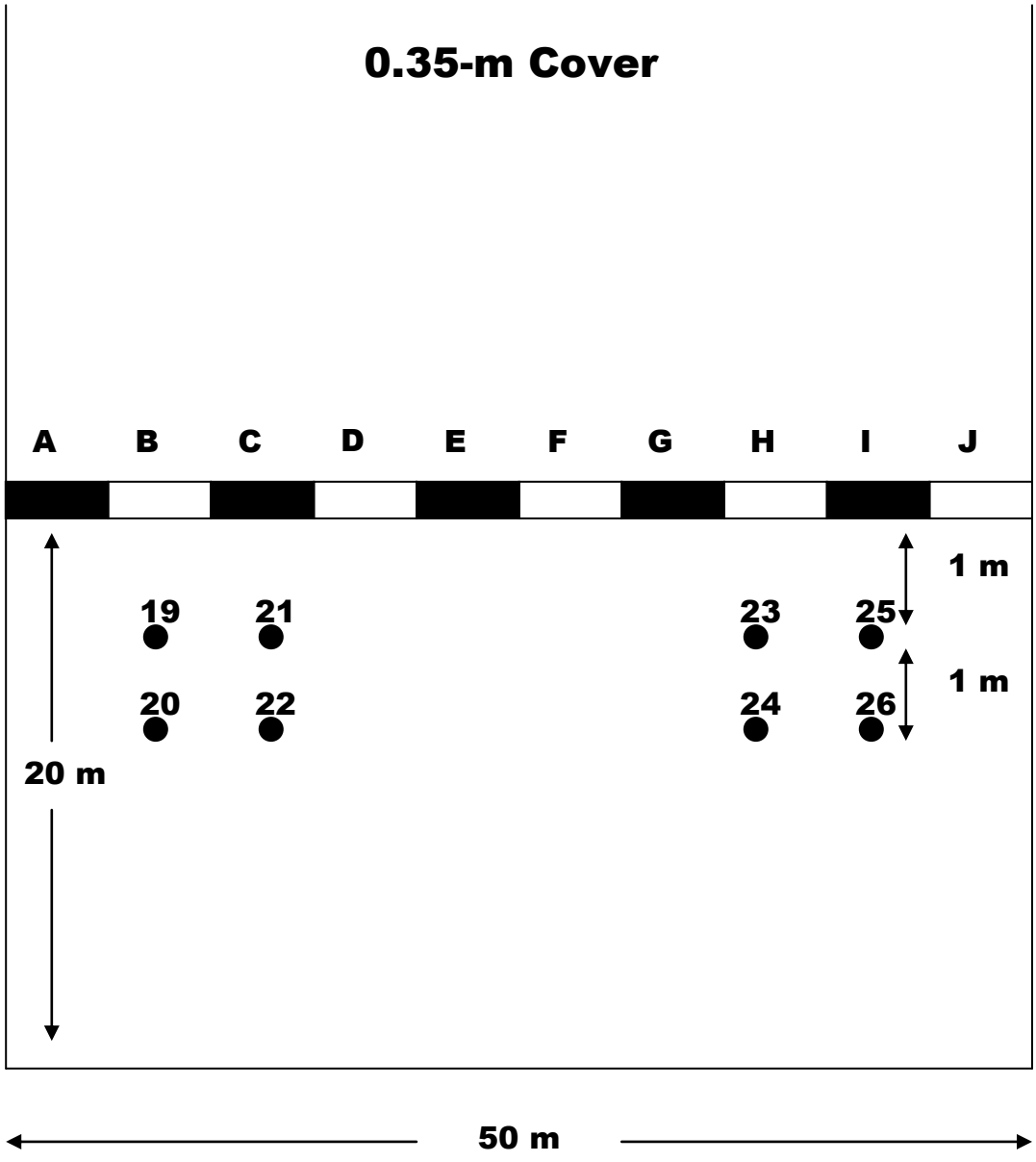

Figure 4.1 Schematic diagram of tracer application and monitoring well locations on the 0.35-m soil cover. Sodium bromide was applied to the soil surface (black boxes) while sodium chloride was applied in the soil trenches (white boxes). The black dots represent the locations of the monitoring wells.

4.2.3 Sampling scheme

Soil samples were collected downslope of the tracer application in September 2004 and June 2005 to track the transport of Br^- and Cl^-. Of the 10 tracer segments, only 6 segments (i.e. A, B, C, D, H, I) were sampled each time to minimize the cost of analysis. Segments H and I were chosen as the final sampling locations due to their proximity to shallow monitoring wells.

Sampling points were determined starting in the middle of each segment and continuing downslope in linear transects at distances of 0.2, 0.4, 0.6, 0.8 and 1 m. The initial location of the tracer application (i.e. the source - distance: 0 m) was sampled by 0.1 m depth increments using a Dutch auger until a depth of 0.5 m was obtained. Downslope sampling points were divided into three sampling depths: 0-0.15 m comprising of peat mix, 0.15-0.35 m consisting of glacial soil, and 0.35-0.50 m to include a shale sample. Samples were collected using a Dutch auger and care was taken to respect material boundaries as much as possible. Approximately 2-3 core holes were needed at each sampling point to reach the desired depth. These samples were combined to form a composite sample at each depth.

Samples were bagged and brought back to the laboratory for analysis. In all, there were 20 soil samples collected at each segment and 6 segments sampled in September 2004, resulting in 120 soil samples for analysis. Following collection, each composite soil sample was sub-sampled for gravimetric soil water content analysis. Remaining sample material was then air-dried and ground to pass a $2x10^{-3}$ m sieve. Preparation of these samples occurred using a 1:2 (soil: water) extraction process (Rhoades, 1982; Hogg and Henry, 1984) where 10 g soil was mechanically shaken with 20 g deionized water for 1 hour prior to extraction. Samples were extracted using vacuum filtration and highly retentive filter paper. Soil water extracts were further filtered using a hand syringe and $4.5x10^{-7}$ m glass fiber filter. Electrical conductivity of the extracts was measured using a dip-type electrical conductivity cell. Basic anion and cation concentrations were measured using high performance liquid chromatography - ion chromatography (IC) at the Syncrude Environmental Research Laboratory.

The same sampling protocols were followed again in June 2005 when follow-up soil sampling occurred. Due to the destructive nature of soil sampling, sample locations were moved approximately 0.05 m east of the previous sampling points. In addition to the 120 sampling points used in 2004, an additional 30 were added for the 2005 collection. Segments C and D were intensively sampled at 0.1 m increments in distance downslope, up from the previous 0.2 m, in hopes of better quantifying tracer transport. Sampling of each segment thus resulted in an additional 15 samples each, resulting in a total of 150 samples being collected in 2005.

Owing to the non-normal distribution of the soil chemistry data, results were analyzed for significance using non-parametric statistical tests. The Kruskal-Wallis H Test was used to determine if the population distributions of three or more populations were identical (e.g. among sampling depth or distance from source). To compare the population distributions between only two samples (e.g. tracer concentrations from year to year or within sampling location), the Wilcoxon Rank Sum Test was used.

Since installation, the shallow monitoring wells were checked daily for the presence of water, starting each year during the spring melt and ceasing after freeze-up. When subsurface water was present, a vacuum pump was used to extract the sample. The sample was sent to the Syncrude Environmental Research Laboratory for basic water quality analysis.

4.3 Results and Discussion

4.3.1 Soil chemistry

Soil sampling to track the movement of Br^- and Cl^- in the 0.35-m soil cover took place over 3 days in September of 2004 and over 4 days in June of 2005. Soil samples within Segments A, C, and I were used to measure the amount of Br^- in a specific soil volume (g m^{-3}), while soil from Segments B, D, and H was used to assess similar Cl^- concentrations (g m^{-3}). The following data is thus presented as the mean of concentrations determined within each of the three sampling segments.

4.3.1.1 2004 sampling program

Soil samples collected at the location of the initial tracer application (i.e. the source) in September 2004 showed the vertical profile of solute concentrations as a function of soil depth (Figure 4.2). There was a great range of variability in the source concentrations among segments, so much so that the standard deviation between concentrations was at times greater than the actual solute concentrations. As such, error bars were not included in Figure 4.2 to minimize the 'noise' in the data profile. Due to the high variability among solute concentrations, the trends seen in Figure 4.2 need to be examined quite liberally.

There were no detectable concentrations of Br^- in the soil prior to the surface application of NaBr. The concentrations of Br^- at soil depths of up to 0.5 m at the source thus showed that infiltrating water transported solutes vertically within the soil profile. Surprisingly, in the year or so since the 1000 g NaBr pulse was applied (per each 5 m x 0.2 m transect), the amount of Br^- recovered at the source was quite low, averaging 3-8 g m^{-3}.

In comparison to Br^- concentrations, there was a considerable difference in the measured concentrations of Cl^- at the source, despite the same rate and volume of irrigation solution being used. Concentrations of Cl^- were in the order of approximately 2-5 times an order of magnitude higher than Br^-, with the difference attributed to high levels of naturally Cl^- occurring in the soil cover. Despite the influence of background Cl^-, it was most surprising to find the highest levels of Cl^- nearest to the soil surface considering that the 1000 g pulse of NaCl was applied at a soil depth of 0.20 m.

To determine if the background concentrations of Cl^- could be removed from the source measurements, Cl^- concentrations were quantified from similar locations in soil segments in which there was no interaction with the NaCl tracer (Appendix B). Measured concentrations of naturally occurring Cl^- were found to be extremely variable, arbitrarily ranging from 4-26 g m^{-3}. Given this large variability in background concentrations, it was impractical to assume a set background concentration of soil Cl^-, and therefore impossible to differentiate the contributions from the applied Cl^- tracer from background levels. As such, the analysis of the

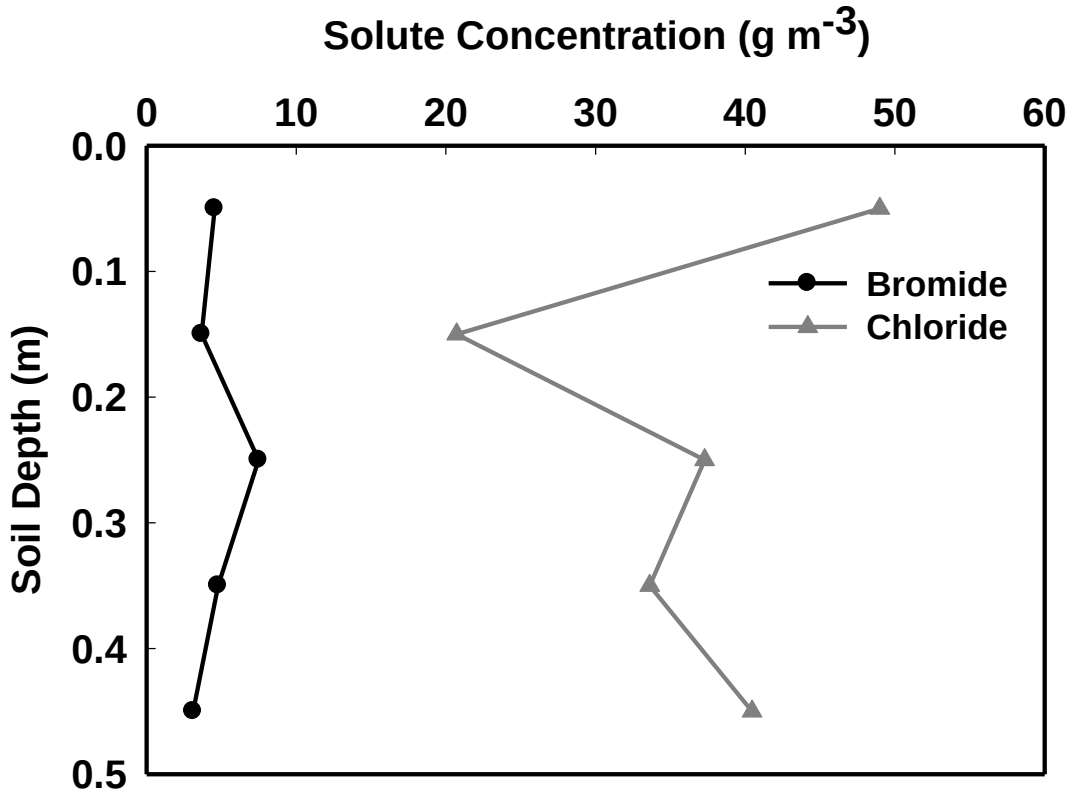

Figure 4.2 Mean concentrations of bromide and chloride (g m^{-3}soil) as a function of soil depth, as measured at the locations of the initial tracer application in September 2004. Error bars were not presented due to the particularly large variability in concentrations.

movement of the applied Cl^- tracer will be henceforth limited to qualitative inferences only.

The mean soil concentrations of Br^- were plotted as a function of distance downslope from source in Figure 4.3 for September 2004 (fall) sampling period. Concentrations of Br^- appeared to decrease with increasing distance from source. This was, however, determined to be statistically insignificant due to the high variability in soil concentrations. The largest concentration of Br^- was consistently found in the upper 0.15 m of the soil. Concentrations decreased significantly at α=0.05 with soil depth for all sample locations.

As the Br^- tracer was applied to the soil surface, there were two possible mechanisms responsible for the observed transport of Br^-: 1) lateral subsurface flow in the upper 0.15 m of the soil, or 2) the interaction between infiltration, lateral subsurface flow at the shale-cover interface, and vertical transport back into the soil cover. For subsurface flow to occur in the upper 0.15 m of the soil, saturated conditions would have had to been present in the peat mix layer. Saturated conditions, in which the soil is saturated from the interface to the soil surface, were unlikely in these soil materials and climatic conditions. However, given that the hydraulic conductivity of the glacial soil is an order of magnitude less than the peat mix soil, there is potential for rainfall to infiltrate the peat mix soil but exceed the infiltration capacity of the glacial soil, thus creating ponding conditions at the layer interface. Upon ponding, the water would flow laterally through the soil in response to the downslope gradient and in this way transport solutes laterally downslope. For this mechanism of solute transport to occur, however, rainfall intensities must be within a narrow range where they do not exceed the conductivity of the peat mix (or overland flow would occur) but exceed the conductivity of the glacial soil. Therefore, only select storm events would result in lateral subsurface flow within the upper 0.15m of the soil.

Alternatively, the interaction between vertical and lateral flow processes could be responsible for the observed solute concentrations. The initial tracer application occurred in July 2003 and soil solute concentrations were measured in September

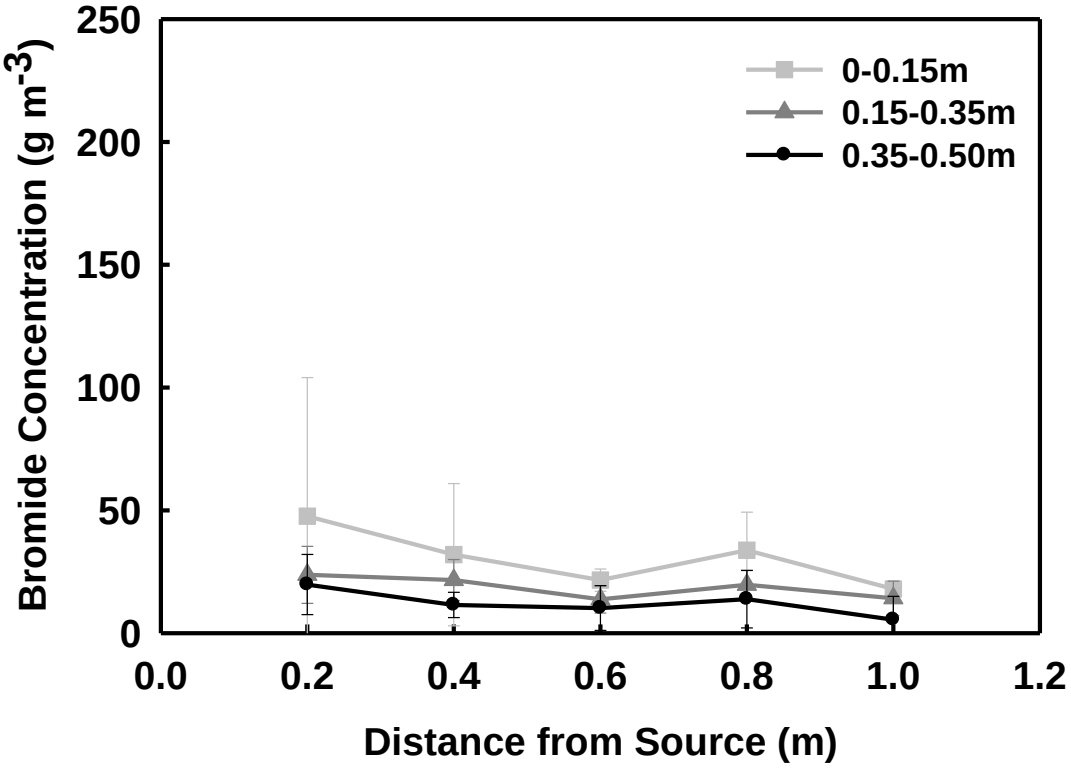

Figure 4.3 Mean concentrations of soil bromide (g m^{-3} soil) as a function of distance downslope from the source (the site of initial tracer application). Measurements occurred during the September 2004 soil sampling program for depths of 0-0.15 m, 0.15-0.35 m, and 0.35-0.50 m. Error bars represent standard deviation. Source data was previously presented in Figure 4.2.

2004. The presence of Br^- near the base of the cover at the site of the initial tracer application, when there was no historical Br^- present in the soil, suggested that vertical flow processes were responsible for leaching solutes from the upper portion of the soil profile and transporting them to depth. Moreover, the small concentrations of Br^- measured at the source following the large pulse of NaBr suggested that considerable vertical flow was needed to leach out the majority of the applied tracer.

These observations suggest two mechanisms for the vertical leaching: flow through the soil matrix and / or preferential flow associated with a large immobile soil region and high rates of mass transfer. Each of these mechanisms accounts for a large interaction with soil solutes. Matrix flow describes the slow transport of infiltrating water that is in contact with all parts of the soil, such that adequate time and contact is available for solute leaching. On the other hand, the large immobile regions and high mass transfer rates associated with preferential flow can result in much transfer between mobile and immobile regions such that soil solutes can also be leached in this manner. As both matrix flow and preferential flow are common to soils, and the results from Chapter 3 confirm the susceptibility of the peat mix soil to preferential flow, the contribution of each mechanism to vertical solute leaching could not be differentiated.

Hence, following tracer application in July 2003, it is speculated that infiltrating water from summer and fall precipitation events flowed either through the soil matrix or between mobile and immobile regions to aid in the leaching of soil Br^-. There were, however, high moisture deficits in the summer and fall of 2003 and 2004 (Kelln et al., 2007), suggesting that the leaching ability of infiltrating water would be limited during these periods. Since significant leaching was observed, it is theorized that these flow mechanisms were not the only sources of vertical leaching.

Rather, it is hypothesized that during the spring snowmelt of 2004, a portion of meltwater infiltrated the soil matrix and helped to leached Br^- vertically within the soil profile. This hypothesis is supported by observations of meltwater infiltrating and flowing through soil matrix of porous, highly organic frozen soils with little resistance (Carey and Woo, 2001). Over the winter, organic surface soil layers

commonly become desiccated by upward vapor flux (Smith and Burn, 1987) so that in the snowmelt period, some meltwater can infiltrate and percolate the organic layer under frozen conditions. Further percolation of the infiltrating water is, however, restricted by the formation of ice in the pores of the underlying mineral soil. In this situation, however, vertical leaching of soil solutes is possible.

Within the same soil cover system, Kelln et al. (2007) concluded that preferential flow, rather than matrix flow, was responsible for transporting meltwater during spring melt. The authors theorized that when the ground was frozen, infiltrating water was transported through preferential flowpaths as infiltration into the soil matrix was restricted due to the presence of pore ice. After the ground thaws, water stored in preferential flow paths was found to migrate into the soil matrix. This concept therefore assumes that soils are near-saturated when autumn freeze-up occurs and that there is no available pore space in the soil matrix for meltwater to infiltrate. In this situation, vertical leaching does not occur within the soil during the spring melt as the matrix is bypassed until ground thaw. By this point, however, a majority of meltwater has already infiltrated the soil and is not available for vertical solute leaching.

Since significant vertical leaching of soil solutes was observed in this study, it is therefore assumed that a portion of the meltwater flowed through the soil matrix during the spring melt of 2004. This explanation shows that infiltration during spring melt is quite complicated, involving both matrix and preferential flow.

The existence of Br^- downslope from the source suggests that some form of subsurface flow was then responsible for the lateral transport of solutes within the landscape. Kelln et al. (2007) observed the formation of a perched water table at the cover-shale interface in response to saturated conditions following the spring melt and ground thaw. This transient water table forms a highly mobile zone of water that can move downslope, thereby transporting soil solutes laterally within the landscape. As such, it appeared that Br^- was transported downslope by subsurface flow at the interface generated in response to the spring snowmelt.

The existence of Br^- near the soil surface at distances downslope from the initial tracer application suggested that following translocation by subsurface flow, Br^- was

transported upwards into the overlying soil. The explanation of Br^- migration could be diffusion or advection related. Bromide could simply be migrating into the overlying soil in response to concentration gradient, as in the case of diffusion. Alternatively, Br^- may be responding to an increase in matric suction due to soil drying and plant uptake, as observed by Kelln et al. (2007).

While the aforementioned flow processes were described as successive events, it should be noted that these flow processes are likely occurring simultaneously within the soil profile. For example, lateral subsurface flow was likely occurring at the same time as vertical infiltration which may also occur at the same time as advective or diffusive transport. Thus, solutes within the soil profile are continuously subjected to downward, lateral, and upward mechanisms of transport, which will ultimately result in highly variable solute concentrations until the source of the solutes is removed from the soil profile.

Soil Cl^- concentrations were plotted as a function of distance from source for all three sampling depths, as determined in the fall 2004 sampling program, in Figure 4.4. There was extensive variability within the Cl^- data and the presence of background Cl^- further clouded any qualitative inferences. What could be determined was that concentrations of Cl^- were considerably different from those evidenced for Br^- for the same fall sampling period. The largest concentrations of Cl^- were not located in the upper portion of the soil profile and did not vary significantly with soil depth at α=0.05, as found for the Br^- tracer. This was, however, somewhat expected given that the Cl^- tracer was applied at 0.2 m.

4.3.1.2 2005 sampling program

Soil samples collected from the source in June 2005 confirmed that matrix flow leached solutes from the upper portions of the soil profile (Figure 4.5). For example, from fall 2004 to spring 2005, there was a general reduction in the mean soil Br^- at depths up to 0.3 m and in the mean Cl^- concentrations at the 0-0.1 m sampling depth. Below these depths, there appeared to be a net gain of soil solutes in each profile, further supporting the concept of matrix flow leaching solutes. There were,

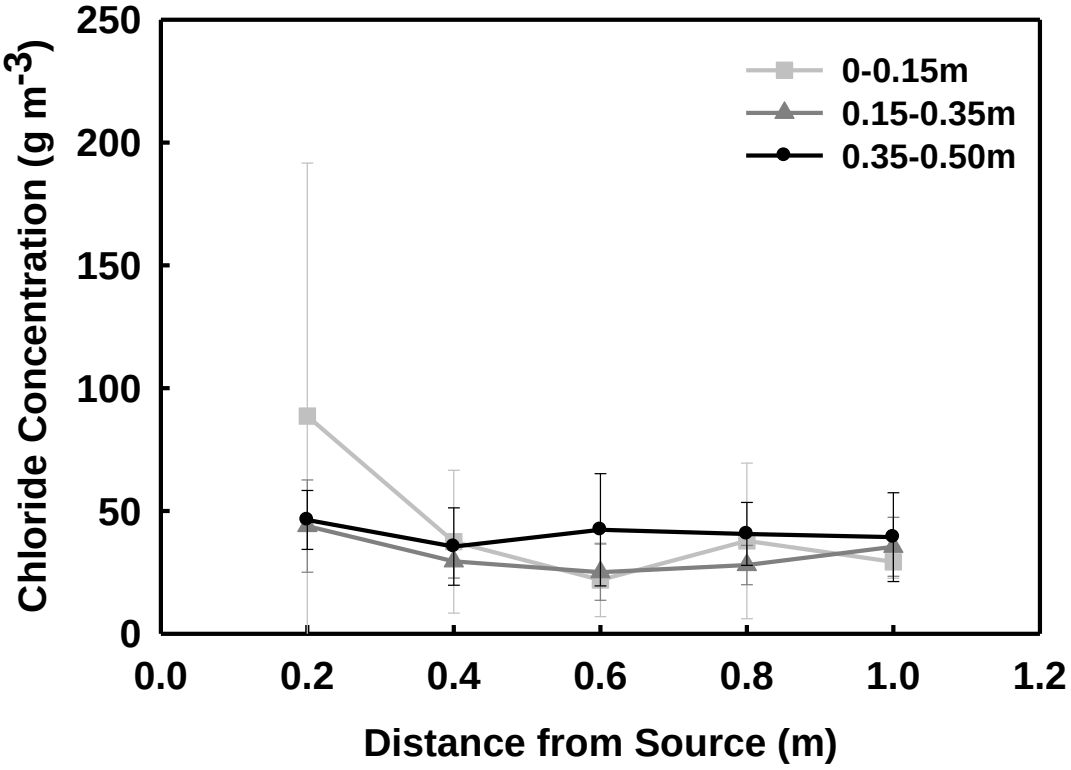

Figure 4.4 Mean concentrations of soil chloride (g m^{-3} soil) as a function of distance downslope from the source (the site of the initial tracer application). Measurements occurred during the September 2004 soil sampling program for depths of 0-0.15 m, 0.15-0.35 m, and 0.35-0.50 m. Error bars represent standard deviation. Source data was previously presented in Figure 4.2.

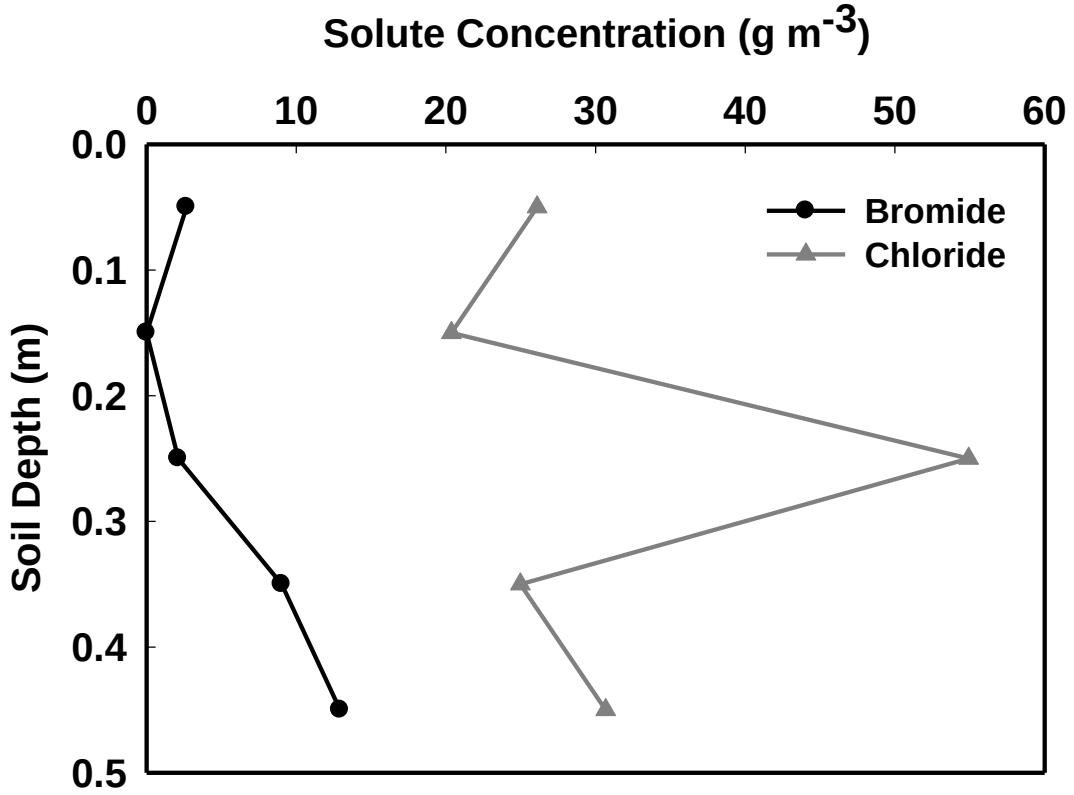

Figure 4.5 Mean concentrations of bromide and chloride (g m^{-3}soil) as a function of soil depth, as measured at the locations of the initial tracer application in June 2005. Error bars were not presented due to the particularly large variability in concentrations.

however, large variations in source concentrations and thus the results are not statistically significant.

Results from the June 2005 (spring) sampling period are presented in Figures 4.6 and 4.7 for the Br^- and Cl^- tracers, respectively. Figure 4.6 shows that there was generally more Br^- found with an increase in soil depth, which is similar to the vertical profile of Br^- concentration with depth at the source. Population distributions were not, however, significantly different with respect to sampling depth at α=0.05. Concentrations of Br^- did not vary significantly with distance from source and thus there were no clear trends were evident. Soil Cl^- concentrations were once more found to be highly variable, showing no true trends in concentrations as a function of distance from source for all three sampling depths (Figure 4.7). There was, however, a large increase in Cl^- noted at 0.6 m from the source in the soil at the base of the cover. Since nearby locations did not show similar elevated concentrations, this spike was likely due to either a) elevated background chloride concentrations at this location, or b) small scale heterogeneity in micro topography which created a depression into which solute rich water collected. No evidence was found to support one explanation over the other.

Concentration distributions of soil Br^- were compared between the fall and spring sampling periods and several changes were observed. There were significant differences in the distribution of Br^- concentrations from the fall to spring for the 0-0.15 m and 0.35-0.50 m soil depths (Figures 4.8 and 4.10, respectively) but not for the 0.15-0.35 m depth (Figure 4.9). Nearest to the soil surface there was a considerable decrease in Br^- concentrations from fall to spring while an increase in concentrations was noted for the same time period for the 0.35-0.50 m depth. This proved that there was a net loss of Br^- near the soil surface and a net gain of Br^- at the lowest sampling depth; suggesting that sometime after sampling in September 2004 and prior to sampling in June 2005, there was a flushing of soil solutes. This strengthens the explanation that meltwater infiltration into the soil matrix during spring melt, along with infiltration from summer and fall precipitation events, was responsible for Br^- transport from upper to lower soil horizons. Thus, the net loss in Br^- concentrations in the 0-0.15 m depth and net gain in the 0.35-0.50 m depth was

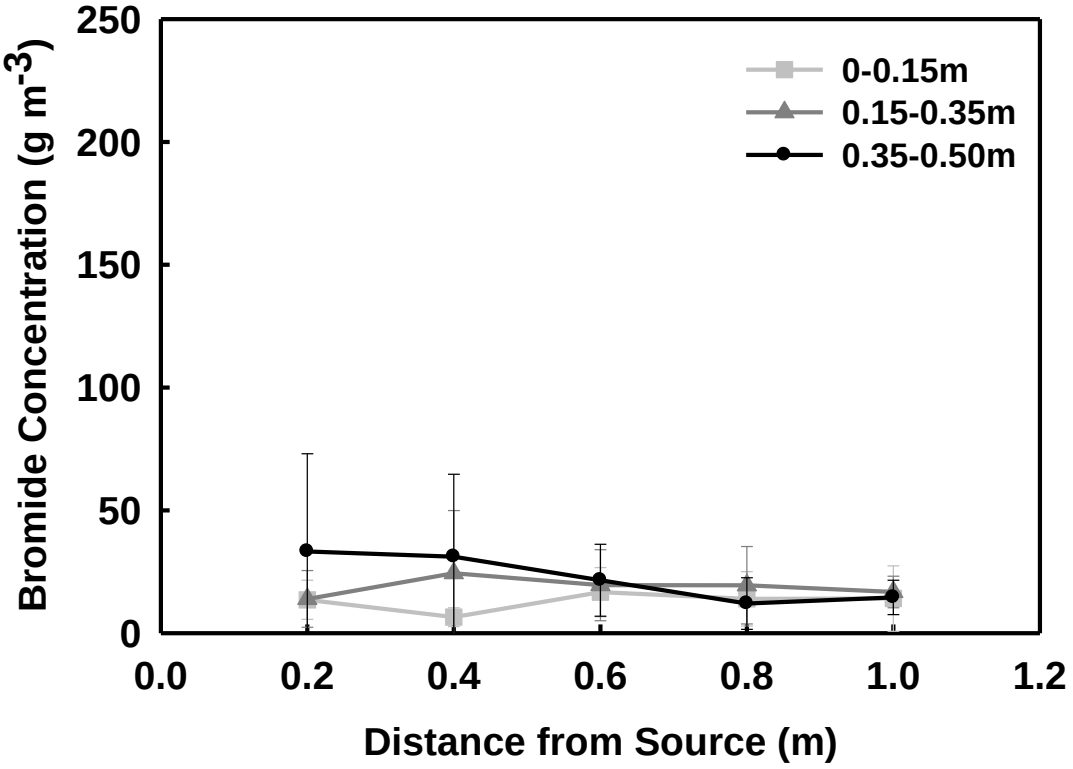

Figure 4.6 Mean concentrations of soil bromide (g m^{-3} soil) as a function of distance downslope from the source, as determined during the June 2005 sampling program for depths of 0-0.15 m, 0.15-0.35 m, and 0.35-0.50 m. Error bars represent standard deviation. Source data was presented previously is Figure 4.5.

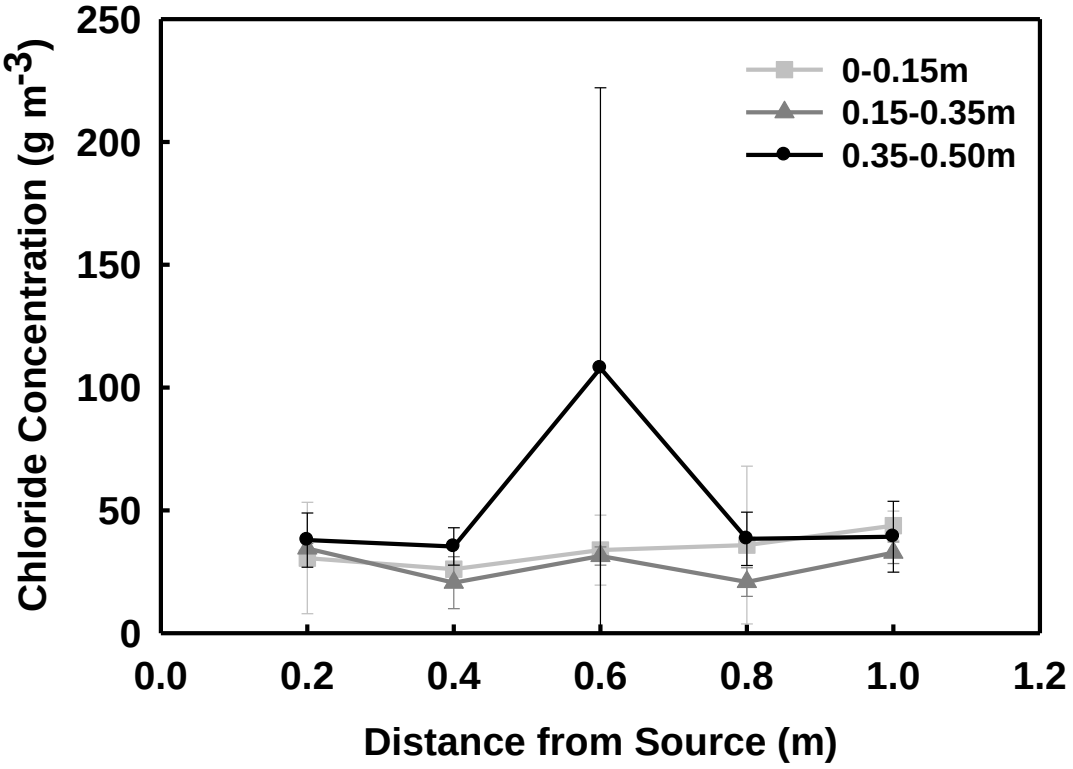

Figure 4.7 Mean concentrations of soil chloride (g m^{-3} soil) as a function of distance downslope from the source, as determined during the June 2005 sampling program for depths of 0-0.15 m, 0.15-0.35 m, and 0.35-0.50 m. Error bars represent standard deviation. Source data was presented previously is Figure 4.5.

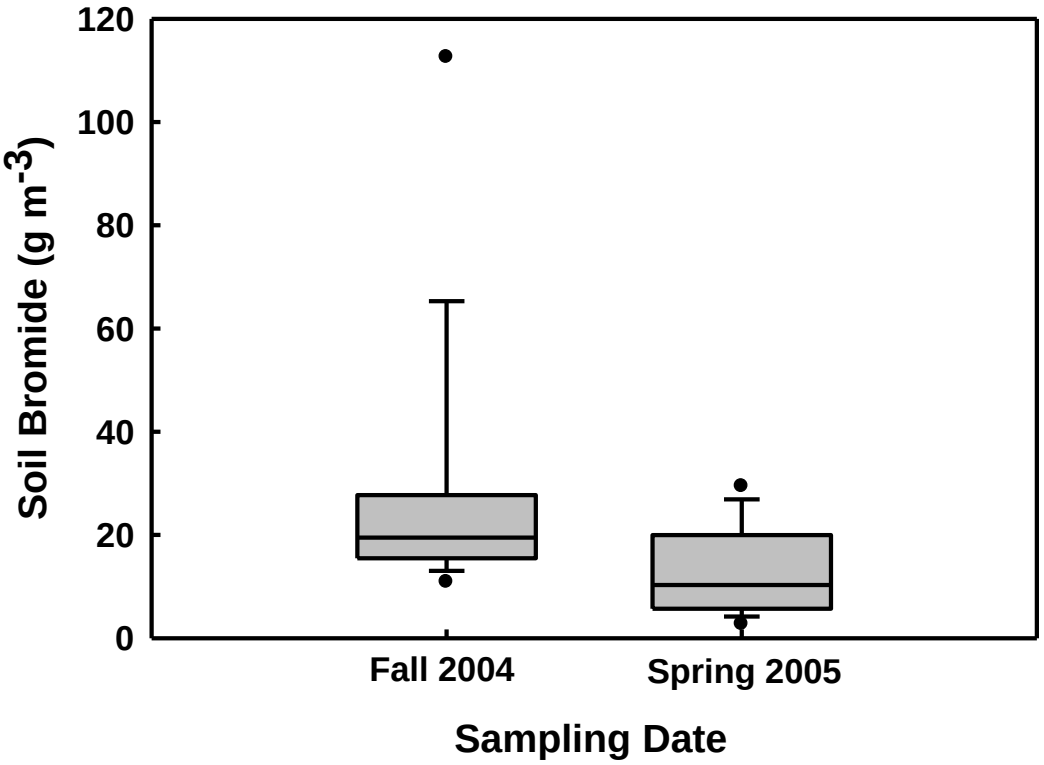

Figure 4.8 Change in soil bromide concentrations at the 0-0.15 m sampling depth from fall 2004 to spring 2005. Box plot illustrates the median, 10th, 25th, 75th, and 90th percentiles. Outliers are shown as black circular dots. Concentration distributions were significantly different at α=0.05 according to the Wilcoxon Rank Sum Test (n= 15).

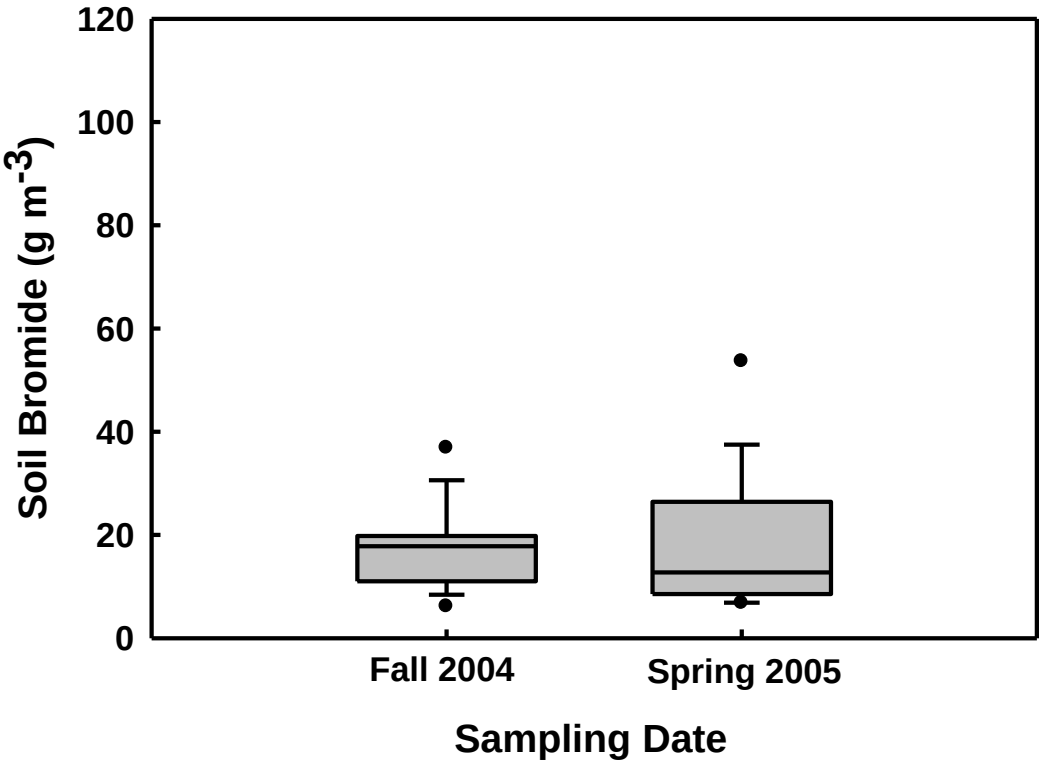

Figure 4.9 Change in soil bromide concentrations at the 0.15-0.35 m sampling depth from fall 2004 to spring 2005. Box plot illustrates the median, 10th, 25th, 75th, and 90th percentiles. Outliers are shown as black circular dots. Results were not statistically different at α=0.05 according to the Wilcoxon Rank Sum Test (n= 15).

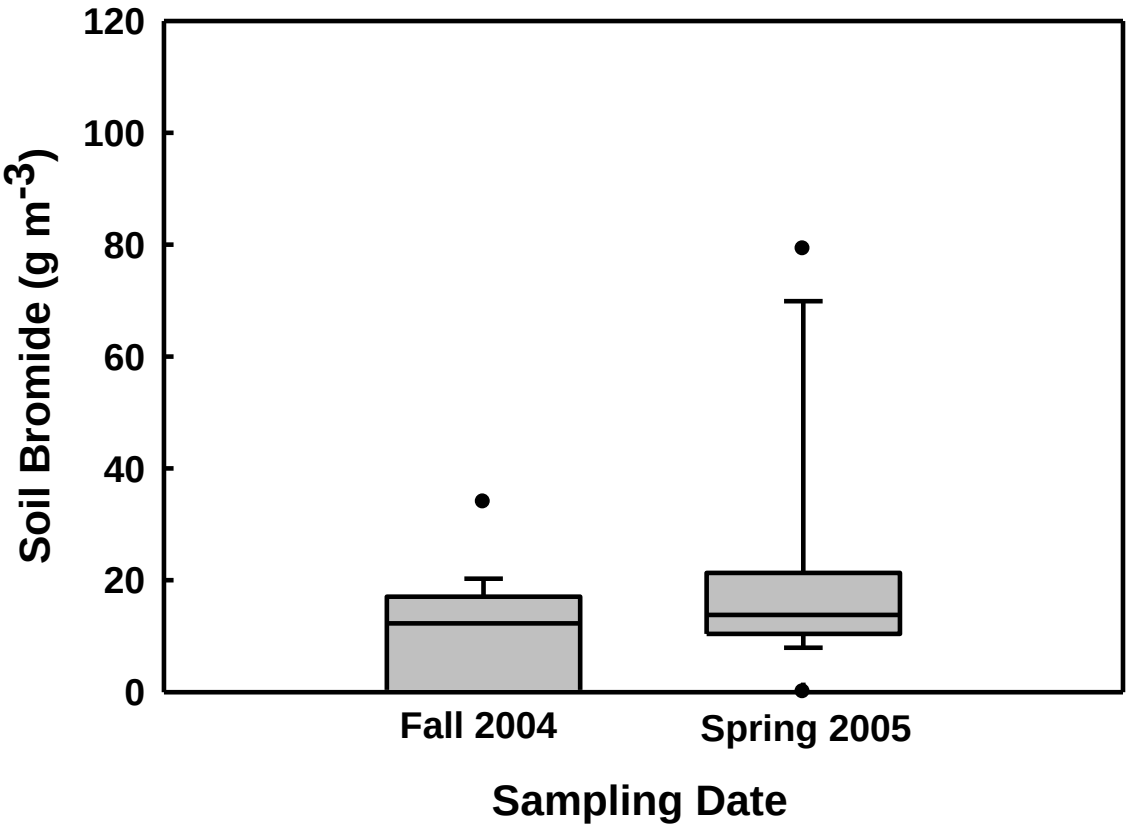

Figure 4.10 Change in soil bromide concentrations at the 0.35-0.50 m sampling depth from fall 2004 to spring 2005. Box plot illustrates the median, 10th, 25th, 75th, and 90th percentiles. Outliers are shown as black circular dots. Concentration distributions were significantly different at α=0.05 according to the Wilcoxon Rank Sum Test (n= 15).

indicative of solutes being transported from upper to lower soil horizons. This was further supported by the non-significant difference in Br^- concentrations at the 0.15-0.35 m depth, as this depth would likely have experienced both a loss and gain of soil solutes. The losses and gains of solutes from the middle depth likely counteracted each other and result in a relatively similar distribution from the fall to spring.

As expected, the comparison of soil Cl^- concentrations from fall to spring showed no significant changes in the population distributions at α=0.05 for any depth. The large variability in the data and the influence of background Cl^- served to mask the true transport of the applied tracer.

The total mass of Br^- tracer measured at each sampling location was calculated and is presented in Tables 4.1 and 4.2 for the fall and spring sampling periods, respectively. This data was not presented for the Cl^- tracer as the background concentrations of Cl^- could not be separated from the mass of the applied tracer. The percentage of Br^- recovered up to 1 m downslope from the source in the fall of 2004 was 18, 24, and 37%, for the A, C, and I segments, respectively. In spring of 2005, the percentages recovered changed to 10%, 24%, and 45% for A, C, and I segments, respectively. For Segment A, there was a significant reduction in the amount of Br^- measured between the fall and spring sampling periods at α=0.05. Conversely, there was no significant change for concentrations determined in Segment C while there was more mass of Br^- measured at Segment I (although it was insignificant statistically).

The spring samples collected in each segment were taken approximately 0.05 m east of the samples collected in fall due to the destructive nature of soil sampling. As such, the mass recovery results suggested that there may have been an initial non-uniform application of NaBr and/or differences in micro topography that resulted in disparities in solute transport and related mass recovery, such that sampling in the middle of each segment was not representative of mean soil solute concentrations. The relatively low percentages of overall tracer recovered were also concerning, suggesting that much of the applied Br^- had already passed 1m in distance downslope. Modeling of the lateral flux by Kelln et al. (2008) was estimated in the

Table 4.1 Mass of bromide ions determined in soil samples downslope of initial tracer application, as measured in September 2004.

	Sampling Location		
Distance Downslope	Segment A	Segment C	Segment I
m	g		
Source (0)	40	43	94
0.2	24	21	92
0.4	23	32	43
0.6	26	27	16
0.8	12	34	27
1.0	17	27	13
Total Mass	140	180	280
Percent (%) of Tracer Applied	18	24	37

Table 4.2 Mass of bromide ions determined in soil samples downslope of initial tracer application, as measured in June 2005.

	Sampling Location		
Distance Downslope	Segment A	Segment C	Segment I
m	g		
Source (0)	17	95	89
0.2	11	16	64
0.4	10	16	67
0.6	13	23	51
0.8	6.0	22	40
1.0	15	16	38
Total Mass	72	190	350
Percent (%) of Tracer Applied	10	24	45

range of 0.7-3 m year^{-1} however good agreement was only obtained near the upper end of the estimation.

4.3.2 Subsurface water chemistry

Eight shallow monitoring wells, used to collect subsurface water flowing along the cover-shale interface, were located downslope of the site of the initial tracer application. Wells 21, 22, 25 and 26 were located below the site of the NaBr application while wells 19, 20, 23, and 24 were below the source of NaCl. Soil water chemistry for samples taken from these wells is presented in Table 4.3 for the wells located downslope of the NaBr application. Soil water chemistry for Cl^- was not presented as the background Cl^- contributions could not be separated from the applied NaCl tracer.

Within Table 4.3, only 4 water quality results for Br^- are listed. Since installation, the shallow monitoring wells were monitored daily for the collection of subsurface water. When samples were present, water chemistry analysis was performed. However, in the years since installation there were only 10 occurrences when water was present in wells 21, 22, 25, and/or 26. The lack of soil water collected in the wedges was contributed to minimal amounts of water flowing along the shale-soil cover interface at these locations rather than due to instrument failure as several successful water samples were gathered. Within the 10 results for water quality, only 4 samples had detectable levels of Br^-.

These results showed that by May 2005 Br^- was being transported in soil water along the shale – soil cover interface. Bromide was not present in the soil prior to the application of NaBr, further confirming that flow during the spring melt was responsible for transporting solutes vertically and laterally downslope. No data was included for dates following the 2005 growing season. The presence of Br^- in wells 22 and 26, both of which are located 2 m downslope of the source, showed that Br^- had indeed traveled further downslope than the soil sampling program was able to characterize. Higher concentrations of Br^- in wells 22 and 26 compared to those located closer to the source, suggested that the rising limb of the solute breakthrough curve may have already passed 2 m in distance from the source.

Table 4.3 Bromide concentrations in subsurface water as collected in downslope shallow monitoring wells.

Location	Date of Sample Collection	Bromide Concentration
		——— mg L^{-1} ———
SW-21	May 8, 2005	3.3
SW-22	May 8, 2005	4.8
SW-25	May 8, 2005	5.5
SW-26	May 8, 2005	7.8

4.4 Conclusions

Vertical and lateral solute transport processes were studied within a reclamation soil cover capping saline-sodic shale using a 2 year tracer study. Approximately 1 year following tracer application, soil sampling determined the majority of applied Br^- had been leached vertically within the soil profile and/or transported downslope. At this time, concentrations of Br^- were greatest in the upper 0.15 m of the soil. By the following spring, this trend was reversed and concentrations of Br^- were highest at the base of the soil cover. Based on these observations, it was hypothesized that matrix flow during the spring melt, combined with matrix flow and / or preferential flow during summer and fall periods, was responsible for leaching Br^-. Subsurface flow at the cover-shale interface in response to the spring melt or subsurface flow at the peat mix-glacial soil interface due to differences in hydraulic conductivity was assumed to be responsible for the lateral transport of Br^-. Following translocation and cessation of subsurface flow, Br^- then migrated into the overlying soil, as a result of diffusive or advective processes.

The 2 year tracer study has therefore determined that solute transport processes occurring within the landscape are complicated and interrelated. While flow processes were described successively, they are recognized as occurring simultaneously within the soil profile. Thus, solutes within the soil profile are continuously subjected to downward, lateral, and upward mechanisms of transport. To conclude, it is apparent that both vertical and lateral flow processes have important implications on water and solute transport within the reconstructed landscape.

5. CONCLUSIONS AND RECOMMENDATIONS

5.1 Summary

Mining the Athabasca oil sands provides a crucial supply of oil to the global energy market and brings with it the need for successful reclamation practices. Following surface mining of the oil sands, highly saline and sodium saturated shales form large volumes of waste material. Current reclamation practices cover the saline-sodic shale with glacial and peat mix soil layers in an effort to reduce the risk of salt redistribution within the landscape. However, despite the soil cover, research has shown that these salts are diffusing upwards into the soil thereby threatening the success of reclamation practices and posing a risk to the ecosystem. The recognition that preferential flow can dramatically affect the mobility of contaminants within the environment has highlighted the need for site-specific research on this mechanism of water and solute transport. As such, the overall objective of this thesis was to examine the existence of preferential flow in reclamation soil covers and assess the impact of this flow on salt redistribution within the reconstructed landscape.

To characterize the susceptibility of the soil covers to preferential flow, the MIM of solute transport was combined with adsorptive dye tracer experiments to characterize solute transport in the soil matrix and soil macropores. Breakthrough patterns obtained during the MIM experiments provided evidence of the early arrival and extended tailing of solutes. Combined with large computed values for the immobile water fraction and high rates of diffusive mass transfer, the MIM results indicate that preferential flow was an important hydrological process governing solute transport in the peat mix soil. Results from adsorptive dye experiments further support this conclusion. Preferential flow as macropore flow, fingering, and / or funneling was observed at each test plot. There was also evidence of large diffusive transfer of solutes into immobile regions within the peat mix. Moreover, the large variability in solute breakthrough and stained flow patterns shows that there is a large spatial variability to flow processes. Therefore, the principal findings of this

study are that the reclamation soil covers are particularly susceptible to preferential flow and that the spatial variability in flow processes may impact salt leaching.

To better understand the effects of vertical and lateral flow processes on solute transport within reconstructed landscapes, conservative tracers were applied to the landscape and monitored over a two year period. Based on observations of vertical leaching, lateral translocation downslope, and upwards movement into overlying soil, it was determined that soil solutes were subjected to downward, lateral, and upward mechanisms of transport. It is speculated that matrix flow during the spring melt, combined with matrix flow and / or preferential flow during summer and fall periods, was responsible for the vertical leaching of solutes. In response to the spring melt or differences in soil layer hydraulic conductivities, subsurface flow generated at layer interfaces was assumed to be responsible for the lateral transport of solutes downslope. Following translocation and the cessation of subsurface flow, soil solutes could then be transported upwards into the overlying soil, as a result of diffusive or advective processes. It is therefore apparent that both vertical and lateral flow processes have important implications on water and solute transport within the reconstructed landscape.

The studies presented in this thesis were designed to test the hypotheses that preferential flow would be an important mechanism of solute transport within the reconstructed landscape and that preferential flow would restrict the vertical and horizontal flushing of salts. Results from the MIM and adsorptive dye experiments confirm the first hypothesis. As predicted, preferential flow was determined to be an important mechanism of solute transport in the reclamation soil covers. Furthermore, the presence of preferential flow was determined to be ubiquitous across the landscape. Results from the two year tracer study do not, however, validate the second hypothesis. Rather, it was observed that despite the existence of preferential flow, there are many other mechanisms of solute transport which serve to leach and flush salts from the soil profile. Moreover, the MIM experiments found preferential flow to be associated with large immobile regions and high rates of mass transfer, indicating that there would be a large interaction with soil solutes such that the flushing of salts may in fact be aided by preferential flow.

5.2 Implications for Design

A goal of this research has been to provide suggestions for the best design of reclamation soil covers such that long-term environmental sustainability of reconstructed landscapes can be achieved. One way to accomplish this would be to limit the amount of salts accumulating in the plant root zone by ensuring the flushing of soil solutes. Preferential flow, which has the potential to reduce the leaching of salts due to its selective nature, was identified as being prevalent throughout the reconstructed landscape. However, vertical flow through the soil matrix combined with lateral transport due to subsurface flow was found to significantly leach and flush salts from the reclamation soil covers. Furthermore, the observed preferential flow was associated with large immobile regions and high rates of mass transfer, indicating that there would be a large interaction with soil solutes such that the flushing of salts may in fact be aided by preferential flow. Therefore, current mechanisms of water transport are acting to attenuate the accumulation of salts in the plant root zone.

Another way to limit the amount of salts accumulating in the plant root zone is to increase the soil cover thickness such that there is a greater distance between the cover-shale interface and the plant root zone. Stained flow patterns from the dye tracer experiments highlighted that macropores from plant roots frequently exceeded 0.4 m in soil depth. These findings suggest that the plant root zone may currently be in direct contact with the highly saline pore water found at the interface of the 0.35-m and 0.50-m covers. Moreover, dye patterns at the middle slope position of the 1-m cover showed two plant-related macropores that neared 1m in depth. Soil cover thicknesses of at least 1 m are therefore recommended. It is also important to note that the depth of the plant root zone will change in response to the succession of vegetative communities as the landscape evolves.

Finally, the existence of preferential flow paths within the reclamation soil covers will also have impacts on the evapotranspiration and aeration of the reconstructed landscape. Preferential flow paths increase soil water storage at depth, thereby reducing evapotranspiration and increasing the plant available water supply.

Preferential flow channels are also empty most of the time, thus leading to better aeration within the soil.

5.3 Recommendations for Future Research

To enhance the understanding of water and solute transport mechanisms in soil, it is recommended that further research be carried out in the areas of snowmelt infiltration and the evolution of preferential flowpaths with time. For example, observations within this study have suggested that a portion of meltwater infiltrates the soil matrix of peat mix when the ground is frozen. These observations are supported by other findings in literature where organic surface layers become porous as a result of desiccation by upward vapor flux. Kelln et al. (2007) concluded that meltwater infiltration within the soil cover is, however, governed by preferential flowpaths as infiltration into the soil matrix is restricted due to the presence of ice in soil pores. As such, there is a need to further investigate how meltwater is transported within the soil covers prior to and during the spring snowmelt to better understand water and solute transport through frozen ground.

Moreover, soil covers are in the early stages of structure development following placement in the reconstructed landscape. As the years go by, physical processes such as freeze-thaw and shrink-swell cycles will begin to influence soil pore development. Once vegetative communities are established on the soil covers, biological processes such as root decay or insect or animal activity will further influence the development of soil structure. It is therefore important to recognize that soil structure within reconstructed landscapes is evolving in time such that preferential flowpaths which exist one year may be replaced by three more the following year. The evolution of soil structure in recently reconstructed landscapes thus necessitates research into how preferential flowpaths develop in the many years subsequent to cover placement.

5.4 Lessons Learned

The data presented in this thesis has taken many years to come to fruition. Over these years there have been many lessons learned, a few of which are outlined below for the benefit of others performing similar research.

The inception of this project occurred in 2003 with another graduate student responsible for the preliminary experimental design. I took over the program in January 2004 and thus inherited certain aspects of the study design. For example, NaCl was used as a tracer of solute movement in soil in which naturally occurring Cl^- was present in highly variable concentrations (Chapter 4). As such, concentrations of soil Cl^- could not provide significant data on the mechanisms of solute transport. It is therefore imperative to first research the study site, and then choose a tracer that can be easily discerned from background concentrations.

Soil chemistry results from the September 2004 sampling program were also not available prior to the June 2005 soil sampling. Had they been pre-determined, it would have been evident that Br^- had traveled further downslope than the soil sampling program was measuring. As such, soil sampling locations could have been revised the following year to better evaluate solute transport. Therefore, in studies employing successive sampling, it would be beneficial to have analyzed the first set of results prior to the collecting the second set of samples.

Furthermore, in studies in which tracer transport is monitored in situ over an extended period, it would be beneficial to increase the frequency of sampling to better coincide with important climatic events. For example, it would have been valuable to obtain transport data in the fall and spring immediately following tracer application to better characterize the influence of matrix flow and the spring snowmelt on solute transport. Ideally, this sampling frequency would have been repeated for the duration of the study to best determine mechanisms of solute transport.

6. REFERENCES

Al-Jabri S.A, R. Horton, D.B. Jaynes, and A.Gaur. 2002. Field determination of soil hydraulic and chemical transport properties. Soil Sci. 167:353-368.

Alletto L., Y. Coquet, P. Vachier, and C. Labat. 2006. Hydraulic conductivity, immobile water content, and exchange coefficient in three soil profiles. Soil Sci. Soc. Am. J. 70:1272-1280.

Barbour, S. L., D. Chapman, C. Qualizza, S. Kessler, C. Boese, R. Shurniak, G. Meiers, M. O'Kane, J. Hendry, and S. Wall. 2004. Tracking the evolution of reclaimed landscapes through the use of instrumented watersheds - a brief history of the Syncrude Southwest 30 overburden reclamation research program. In: International Instrumented Watershed Symposium (Edmonton, Canada, June 22-25).

Bear, J. 1972. Dynamics of fluids in porous media. Elsevier, New York.

Beven, K.J., and P. Germann. 1982. Macropores and water flow in soils. Water Resour. Res. 18:1311-1325.

Boese, C.D. 2003. The design and installation of field instrumentation program for the evaluation of soil-atmosphere water fluxes in a vegetated cover over saline/sodic shale overburden. M.Sc. Thesis. Univ. of Saskatchewan, Saskatoon.

Booltink, H.W.G., R. Hatano, and J. Bouma. 1993. Measurement and simulation of bypass flow in a structured clay soil - a physicomorphological approach. J. Hydrol. 148:149-168.

Booltink, H.W.G., and J. Bouma. 1991. Physical and morphological characterization of bypass flow in a well-structured clay soil. Soil Sci. Soc. Am. J. 55:1249-1254.

Buczko, U., O. Bens, and R.F. Huttl. 2006. Tillage effects on hydraulic properties and macroporosity in silty and sandy soils. Soil Sci. Soc. Am. J. 70:1998-2007.

Butters, G.L., W.A. Jury, and F.F. Ernst. 1989. Field scale transport of bromide in an unsaturated soil, 1. Experimental methodology and results. Water Resour. Res. 25:1575-1581.

Buttle, J.M., and D.J. McDonald. 2002. Coupled vertical and lateral preferential flow on a forested slope. Water Resour. Res. 38:1-17.

Camobreco, V.J., B.K. Richards, T.S. Steenhuis, J.H. Peverly, and M.B. McBride. 1996. Movement of heavy metals through undisturbed and homogenized soil columns. Soil Sci. 161:740-750.

Carey, S. and M. Woo. 2001. Slope runoff processes and flow generation in a subarctic, subalpine catchment. J. Hydrol. 253:110-129.

Casey, F. X. M., S.D. Logsdon, R. Horton, and D.B. Jaynes. 1998. Measurement of field soil hydraulic and solute transport parameters. Soil Sci. Soc. Am. J. 62:1172-1178.

Cassel, D.K. 1971. Water and solute movement in Svea loam for 2 water management regimes. Soil Sci. Soc. Am. Proc. 35:859-.

Chen, C., and R.J. Wagenet. 1992. Simulation of water and chemicals in macropore soils 1. Representation of the equivalent macropore influence and its effect on soil water flow. J. Hydrol. 130:105-126.

Coats, K.H., and B.D. Smith. 1964. Dead-end pore volume and dispersion in porous media. SPE Journal 46:73-84.

Collins R, A. Jenkins, and M. Harrow. 2000. The contribution of old and new water to a storm hydrograph determined by tracer addition to a whole catchment. Hydrol. Processes 14: 701-711.

Comegna, V., A. Coppola, and A. Sommella. 1999. Nonreactive solute transport in variously structured soil materials as determined by laboratory-based time domain reflectometry (TDR). Geoderma 92:167-184.

Dalton, F.N., W.N. Herkelrath, D.S. Rawlins, and J.D. Rhoades. 1984. Time domain reflectometry – simultaneous measurement of soil water content and electrical conductivity with a single probe. Science 224: 989-990.

Davis, S.N., G.M. Thompson, H.W. Bentley, and G. Stiles. 1980. Ground water tracers - A short review. Ground Water 18:14-23.

de Rooij, G.H. 2000. Modeling fingered flow of water in soils owing to wetting front instability: a review. J. Hydrol. 231:277-294.

Dingman, S.L. 2002. Physical hydrology. 2nd ed. Prentice-Hall, Inc., New Jersey.

Dunne, T. 1983. Relation of field study and modeling in the prediction of storm flow. J. Hydrol. 65:25-48.

Dunne, T.and R.D. Black. 1970. Partial area contributions to storm runoff in a small New England watershed. Water Resour. Res. 6:1296-1311.

Elshorbagy, A., A. Jutla, S.L. Barbour, and J. Kells. 2005. System dynamics approach to assess the sustainability of reclamation of disturbed watersheds. Can. J. Civ. Eng. 32:144-158.

Everts, C.J., R.S. Kanwar, E.C. Alexander, and S.C. Alexander. 1989. Comparison of tracer mobilities under laboratory and field conditions. J. Environ. Qual. 18:491-498.

Fetter, C.W. 1999. Contaminant hydrogeology. Prentice-Hall, Inc., New Jersey.

Feyen, H., H. Wunderli, H. Wydler, and A. Papritz. 1999. A tracer experiment to study flow paths of water in a forest soil. J. Hydrol. 225:155-167.

Feyen, J., D. Jacques, A. Timmerman, and J. Vanderborght. 1998. Modeling water flow and solute transport in heterogeneous soils: A review of recent approaches. J. Agric. Eng. Res.70:231-256.

Flury, M., and H. Fluhler. 1994. Brilliant blue FCF as a dye tracer for solute transport studies – a toxicological review. J. Environ. Qual. 23:1108-1112.

Flury, M., and H. Fluhler. 1995. Tracer characteristics of brilliant blue fcf. Soil Sci. Soc. Am. J. 59:22-27.

Flury, M., and N.N. Wai. 2003. Dyes as tracers for vadose zone hydrology. Reviews of Geophysics 41.

Flury, M., H. Fluhler, W.A. Jury, and J. Leuenberger. 1994. Susceptibility of soils to preferential flow of water - a field-study. Water Resour. Res. 30:1945-1954.

Forrer I, A. Papritz, R. Kasteel, H. Fluhler, and D. Luca. 2000. Quantifying dye tracers in soil profiles by image processing. Euras. Soil Sci. 51:313-322.

Freeze, R.A. 1972. Role of subsurface flow in generating surface runoff. 1. Base flow contributions to channel flow. Water Resour. Res. 8:609-623.

Gamerdinger, A.P., R.J. Wagenet, and M.T. van Genuchten. 1990. Application of 2 site 2 region models for studying simultaneous nonequilibrium transport and degradation of pesticides. Soil Sci. Soc. Am. J. 54:957-963.

Ghodrati, M., and W.A. Jury. 1990. A field-study using dyes to characterize preferential flow of water. Soil Sci. Soc. Am. J. 54:1558-1563.

Ghodrati, M., and W.A. Jury. 1992. A field-study of the effects of soil structure and irrigation methods on preferential flow of pesticides in unsaturated soil. J. Contam. Hydrol. 11:101-125.

Glass, R.J., J.Y. Parlange, and T.S. Steenhuis. 1989. Wetting front instability. I. Theoretical discussion and dimensional analysis. Water Resour. Res. 25:1187-1194.

Glass, R.J., T.S. Steenhuis, and J.Y. Parlange. 1988. Wetting front instability as a rapid and far-reaching hydrologic process in the vadose zone. J. Contam. Hydrol. 3:207-226.

Hill, D.E., and J.Y. Parlange. 1972. Wetting front instability in layered soils. Soil Sci. Soc. Am. Proc. 36:697-702.

Hillel, D., and R.S. Baker. 1988. A descriptive theory of fingering during infiltration into layered soils. Soil Sci. 146:51-56.

Hogg, T.J., and J.L. Henry. 1984. Comparison of 1:1 and 1:2 suspensions and extracts with the saturation extract in estimating salinity in Saskatchewan soils. Can. J. Soil Sci. 64:699-704.

Hornberger, G.M., P.F. Germann, and K.J. Beven. 1991. Throughflow and solute transport in an isolated sloping soil block in a forested catchment. J. Hydrol. 124:81-99.

Ilsemann J., R.R. van der Ploeg, R. Horton, and J. Bachmann. 2002. Laboratory method for determining immobile soil water content and mass exchange coefficient. J. Plant Nutr. Soil Sci. 165:332-338.

Jarvis, N. 2007. A review of non-equilibrium water flow and solute transport in soil macropores: principles, controlling factors and consequences for water quality. Euras. Soil Sci. 58:523-546.

Jaynes, D.B., S.D. Logsdon, and R. Horton. 1995. Field methods for measuring mobile/immobile water content and solute transfer rate coefficient. Soil Sci. Soc. Am. J. 59:352-356.

Ju, S.H., K.J.S. Kung, and C.S. Helling. 1997. Simulating impact of funnel flow on contaminant sampling. Soil Sci. Soc. Am. J. 61:427-435.

Jury, W.A., H. Elabd, and M. Resketo. 1986. Field study of napropamide movement through unsaturated soil. Water Resour. Res. 72:749-755.

Jury, W.A., W.R. Gardner, and W.H. Gardner. 1991. Soil physics. 5th ed. John Wiley & Sons, Inc., United States of America.

Kachanoski, R.G., E. Pringle, and A. Ward. 1992. Field measurement of solute travel times using time domain reflectometry. Soil Sci. Soc. Am. J. 56:47-52.

Kachanoski, R.G., J.L. Thony, M. Vauclin, G. Vachaud, and R. Laty. 1994. Measurement of solute transport during constant infiltration from a point source. Soil Sci. Soc. Am. J. 58:304-309.

Kelln, C., S. L. Barbour, and C. Qualizza. 2007. Preferential flow in a reclamation cover: hydrological and geochemical response. J. Geotech. Geoenviron. Eng. 133:1277-1289.

Kelln, C., S. L. Barbour, and C. Qualizza. 2008. Controls on the spatial distribution of soil moisture and solute transport in a sloping reclamation cover. Can. Geotech. J. 45:351-366.

Kessler, S. 2007. Salinity profiles in reconstructed soils over saline-sodic waste from the oil sands industry. M. Sc. Thesis. Univ. of Saskatchewan, Saskatoon.

Khan, A.U., and W.A. Jury. 1990. A laboratory study of the dispersion SCA column outflow experiments. J. Contam. Hydrol. 5: 119-131.

Kim, Y.J., C.J.G. Darnault, N.O. Bailey, J.Y. Parlange, and T.S. Steenhuis. 2005. Equation for describing solute transport in field soils with preferential flow paths. Soil Sci. Soc. Am. J. 69:291-300.

Kirkby, M.J. 1988. Hillslope runoff processes and models. J. Hydrol. 100:315-339.

Kladivko, E.J., G.E. Vanscoyoc, E.J. Monke, K.M. Oates, and W. Pask. 1991. Pesticide and nutrient movement into subsurface tile drains on a silt loam soil in Indiana. J. Environ. Qual. 20:264-270.

Kung, K.J.S. 1990a. Preferential flow in a sandy vadose zone: 1. Field observation. Geoderma 46:51-58.

Kung, K.J.S. 1990b. Preferential flow in a sandy vadose zone: 2. Mechanism and implications. Geoderma 46:59-71.

Kung, K.J.S., E.J. Kladivko, T.J. Gish, T.S. Steenhuis, G. Bubenzer, and C.S. Helling. 2000a. Quantifying preferential flow by breakthrough of sequentially applied tracers: Silt loam soil. Soil Sci. Soc. Am. J. 64:1296-1304.

Kung, K.J.S., T.S. Steenhuis, E.J. Kladivko, T.J. Gish, G. Bubenzer, and C.S. Helling. 2000b. Impact of preferential flow on the transport of adsorbing and non-adsorbing tracers. Soil Sci. Soc. Am. J. 64:1290-1296.

Lee, J., R. Horton, K. Noborio, and D.B. Jaynes. 2001. Characterization of preferential flow in undisturbed, structured soil columns using a vertical TDR probe. J. Contam. Hydrol. 51:131-144.

Li, Y.M., and M. Ghodrati. 1994. Preferential transport of nitrate through soil columns containing root channels. Soil Sci. Soc. Am. J. 58:653-659.

Luxmoore, R.J. 1981. Micro-, meso-, and macroporosity of soil. Soil Sci. Soc. Am. J. 45:671-672.

Mallants, D., M. Vanclooster, M. Meddahi, and J. Feyen. 1994. Estimating solute transport in undisturbed soil columns using time- domain reflectometry. J. Cont. Hydrol. 17: 91-109.

Mallants, D., M. Vanclooster, N. Toride, J. Vanderborght, M. T. van Genuchten, and J. Feyen. 1996. Comparison of three methods to calibrate TDR for monitoring solute movement in undisturbed soil. Soil Sci. Soc. Am. J. 60: 747-754.

McDonnell, J.J. 1990. A rationale for old water discharge through macropores in a steep, humid catchment. Water Resour. Res. 26:2821-2832.

McKnight, T.L. and D. Hess. 2005. Physical Geography: A landscape appreciation, Pearson Prentice-Hall, Upper Saddle River, N.J.

Meiers, G. P., S.L. Barbour, and C.V. Qualizza. 2003. The use of field measurements of hydraulic conductivity to characterize the performance of reclamation soil covers with time. Proc., 6th Int. Conf. on Acid Rock Drainage, International Network for Acid Prevention. Tehachapi, CA.

Meier, D. 2003. The deep hydrogeology of the SW overburden hill. M.Sc. Thesis. Univ. of Saskatchewan, Saskatoon.

Meier, G.P. 2002. Use of field measurements of hydraulic conductivity to characterize the performance of reclamation soil covers with time. M.Sc. Thesis. Univ. of Saskatchewan, Saskatoon.

Miyazaki, T. 1993. Water flow in soils. Marcel Dekker, Inc., New York, NY.

Morris, C., and S.J. Mooney. 2004. A high-resolution system for the quantification of preferential flow in undisturbed soil using observations of tracers. Geoderma 118:133-143.

Mosley, M.P. 1979. Streamflow generation in a forested watershed, New Zealand. Water Resour. Res. 15:795-806.

Nissen, H.H., P. Moldrup, and K.Henriksen. 1998. High-resolution time domain reflectometry coil probe for measuring soil water content. Soil Sci. Soc. Am. J. 62: 1203-1211.

Nkedi-Kizza, P., J.W. Biggar, H.M. Selim, M.T. van Genuchten, P.J. Weirenga, J.M. Davidson, and D.R. Nielsen. 1984. On the equivalence of two conceptual models for describing ion exchange during transport through an aggregated oxisol. Water Resour. Res. 20:1123-1130.

Nkedi-Kizza, P., J.W. Biggar, M.T. van Genuchten, P.J. Weirenga, H.M. Selim, J.M. Davidson, and D.R. Nielsen. 1983. Modeling tritium and chloride 36 transport through an aggregated oxisol. Water Resour. Res. 19:691-700.

Noguchi, S., Y. Tsuboyama, R.C. Sidle, and I. Hosoda. 1999. Morphological characteristics of macropores and the distribution of preferential flow pathways in a forested slope segment. Soil Sci. Soc. Am. J. 63:1413-1423.

Noguchi, S., Y. Tsuboyama, R.C. Sidle, and I. Hosoda. 2001. Subsurface runoff characteristics from a forest hillslope soil profile including macropores, Hitachi Ohta, Japan. Hydrol. Processes 15:2131-2149.

Ohrstrom P., M. Persson, J. Albergel, P. Zante, S. Nasri, R. Berndtsson, and J. Olsson. 2002. Field-scale variation of preferential flow as indicated from dye coverage. J. Hydrol. 257:164-173.

Ohrstrom P., Y. Hamed, M. Persson, and R. Berndtsson. 2004. Characterizing unsaturated solute transport by simultaneous use of dye and bromide. J. Hydrol. 289:23-35.

OSERN, Univ. of Alberta. 2004. Oil sands environmental research network [Online]. Available at http://www.osern.rr.ualberta.ca/vmssob.htm.

Parker, J.C. and M.T. van Genuchten. 1984. Flux-averaged and volume-averaged concentrations in continuum approaches to solute transport. Water Resour. Res. 20:866-872.

Pearce, A.J., M.K. Stewart, and M.G. Sklash. 1986. Storm runoff generation in humid headwater catchments. 1. Where does the water come from? Water Resour. Res. 22:1263-1272.

Philip, J.R. 1975. Stability analysis of infiltration. Soil Sci. Soc. Am. Proc. 39:1049-1053.

Price, A.G., and L.K. Hendrie. 1983. Water motion in a deciduous forest during snowmelt. J. Hydrol. 64:339-356.

Raats, P.A.C. 1973. Unstable wetting fronts in uniform and non-uniform soils. Soil Sci. Soc. Am. Proc. 37:681-685.

Rhoades, J.D. 1982. Soluble salts., *In* A. L. Page, R.H. Miller, and D.R. Keeney, ed. Methods of soil analysis. Part 2. Chemical and microbiological properties., 2nd ed. American Society of Agronomy, Wisconsin.

Ritsema, C.J., and L.W. Dekker. 1994. How water moves in a water repellent sandy soil .2. Dynamics of fingered flow. Water Resour. Res. 30:2519-2531.

Ritsema C.J., L.W. Dekker, J.L. Nieber, and T.S. Steenhuis. Modeling and field evidence of finger formation and finger recurrence in a water repellent sandy soil. Water Resour. Res. 34:555-567.

Saffigna, P.G., D.R. Kenney, and C.B. Tanner. 1977. Lysimeter and field measurements of chloride and bromide leaching in an uncultivated loamy sand. Soil Sci. Soc. Am. J. 41: 478–482.

Schwartz, R.C., K.J. McInnes, A.S.R. Juo, and C.E. Cervantes. 1999. The vertical distribution of a dye tracer in a layered soil. Soil Sci. 164:561-573.

Selker, J., T.S. Steenhuis, and J.Y. Parlange. 1992. Wetting front instability in homogenous sandy soils under continuous infiltration. Soil Sci. Soc. Am. J. 56:1346-1350.

Seo, Y., and J. Lee. 2005. Characterizing preferential flow of nitrate and phosphate in soil using time domain reflectometry. Soil Sci. 170:47-54.

Shurniak, R.E. 2003. Predictive modeling of moisture movement within soil cover systems for saline/sodic overburden piles. M.Sc. Thesis. Univ. of Saskatchewan, Saskatoon.

Sidle, R.C., S. Noguchi, Y. Tsuboyama, and K. Laursen. 2001. A conceptual model of preferential flow systems in forested hillslopes: evidence of self-organization. Hydrol. Processes 15:1675-1692.

Simunek, J., N.J. Jarvis, M.T. van Genuchten, and A. Gardenas. 2003. Review and comparison of models for describing non-equilibrium and preferential flow and transport in the vadose zone. J. Hydrol. 272:14-35.

Smettem, K.R.J., D.J. Chittleborough, B.G. Richards, and F.W. Leaney. 1991. The influence of macropores on runoff generation from a hillslope soil with a contrasting textural class. J. Hydrol. 122:235-252.

Smith, M.W., and C.R. Burn. 1987. Outward flux of vapor from frozen soils at Mayo, Yukon, Canada: results and interpretation. Cold Reg. Sci. Tech. 13: 143-152.

Steenhuis, T.S., J. Boll, G. Shalit, J.S. Selker, and I.A. Merwin. A simple equation for predicting preferential flow solute concentrations. J. Environ. Qual. 23:1058-1064.

Tamai, N., T. Asaeda, and C.G. Jeevaraj. 1987. Fingering in two-dimensional, homogenous, unsaturated porous media. Soil Sci. 144:107-112.

Till, A.R. and T.P. McCabe. 1976. Sulfur leaching and lysimeter characterization. Soil Sci. 121: 44–47.

Topp, G.C., J.L. Davis, A.P. Annan. 1980. Electromagnetic determination of soil water content: Measurement in coaxial cable lines. Water Resour. Res. 16:574-582.

Topp, G.C., J.L. Davis, A.P. Annan. 1982. Electromagnetic determination of soil water content using TDR 1. Applications to wetting fronts and steep gradients. Soil Sci. Soc. Am. J. 46:672-684.

Topp, G.C., and J.L. Davis. 1985. Measurement of soil water content using time-domain reflectometry (TDR) – a field evaluation. Soil Sci. Soc. Am. J. 49:19-24.

Toride, N., F.J. Leij, and M. Th. van Genuchten. 1999. The CXTFIT code for estimating transport parameters from laboratory or field tracer experiments. Release 2.1. U.S. Salinity Laboratory Agricultural Research Service, U. S. Department of Agriculture, California.

Tsuboyama, Y., R.C. Sidle, S. Noguchi, and I. Hosoda. 1994. Flow and solute transport through the soil matrix and macropores of a hillslope segment. Water Resour. Res. 30:879-890.

Turton, D.J., D.R. Barnes, and J. de Jesus-Havar. 1995. Old and new water in subsurface flow from a forest soil block. J. Environ. Qual. 24:139-146.

vanClooster, M., D. Mallants, J. Diels, and J. Feyen. 1993. Determining local scale solute transport parameters using time domain reflectometry (TDR). J. Hydrol. 148: 93-107.

van Dam, J.C., J.M.H. Hendrickx, H.C. van Ommen, M.H. Bannink, M. Th. van Genuchten, and L.W. Dekker. 1990. Water and solute movement in a coarse-textured water repellent field soil. J. Hydrol. 120:359-379.

van Genuchten, M.T., and R.J. Wagenet. 1989. Two-site/two-region models for pesticide transport and degradation: theoretical development and analytical solutions. Soil Sci. Soc. Am. J. 53:1303-1310.

van Genuchten, M.T., and P.J. Wierenga. 1977. Mass transfer studies in sorbing porous media: III. Experimental evaluation with 2,4,5,-T. Soil Sci. Soc. Am. J. 41:278-285.

Wall, S.N. 2005. Characterizing geochemical reactions in the South Bison Hill overburden waste pile. M.Sc. Thesis. Univ. of Saskatchewan, Saskatoon.

Ward, A.L., R.G. Kachanoski, and D.L. Elrick. 1994. Laboratory measurements of solute transport using time domain reflectometry. Soil Sci. Soc. Am. J. 58:1031-1039.

Ward, A.L., R.G. Kachanoski, and D.L. Elrick. 1995. Analysis of water and solute transport away from a surface point source. Soil Sci. Soc. Am. J. 59:699-706.

Watson, K.W., and R.J. Luxmoore. 1986. Estimating macroporosity in a forested watershed by use of a tension infiltrometer. Soil Sci. Soc. Am. J. 50:578-582.

Weiler, M., and H. Fluhler. 2004. Inferring flow types from dye patterns in macroporous soils. Geoderma 120:137-153.

Weiler M., and F. Naef. 2003. An experimental tracer study of the role of macropores in infiltration in grassland soils. Hydrol. Processes 17:477-493.

Whipkey, R.Z. 1965. Subsurface storm flow from forested slopes. Bull. Int. Assoc. Sci. Hydrol. 10:25-33.

Wildenschild, D., K.H. Jensen, K. Villholth, and T.H. Illangasekare. 1994. A laboratory analysis of the effect of macropores on solute transport. Ground Water 32:381-389.

Wraith, J.M., S.D. Comfort, B.L. Woodbury, and W.P. Inskeep. 1993. A simplified wave-form analysis approach for monitoring solute transport using time-domain reflectometry. Soil Sci. Soc. Am. J. 57:637-642.

Yao, T.M., and J.M.H. Hendrickx. 1996. Stability of wetting fronts in dry homogeneous soils under low infiltration rates. Soil Sci. Soc. Am. J. 60:20-28.

APPENDIX A
NON-LINEAR LEAST SQUARES ANALYSIS FOR ESTIMATION OF TRANSPORT PARAMETERS

Table A1. 95% Confidence Limits for Analysis of Transport in C6 0.1 m Depth where q=0.002 m hr^{-1}.

NAME	VALUE	S.E.COEFF.	T-VALUE	LOWER	UPPER
D_m (m^2 hr^{-1})	2.4×10^{-1}	4.3×10^{2}	5.5×10^{-4}	-1.2×10^{3}	1.2×10^{3}
β (%)	2.2×10^{-3}	5.5×10^{-1}	4.0×10^{-3}	-1.5×10^{0}	1.5×10^{0}
α (h^{-1})	2.0×10^{0}	5.7×10^{1}	3.5×10^{-2}	-1.5×10^{-2}	1.6×10^{2}

Table A2. 95% Confidence Limits for Analysis of Transport in C16 0.1 m Depth where q=0.002 m hr^{-1}.

NAME	VALUE	S.E.COEFF.	T-VALUE	LOWER	UPPER
D_m (m^2 hr^{-1})	9.1×10^{-1}	1.9×10^{-2}	4.8×10^{1}	8.7×10^{-1}	9.5×10^{-1}
β (%)	9.7×10^{-2}	2.7×10^{-4}	3.6×10^{2}	9.6×10^{-2}	9.7×10^{-2}
α (h^{-1})	2.4×10^{-1}	8.5×10^{-3}	2.9×10^{1}	2.2×10^{-1}	2.6×10^{-1}

Table A3. 95% Confidence Limits for Analysis of Transport in C25 0.1 m Depth where q=0.002 m hr^{-1}.

NAME	VALUE	S.E.COEFF.	T-VALUE	LOWER	UPPER
D_m (m^2 hr^{-1})	1.1×10^{2}	5.8×10^{-2}	3.0×10^{1}	1.6×10^{0}	1.8×10^{0}
β (%)	4.2×10^{-2}	3.3×10^{-4}	1.5×10^{2}	4.9×10^{-2}	5.0×10^{-2}
α (h^{-1})	3.0×10^{-1}	1.4×10^{-2}	2.3×10^{1}	2.9×10^{-1}	3.5×10^{-1}

Table A4. 95% Confidence Limits for Analysis of Transport in C25 0.1 m Depth where q=0.010 m hr^{-1}.

NAME	VALUE	S.E.COEFF.	T-VALUE	LOWER	UPPER
D_m (m^2 hr^{-1})	1.5 x 10^0	1.7 x 10^{-1}	9.0 x 10^0	1.2 x 10^0	1.8 x 10^0
β (%)	1.1 x 10^{-1}	3.0 x 10^{-3}	3.8 x 10^1	1.1 x 10^{-1}	1.2 x 10^{-1}
α (h^{-1})	1.2 x 10^0	4.6 x 10^{-2}	2.6 x 10^1	1.1 x 10^0	1.3 x 10^0

Table A5. 95% Confidence Limits for Analysis of Transport in C3 0.1 m Depth where q=0.010 m hr^{-1}.

NAME	VALUE	S.E.COEFF.	T-VALUE	LOWER	UPPER
D_m (m^2 hr^{-1})	6.9 x 10^0	3.0 x 10^{-1}	2.3 x 10^1	6.3 x 10^0	7.5 x 10^0
β (%)	2.0 x 10^{-1}	4.2 x 10^{-3}	4.7 x 10^1	1.9 x 10^{-1}	2.1 x 10^{-1}
α (h^{-1})	1.5 x 10^{-1}	2.4 x 10^{-2}	5.9 x 10^0	9.5 x 10^{-2}	1.9 x 10^{-1}

Table A6. 95% Confidence Limits for Analysis of Transport in C25 0.1 m Depth where q=0.010 m hr^{-1}.

NAME	VALUE	S.E.COEFF.	T-VALUE	LOWER	UPPER
D_m (m^2 hr^{-1})	1.7 x 10^0	5.8 x 10^{-2}	3.0 x 10^1	1.6 x 10^0	1.8 x 10^0
β (%)	4.9 x 10^{-2}	3.3 x 10^{-4}	1.5 x 10^2	4.9 x 10^{-2}	5.0 x 10^{-2}
α (h^{-1})	3.3 x 10^{-1}	1.4 x 10^{-2}	2.3 x 10^1	3.0 x 10^{-1}	3.5 x 10^{-1}

APPENDIX B
SOIL WATER CHEMISTRY FROM SOIL SAMPLING PROGRAM

Table B1. Chloride and bromide concentrations (mg g^{-1} soil) measured in leachate water from the 2004/2005 soil sampling program - Segment A

Sample ID	Sample Depth	Sample Origin	Soil Material	Tracer Applied	2004			2005		
					Lab Cond (µS/cm)	Cl	Br	Lab Cond (µS/cm)	Cl	Br
A1	0-10 cm	Middle of Source	Peat Mix	NaBr	1395	63	14.1	463	25.0	BDL
A2	10-20 cm	Middle of Source	Peat Mix	NaBr	980	27	6.9	486	23.0	BDL
A3	20-30 cm	Middle of Source	Mineral Soil	NaBr	1520	31	13	759	29.0	5.4
A4	30-40 cm	Middle of Source	Shale Interface	NaBr	3130	33	BDL	1873	40.0	8.1
A5	40-50 cm	Middle of Source	Shale OB	NaBr	4090	46	BDL	3910	49.0	0.0
A6	0-15 cm	20 cm from Source	Peat Mix	NaBr	1794	75	33	960	31.0	9.1
A7	15-35 cm	20 cm from Source	Mineral Soil	NaBr	1383	27	28	1080	31.0	13.0
A8	35-45 cm	20 cm from Source	Shale OB	NaBr	3090	31	22	2810	39.0	17.0
A9	0-15 cm	40 cm from Source	Peat Mix	NaBr	660	28	24	630	24.0	6.2
A10	15-35 cm	40 cm from Source	Mineral Soil	NaBr	994	26	27	800	28.0	12.0
A11	35-45 cm	40 cm from Source	Shale OB	NaBr	2400	32	18	2820	38.0	17.0
A12	0-15 cm	60 cm from Source	Peat Mix	NaBr	1000	39	44	860	32.0	12.0
A13	15-35 cm	60 cm from Source	Mineral Soil	NaBr	1060	27	27	1110	30.0	16.0
A14	35-45 cm	60 cm from Source	Shale OB	NaBr	3420	47	22	2470	40.0	19.0
A15	0-15 cm	80 cm from Source	Peat Mix	NaBr	1215	39	26.4	730	25.0	7.7
A16	15-35 cm	80 cm from Source	Mineral Soil	NaBr	1290	26	18	1280	33.0	15.0
A17	35-45 cm	80 cm from Source	Shale OB	NaBr	4500	59	BDL	3450	65.0	0.0
A18	0-15 cm	100 cm from Source	Peat Mix	NaBr	1290	48	30	1140	42.0	16.8
A19	15-35 cm	100 cm from Source	Mineral Soil	NaBr	2170	42	30	1530	40.0	18.0
A20	35-45 cm	100 cm from Source	Shale OB	NaBr	4370	60	BDL	2580	48.0	13.0

* with 20 grams deionized water to 10 grams soil; samples filtered with 0.45µm

BDL - Below detection limit (<0.001).

Table B2. Chloride and bromide concentrations (mg g^{-1} soil) measured in leachate water from the 2004/2005 soil sampling program - Segment B

Sample ID	Sample Depth	Sample Origin	Soil Material	Tracer Applied	2004			2005		
					Lab Cond (µS/cm)	Cl	Br	Lab Cond (µS/cm)	Cl	Br
B1	0-10 cm	Middle of Source	Peat Mix	NaCl	678	30	BDL	520	18.0	BDL
B2	10-20 cm	Middle of Source	Peat Mix	NaCl	1650	66	BDL	550	23.0	BDL
B3	20-30 cm	Middle of Source	Mineral Soil	NaCl	1974	90	BDL	780	27.0	BDL
B4	30-40 cm	Middle of Source	Shale Interface	NaCl	1987	51	BDL	1560	36.0	BDL
B5	40-50 cm	Middle of Source	Shale OB	NaCl	4140	54	BDL	1090	10.0	BDL
B6	0-15 cm	20 cm from Source	Peat Mix	NaCl	907	39	BDL	930	31.0	BDL
B7	15-35 cm	20 cm from Source	Mineral Soil	NaCl	2187	75	BDL	1240	34.0	BDL
B8	35-45 cm	20 cm from Source	Shale OB	NaCl	3230	67	BDL	3220	58.0	BDL
B9	0-15 cm	40 cm from Source	Peat Mix	NaCl	993	48	BDL	920	28.0	BDL
B10	15-35 cm	40 cm from Source	Mineral Soil	NaCl	1342	42	BDL	1750	31.0	BDL
B11	35-45 cm	40 cm from Source	Shale OB	NaCl	3410	65	BDL	3540	38.0	BDL
B12	0-15 cm	60 cm from Source	Peat Mix	NaCl	1046	51	BDL	790	24.0	BDL
B13	15-35 cm	60 cm from Source	Mineral Soil	NaCl	1850	52	BDL	1000	31.0	BDL
B14	35-45 cm	60 cm from Source	Shale OB	NaCl	3800	84	BDL	2620	32.0	BDL
B15	0-15 cm	80 cm from Source	Peat Mix	NaCl	1030	43	BDL	630	24.0	BDL
B16	15-35 cm	80 cm from Source	Mineral Soil	NaCl	1471	55	BDL	1130	37.0	BDL
B17	35-45 cm	80 cm from Source	Shale OB	NaCl	3160	60	BDL	2990	56.0	BDL
B18	0-15 cm	100 cm from Source	Peat Mix	NaCl	980	54	BDL	860	37.0	BDL
B19	15-35 cm	100 cm from Source	Mineral Soil	NaCl	1356	77	BDL	1100	39.0	BDL
B20	35-45 cm	100 cm from Source	Shale OB	NaCl	3510	74	BDL	3500	65.0	BDL

* with 20 grams deionized water to 10 grams soil; samples filtered with 0.45µm

BDL - Below detection limit (<0.001).

Table B3. Chloride and bromide concentrations (mg g^{-1} soil) measured in leachate water from the 2004/2005 soil sampling program - Segment C

Sample ID	Sample Depth	Sample Origin	Soil Material	Tracer Applied	2004			2005		
					Lab Cond (µS/cm)	Cl	Br	Lab Cond (µS/cm)	Cl	Br
C1	0-10 cm	Middle of Source	Peat Mix	NaBr	470	28	3.8	195	52.0	10.4
C2	10-20 cm	Middle of Source	Peat Mix	NaBr	389	11	4.7	468	11.0	0.0
C3	20-30 cm	Middle of Source	Mineral Soil	NaBr	625	18	11	576	40.0	9.0
C4	30-40 cm	Middle of Source	Shale Interface	NaBr	982	25	11	434	64.0	24.8
C5	40-50 cm	Middle of Source	Shale OB	NaBr	2800	37	BDL	3400	51.0	18.0
C6	0-15 cm	10 cm from Source	Peat Mix	NaBr	N/A	N/A	N/A	280	32.0	9.2
C7	15-35 cm	10 cm from Source	Mineral Soil	NaBr	N/A	N/A	N/A	720	24.0	14.0
C8	35-45 cm	10 cm from Source	Shale OB	NaBr	N/A	N/A	N/A	2710	41.0	28.0
C9	0-15 cm	20 cm from Source	Peat Mix	NaBr	615	15	33	289	33.0	8.7
C10	15-35 cm	20 cm from Source	Mineral Soil	NaBr	1035	20	33	789	24.0	13.0
C11	35-45 cm	20 cm from Source	Shale OB	NaBr	2880	30	18	1998	36.0	18.0
C12	0-15 cm	30 cm from Source	Peat Mix	NaBr	N/A	N/A	N/A	258	32.0	9.2
C13	15-35 cm	30 cm from Source	Mineral Soil	NaBr	N/A	N/A	N/A	1161	28.0	29.0
C14	35-45 cm	30 cm from Source	Shale OB	NaBr	N/A	N/A	N/A	2660	44.0	37.0
C15	0-15 cm	40 cm from Source	Peat Mix	NaBr	860	23	44	703	26.0	11.0
C16	15-35 cm	40 cm from Source	Mineral Soil	NaBr	1500	27	46	829	28.0	19.0
C17	35-45 cm	40 cm from Source	Shale OB	NaBr	3100	31	24	2640	39.0	20.0
C18	0-15 cm	50 cm from Source	Peat Mix	NaBr	N/A	N/A	N/A	640	26.0	13.0
C19	15-35 cm	50 cm from Source	Mineral Soil	NaBr	N/A	N/A	N/A	1240	31.0	27.0
C20	35-45 cm	50 cm from Source	Shale OB	NaBr	N/A	N/A	N/A	3140	48.0	34.0

Table B3. Continued

Sample ID	Sample Depth	Sample Origin	Soil Material	Tracer Applied	2004			2005		
					Lab Cond (µS/cm)	Cl	Br	Lab Cond (µS/cm)	Cl	Br
C21	0-15 cm	60 cm from Source	Peat Mix	NaBr	793	29	36	880	30.0	19.0
C22	15-35 cm	60 cm from Source	Mineral Soil	NaBr	1200	36	33	1010	34.0	25.0
C23	35-45 cm	60 cm from Source	Shale OB	NaBr	3060	29	24	2760	42.0	26.0
C24	0-15 cm	70 cm from Source	Peat Mix	NaBr	N/A	N/A	N/A	450	32.0	16.0
C25	15-35 cm	70 cm from Source	Mineral Soil	NaBr	N/A	N/A	N/A	1370	43.0	21.0
C26	35-45 cm	70 cm from Source	Shale OB	NaBr	N/A	N/A	N/A	3730	69.0	24.0
C27	0-15 cm	80 cm from Source	Peat Mix	NaBr	953	38	72	810	29.0	13.0
C28	15-35 cm	80 cm from Source	Mineral Soil	NaBr	1070	40	33	1150	43.0	21.0
C29	35-45 cm	80 cm from Source	Shale OB	NaBr	2650	39	30	4460	70.0	25.0
C30	0-15 cm	90 cm from Source	Peat Mix	NaBr	N/A	N/A	N/A	790	32.0	19.0
C31	15-35 cm	90 cm from Source	Mineral Soil	NaBr	N/A	N/A	N/A	990	31.0	16.0
C32	35-45 cm	90 cm from Source	Shale OB	NaBr	N/A	N/A	N/A	4140	55.0	0.0
C33	0-15 cm	100 cm from Source	Peat Mix	NaBr	704	23	48	620	16.0	10.0
C34	15-35 cm	100 cm from Source	Mineral Soil	NaBr	730	23	33	820	30.0	22.0
C35	35-45 cm	100 cm from Source	Shale OB	NaBr	2420	37	29	3200	52.0	24.0

* with 20 grams deionized water to 10 grams soil; samples filtered with 0.45µm

BDL - Below detection limit (<0.001).

N/A - Not available. In 2005 the sampling program was expanded for segments C and D.

Table B4. Chloride and bromide concentrations (mg g^{-1} soil) measured in leachate water from the 2004/2005 soil sampling program - Segment D

Sample ID	Sample Depth	Sample Origin	Soil Material	Tracer Applied	2004			2005		
					Lab Cond (µS/cm)	Cl	Br	Lab Cond (µS/cm)	Cl	Br
D1	0-10 cm	Middle of Source	Peat Mix	NaCl	1725	114	BDL	530	35.0	BDL
D2	10-20 cm	Middle of Source	Peat Mix	NaCl	696	33	BDL	610	24.0	BDL
D3	20-30 cm	Middle of Source	Mineral Soil	NaCl	798	79	BDL	454	40.0	BDL
D4	30-40 cm	Middle of Source	Shale Interface	NaCl	1130	99	BDL	905	58.0	BDL
D5	40-50 cm	Middle of Source	Shale OB	NaCl	2080	110	BDL	2040	77.0	BDL
D6	0-15 cm	10 cm from Source	Peat Mix	NaCl	N/A	N/A	N/A	118	32.8	BDL
D7	15-35 cm	10 cm from Source	Mineral Soil	NaCl	N/A	N/A	N/A	1550	76.0	BDL
D8	35-45 cm	10 cm from Source	Shale OB	NaCl	N/A	N/A	N/A	3230	82.0	BDL
D9	0-15 cm	20 cm from Source	Peat Mix	NaCl	2112	219	BDL	189	34.8	BDL
D10	15-35 cm	20 cm from Source	Mineral Soil	NaCl	1344	97	BDL	1800	72.0	BDL
D11	35-45 cm	20 cm from Source	Shale OB	NaCl	2880	54	BDL	3340	66.0	BDL
D12	0-15 cm	30 cm from Source	Peat Mix	NaCl	N/A	N/A	N/A	340	42.0	4.0
D13	15-35 cm	30 cm from Source	Mineral Soil	NaCl	N/A	N/A	N/A	1180	73.0	BDL
D14	35-45 cm	30 cm from Source	Shale OB	NaCl	N/A	N/A	N/A	1690	62.0	4.8
D15	0-15 cm	40 cm from Source	Peat Mix	NaCl	1089	96	BDL	210	26.0	BDL
D16	15-35 cm	40 cm from Source	Mineral Soil	NaCl	1090	54	BDL	1940	84.0	BDL
D17	35-45 cm	40 cm from Source	Shale OB	NaCl	2460	51	BDL	3940	66.0	BDL
D18	0-15 cm	50 cm from Source	Peat Mix	NaCl	N/A	N/A	N/A	213	29.4	BDL
D19	15-35 cm	50 cm from Source	Mineral Soil	NaCl	N/A	N/A	N/A	1630	87.0	BDL
D20	35-45 cm	50 cm from Source	Shale OB	NaCl	N/A	N/A	N/A	3710	73.0	BDL

Table B4. Continued

Sample ID	Sample Depth	Sample Origin	Soil Material	Tracer Applied	2004 Lab Cond (µS/cm)	2004 Cl	2004 Br	2005 Lab Cond (µS/cm)	2005 Cl	2005 Br
D21	0-15 cm	60 cm from Source	Peat Mix	NaCl	576	46	BDL	154	36.4	BDL
D22	15-35 cm	60 cm from Source	Mineral Soil	NaCl	1051	47	BDL	1766	77.0	BDL
D23	35-45 cm	60 cm from Source	Shale OB	NaCl	2840	55	BDL	4030	82.0	BDL
D24	0-15 cm	70 cm from Source	Peat Mix	NaCl	N/A	N/A	N/A	560	37.0	BDL
D25	15-35 cm	70 cm from Source	Mineral Soil	NaCl	N/A	N/A	N/A	1566	72.0	BDL
D26	35-45 cm	70 cm from Source	Shale OB	NaCl	N/A	N/A	N/A	4130	75.0	BDL
D27	0-15 cm	80 cm from Source	Peat Mix	NaCl	1656	83	BDL	403	42.0	BDL
D28	15-35 cm	80 cm from Source	Mineral Soil	NaCl	1272	53	BDL	1266	56.0	BDL
D29	35-45 cm	80 cm from Source	Shale OB	NaCl	3990	63	BDL	3280	63.0	BDL
D30	0-15 cm	90 cm from Source	Peat Mix	NaCl	N/A	N/A	N/A	702	41.0	BDL
D31	15-35 cm	90 cm from Source	Mineral Soil	NaCl	N/A	N/A	N/A	1215	57.0	BDL
D32	35-45 cm	90 cm from Source	Shale OB	NaCl	N/A	N/A	N/A	2740	61.0	BDL
D33	0-15 cm	100 cm from Source	Peat Mix	NaCl	915	42	BDL	425	40.0	BDL
D34	15-35 cm	100 cm from Source	Mineral Soil	NaCl	1336	57	BDL	1553	56.0	BDL
D35	35-45 cm	100 cm from Source	Shale OB	NaCl	2850	57	BDL	3410	52.0	BDL

* with 20 grams deionized water to 10 grams soil; samples filtered with 0.45µm

BDL - Below detection limit (<0.001).

N/A - Not available. In 2005 the sampling program was expanded for segments C and D.

Table B5. Chloride and bromide concentrations (mg g^{-1} soil) measured in leachate water from the 2004/2005 soil sampling program - Segment H

Sample ID	Sample Depth	Sample Origin	Soil Material	Tracer Applied	2004			2005		
					Lab Cond (µS/cm)	Cl	Br	Lab Cond (µS/cm)	Cl	Br
H1	0-10 cm	Middle of Source	Peat Mix	NaCl	420	16	BDL	426	18.0	BDL
H2	10-20 cm	Middle of Source	Peat Mix	NaCl	405	9	BDL	204	22.0	BDL
H3	20-30 cm	Middle of Source	Mineral Soil	NaCl	839	8	BDL	187	95.0	BDL
H4	30-40 cm	Middle of Source	Shale Interface	NaCl	2100	9	BDL	2030	13.0	BDL
H5	40-50 cm	Middle of Source	Shale OB	NaCl	2760	14	BDL	3310	17.0	BDL
H6	0-15 cm	20 cm from Source	Peat Mix	NaCl	3090	64	BDL	630	13.0	BDL
H7	15-35 cm	20 cm from Source	Mineral Soil	NaCl	1220	40	BDL	780	25.0	BDL
H8	35-45 cm	20 cm from Source	Shale OB	NaCl	685	33	BDL	2500	38.0	BDL
H9	0-15 cm	40 cm from Source	Peat Mix	NaCl	2370	52	BDL	230	22.8	BDL
H10	15-35 cm	40 cm from Source	Mineral Soil	NaCl	824	30	BDL	780	27.0	BDL
H11	35-45 cm	40 cm from Source	Shale OB	NaCl	703	27	BDL	2560	32.0	BDL
H12	0-15 cm	60 cm from Source	Peat Mix	NaCl	576	20	BDL	390	22.0	BDL
H13	15-35 cm	60 cm from Source	Mineral Soil	NaCl	736	22	BDL	810	33.0	BDL
H14	35-45 cm	60 cm from Source	Shale OB	NaCl	2060	39	BDL	2460	195.0	BDL
H15	0-15 cm	80 cm from Source	Peat Mix	NaCl	834	63	BDL	106	7.0	BDL
H16	15-35 cm	80 cm from Source	Mineral Soil	NaCl	844	31	BDL	1243	36.0	BDL
H17	35-45 cm	80 cm from Source	Shale OB	NaCl	2380	39	BDL	3170	42.0	BDL
H18	0-15 cm	100 cm from Source	Peat Mix	NaCl	920	58	BDL	720	27.0	BDL
H19	15-35 cm	100 cm from Source	Mineral Soil	NaCl	1455	35	BDL	677	28.0	BDL
H20	35-45 cm	100 cm from Source	Shale OB	NaCl	2530	31	BDL	1983	33.0	BDL

* with 20 grams deionized water to 10 grams soil; samples filtered with 0.45µm

BDL - Below detection limit (<0.001).

Table B6. Chloride and bromide concentrations (mg g^{-1} soil) measured in leachate water from the 2004/2005 soil sampling program - Segment I

Sample ID	Sample Depth	Sample Origin	Soil Material	Tracer Applied	2004			2005		
					Lab Cond (µS/cm)	Cl	Br	Lab Cond (µS/cm)	Cl	Br
I1	0-10 cm	Middle of Source	Peat Mix	NaBr	650	16	7.8	584	14.0	BDL
I2	10-20 cm	Middle of Source	Peat Mix	NaBr	418	11	18	327	11.0	BDL
I3	20-30 cm	Middle of Source	Mineral Soil	NaBr	1154	10	21	193	22.0	BDL
I4	30-40 cm	Middle of Source	Shale Interface	NaBr	2840	12	19	1830	9.8	7.6
I5	40-50 cm	Middle of Source	Shale OB	NaBr	3710	15	18	3460	13.0	20.0
I6	0-15 cm	20 cm from Source	Peat Mix	NaBr	888	16	160	590	15.0	12.0
I7	15-35 cm	20 cm from Source	Mineral Soil	NaBr	874	11	92	520	13.0	22.0
I8	35-45 cm	20 cm from Source	Shale OB	NaBr	3480	14	83	1730	14.0	59.0
I9	0-15 cm	40 cm from Source	Peat Mix	NaBr	700	16	75	467	13.0	8.6
I10	15-35 cm	40 cm from Source	Mineral Soil	NaBr	728	14	36	642	16.0	46.0
I11	35-45 cm	40 cm from Source	Shale OB	NaBr	3030	17	17	2410	18.0	52.0
I12	0-15 cm	60 cm from Source	Peat Mix	NaBr	617	13	39	520	15.0	16.0
I13	15-35 cm	60 cm from Source	Mineral Soil	NaBr	688	21	23	540	15.0	29.0
I14	35-45 cm	60 cm from Source	Shale OB	NaBr	3400	19	BDL	2140	20.0	29.0
I15	0-15 cm	80 cm from Source	Peat Mix	NaBr	750	18	65	550	15.0	20.0
I16	15-35 cm	80 cm from Source	Mineral Soil	NaBr	715	15	22	630	20.0	29.0
I17	35-45 cm	80 cm from Source	Shale OB	NaBr	3330	19	BDL	2620	21.0	14.0
I18	0-15 cm	100 cm from Source	Peat Mix	NaBr	647	12	38	550	17.0	19.0
I19	15-35 cm	100 cm from Source	Mineral Soil	NaBr	871	12	18	500	17.0	23.0
I20	35-45 cm	100 cm from Source	Shale OB	NaBr	3110	13	BDL	1090	19.0	19.0

* with 20 grams deionized water to 10 grams soil; samples filtered with 0.45µm

BDL - Below detection limit (<0.001).

N/A - Not available. In 2005 the sampling program was expanded for segments C and D.